# INFORMATION TO USERS

This manuscript has been reproduced from the microfilm master. UMI films the text directly from the original or copy submitted. Thus, some thesis and dissertation copies are in typewriter face, while others may be from any type of computer printer.

**The quality of this reproduction is dependent upon the quality of the copy submitted.** Broken or indistinct print, colored or poor quality illustrations and photographs, print bleedthrough, substandard margins, and improper alignment can adversely affect reproduction.

In the unlikely event that the author did not send UMI a complete manuscript and there are missing pages, these will be noted. Also, if unauthorized copyright material had to be removed, a note will indicate the deletion.

Oversize materials (e.g., maps, drawings, charts) are reproduced by sectioning the original, beginning at the upper left-hand corner and continuing from left to right in equal sections with small overlaps. Each original is also photographed in one exposure and is included in reduced form at the back of the book.

Photographs included in the original manuscript have been reproduced xerographically in this copy. Higher quality 6" x 9" black and white photographic prints are available for any photographs or illustrations appearing in this copy for an additional charge. Contact UMI directly to order.

U·M·I

University Microfilms International
A Bell & Howell Information Company
300 North Zeeb Road, Ann Arbor, MI 48106-1346 USA
313/761-4700 800/521-0600

Order Number 9202248

# Phase morphology and its relationship to fracture of injection molded polycarbonate and ABS blends

Lee, Ming-Peng, Ph.D.

Case Western Reserve University, 1991

U·M·I
300 N. Zeeb Rd.
Ann Arbor, MI 48106

# PHASE MORPHOLOGY AND ITS RELATIONSHIP TO FRACTURE OF INJECTION MOLDED POLYCARBONATE AND ABS BLENDS

by

MING-PENG LEE

Submitted in partial fulfillment of the requirements

for the degree of Doctor of Philosophy

Thesis Advisors: Dr. Anne Hiltner

Dr. Eric Baer

Department of Macromolecular Science

CASE WESTERN RESERVE UNIVERSITY

May 17, 1991

CASE WESTERN RESERVE UNIVERSITY

GRADUATE STUDIES

We hereby approve the thesis of

Ming-Peng Lee

candidate for the Ph.D.

degree.*

Signed: _____ (Chairman)

_____

_____

_____

_____

Date Sept 24, 1990

*We also certify that written approval has been obtained for any proprietary material contained therein.

# PHASE MORPHOLOGY AND ITS RELATIONSHIP TO FRACTURE OF INJECTION MOLDED POLYCARBONATE AND ABS BLENDS

Abstract

by

MING-PENG LEE

Professor Hull , in the preface of his book, **an Introduction to Composite Materials**, has pointed out that " The essence of composite materials technology is the ability to put strong stiff fibers in the right place, in the right orientation with the right volume fraction. " I would like to paraphrase his statement for the blends as following : " The essence of polymer blends technology is the ability to put soft deformable phases in the right place, in the right shape and orientation with the right volume fraction ".

How do we know what the right microstructure is to obtain the optimum macroscopic performance? A physical understanding of the deformation mechanisms and fracture processes will bridge the gap between these two hierarchical levels. The blends of polycarbonate(PC) and ABS are commercially successful. Basic studies to understand morphology-fracture relationships will provide routes to further upgrade the properties of these

blends.

In the first chapter, the formation and breakup mechanisms of an unusual bead-and-string ABS domain morphology during injection molding of a blend with 10% by weight ABS were described. Based on these mechanisms as well as the flow and thermal histories in mold, the origin of the phase morphology gradient through the thickness was elucidated.

In the second chapter, the phase morphology gradient of injection molded blends of PC and ABS has been characterized across the entire composition range. Based on the morphological features, three composition ranges were identified and an explanation of the origin of the gradient structure was also provided for each region.

In the third chapter, fracture processes were examined as the composition was systematically varied. Three ductile fracture modes, shear tearing, "pop-in" with shear lips and herringbone fracture, occurred coincidentally with the three composition ranges as characterized in the morphological studies described in the second chapter. Correlations between fracture and morphology were also provided.

In the fourth chapter, based on the results of the third chapter , the herringbone and reverse herringbone fracture of the most brittle blend with 30% by weight PC has been studied in more detail. The role of the morphology gradient in the anisotropic fracture was described too.

## DEDICATION

This dissertation is dedicated to my mother and my brother who gave me the love, encouragement and support during the work and to the loving memory of my father.

## ACKNOWLEDGEMENTS

I wish to thank my advisors, Professor Anne Hiltner and Professor Eric Baer for their guidance and support throughout the research project. Financial support for this research was provided by The Dow Chemical Company.

## TABLE OF CONTENTS

PAGE

ABSTRACT.....ii

DEDICATION.....v.

ACKNOWLEDGEMENTS.....vi.

TABLE OF CONTENTS.....vii

LIST OF FIGURES.....xi.

**CHAPTER 1 FORMATION AND BREAKUP OF A BEAD-AND-STRING STRUCTURE DURING INJECTION MOLDING OF A POLYCARBONATE/ABS BLEND**

**PAGE**

1. INTRODUCTION.....1.

2. EXPERIMENTAL.....3

3. RESULTS AND DISCUSSION.....7.

3.1 Morphology.....7.

3.2 Formation of Bead-and-String Structure.....11

3.3 Breakup of Bead-and String Structure.....13

3.4 Effect of Annealing .....15.

3.5 Origin of the Morph logy Gradient.....17.

4. CONCIUSIONS.....22

FIGURES.....24

**CHAPTER 2 PHASE MORPHOLOGY OF INJECTION MOLDED PC/ABS BLENDS**

1. INTRODUCTION.....40

2. EXPERIMENTAL.....42

3. RESULTS AND DISCUSSION.....43

3.1 PC-Rich Compositions.....44

3.1.1 PC/ABS 90/10.....44

3.1.2 PC/ABS 70/30.....47

3.2 Intermediate Blend Compositions.....49

3.2.1 PC/ABS 60/40.....49

3.2.2 PC/ABS 50/50.....51

3.2.3. PC/ABS 40/60.....56

3.3 ABS-Rich Blend Compositions.....58

3.3.1 PC/ABS 30/70.....58

3.3.2 PC/ABS 10/90.....59

3.4 Effects of Composition.....60

4. CONCLUSIONS.....63

FIGURES.....66.

CHAPTER 3 FRACTOGRAPHY OF INJECTION MOLDED POLYCARBONATE/ABS BLENDS

1. INTRODUCTION.....90

2. EXPERIMENTAL.....93

3. RESULTS and DISCUSSIONS.....94

3.1 Ductile Fracture Modes.....94.

3.2 Ductile-to-Brittle Transition.....97

3.3 PC-Rich Compositions.....100

3.4 Intermediate Compositions.....103.

3.5 ABS-Rich Compositions.....107.

4. CONCLUSIONS.....110

FIGURES.....112.

CHAPTER 4 THE HERRINGBONE FRACTURE OF A POLYCARBONATE/ABS BLEND

1. INTRODUCTION.....131.

2. EXPERIMENTAL.....133

3. RESULTS and DISCUSSION.....135

3.1 Stress-Displacement Behavior.....135.

3.2 Fractography of Parallel Orientation.....136

3.3 Fractography of perpendicular Orientation.....138

3.4 Formation of Herringbone and Reverse Herringbone Patterns.....141

3.5 Morphology.....144

3.6 Microstructure of Fracture Surfaces.....147

4. CONCLUSIONS.....152

FIGURES.....154.

REFERENCES.....182.

## LIST OF FIGURES

**CHAPTER 1 FORMATION AND BREAKUP OF A BEAD-AND-STRING STRUCTURE DURING INJECTION MOLDING OF A POLYCARBONATE/ABS BLEND**


PAGE

Figure 1 Scanning electron micrographs of the injection molded PC/ABS 90/10 blend at various positions through the thickness.....24

Figure 2 Views parallel to the injection direction near the center of the plaque.....29.

Figure 3 The relative number density of spherical SAN particles on micrographs.....30.

Figure 4 Schematic representation of the morphology of the injection molded PC/ABS 90/10 blend.....31

Figure 5 Etched surfaces showing SAN strings in various stages of breakup.....32.

Figure 6 Etched surfaces showing various stages of end-pinching...34

Figure 7 The annealed blend viewed parallel to the injection direction near the edge of the plaque..... .....36

Figure 8 Shear rate profile through the thickness during mold

filling, estimated for the PC/ABS 90/10 blend.....38

Figure 9. Schematic representation showing the formation of the bead-and-string structure at the melt front.....39

**CHAPTER 2 PHASE MORPHOLOGY OF INJECTION MOLDED PC/ABS BLENDS**

Figure 1 Scanning electron micrographs of injection molded PC/ABS 90/10 blend.....66.

Figure 2 The relative number density of SAN particles on micrographs of a PC/ABS 90/10 parallel fracture surface at various positions through the thickness.....68

Figure 3 Scanning electron micrographs of injection molded PC/ABS 70/30 blend.....69.

Figure 4. Scanning electron micrographs of injection molded PC/ABS 60/40 blend.....72.

Figure 5 Scanning electron micrographs of injection molded PC/ABS 50/50 blend at various positions through the thickness.....75

Figure 6 The reciprocal Chalkley parameter $C^{-1}$ through the thick-

ness of the PC/ABS 50/50 blend.....79

Figure 7 Schematic representation of the morphology of the morphology of the PC/ABS 50/50 blend.....80.

Figure 8 The annealed PC/ABS 50/50 blend viewed parallel to the injection direction near the edge.....81.

Figure 9 Scanning electron micrographs of injection molded PC/ABS 40/60 blend.....82.

Figure 10 Scanning electron micrographs of injection molded PC/ABS 30/70 blend.....85.

Figure 11 The length to width ratio of the PC domains through the thickness of the PC/ABS 30/70 blend.....87

Figure 12 The annealed PC/ABS 30/70 blend viewed parallel to the injection direction near the edge.....88

Figure 13 Scanning electron micrographs of injection molded PC/ABS 10/90 blend.....89.

**CHAPTER 3 FRACTOGRAPHY OF INJECTION MOLDED POLYCARBONATE/ABS BLENDS**

Figure 1 Ductile fracture surfaces obtained at room temperature with a crosshead speed of 229 mm/min as viewed in the

stereoscan optical microscope.....112.

Figure 2 Brittle fracture surface of PC obtained at -20°C and a crosshead speed of 229 mm/min as viewed in the optical microscope with reflected light.....115

Figure 3 The ductile-to-brittle transition for PC/ABS blends for a crosshead speed of 229 mm/min.....116

Figure 4 Fracture surfaces in the ductile-to-brittle transition region with a crosshead speed of 229 mm/min as viewed in the stereoscan optical microscope.....117.

Figure 5 Scanning electron micrographs of the fracture surface in Figure 4a of PC/ABS 90/10.....119

Figure 6 Scanning electron micrographs of a fracture surface of PC/ABS 50/50 obtained at -65°C and a crosshead speed of 229 mm/min.....121.

Figure 7 Schematic representation of craze growth in the pop-in region.....123

Figure 8 Scanning electron micrographs of fracture surfaces of PC/ABS 50/50 obtained at room temperature with a crosshead speed of 0.1 mm/min.....124

Figure 9 Scanning electron micrograph of the fracture surface of a PC/ABS 50/50 specimen machined perpendicular to

the injection direction and tested at -10°C with a crosshead speed of 229 mm/min.....126

Figure 10 Scanning electron micrographs of the herringbone fracture surface of PC/ABS 30/70 obtained at -25°C and a crosshead speed of 229 mm/min.....127

Figure 11 Schematic representation for craze growth in the crack initiation region of the herringbone.....129

Figure 12 Scanning electron micrograph of the reverse herringbone fracture surface of a PC/ABS 30/70 specimen machined perpendicular to the injection direction and tested at -10°C and a crosshead speed of 229 mm/min.....130

**CHAPTER 4 THE HERRING BONE FRACTURE OF A POLYCARBONATE/ABS BLEND**

Figure 1 Typical stress-displacement curves for parallel and perpendicular specimens tested at room temperature with a crosshead speed of 0.5mm/min.....154

Figure 2 Typical fracture surfaces of parallel specimens tested at a crosshead speed of 229 mm/min and

various temperature.....155.

Figure 3 Final three frames showing fracture of a parallel specimen viewed ind-on from the notched end.....157

Figure 4 Typical fracture surfaces of perpendicular specimens tested at a crosshead speed of 229 mm/min and various temperatures.....159

Figure 5 The reverse herringbone pattern.....161

Figure 6 Temperature contours showing fracture of a perpendicular specimen viewed end-on from the unnotched end.163

Figure 7 Proposed mechanism for formation for the herringbone pattern.....165

Figure 8 Proposed mechanism for formation for the reverse herringbone pattern.....167

Figure 9 Scanning electron micrographs of the unetched fracture surface of a perpendicular specimen tested at -70°C with a crosshead speed of 229 mm/min.....169

Figure 10 Scanning electron micrographs of etched cryogenic fracture surfaces at various positions through the thickness.....170

Figure 11 Scanning electron micrograph of etched mold-contacting edge.....174

Figure 12 Schematic representation of the morphology.....175

Figure 13 Transmission electron micrographs of $OsO_4$-stained sections.....176

Figure 14 The length to thickness ratio for the PC domains and the rubber particles through the thickness for the 3mm thick plaque at its midpoint.....177

Figure 15 Scanning electron micrographs showing various regions of the fracture surface in Figure 2a.....178

Figure 16 Scanning electron micrographs of the fracture surface in Figure 4c.....180

Figure 17 Schematic representation showing how the anisotropic morphology produced the herringbone and raverse herringbone.....181.

# CHAPTER 1

## FORMATION AND BREAKUP OF A BEAD-AND-STRING STRUCTURE DURING INJECTION MOLDING OF A POLYCARBONATE/ABS BLEND

### 1. INTRODUCTION

Injection molding is one of the most important plastics fabrication operations, and is frequently employed for melt forming blends of immiscible polymers. Although it is well known that the improved physical and mechanical properties of polymer blends are highly dependent on the phase morphology, the non-steady state conditions during injection molding make it particularly difficult to predict and control the solid state morphology achieved in injection molded parts. Material properties of the components, such as interfacial tension and rheological characteristics, have a major effect on size and shape of domains that are formed by the complex shear and elongational flow fields of the mold filling process. After cessation of flow, the domain morphologies created by the flow patterns during mold filling relax to a greater or lesser extent depending upon the rate of cooling. As a result, skin-core structures that have a gradient in phase morphology through the thickness are characteristic of injection molded parts.

Elongated domains of the dispersed component are frequently

observed in the skin at the mold-contacting surface where the melt experiences elongational flow at the front of the fountain flow pattern (1) and where rapid freezing favors retention of the melt morphology in the solid state. For example, dispersed particles of EPDM in polypropylene were observed to be highly elongated in the skin layer (2), as were SAN domains in blends with polycarbonate (3, 4). When other variables are held constant, the viscosity ratio of the two components is the decisive factor controlling the extent to which the dispersed phase is elongated in the flowing melt (5). The elongated domain morphology is sustained by the flow field, but after cessation of flow may relax to a spherical shape, or, if the aspect ratio is sufficiently large, it has been suggested that the domains may breakup by an interfacial instability mechanism (6-8) which has been described analytically for Newtonian liquids (9-12).

Blends with ABS as one of the components have an additional complication in that the ABS is itself a heterogeneous material and consists of a free SAN component together with composite rubber particles with a grafted SAN shell and SAN sub-inclusions. Because of the recent interest in blends of polycarbonate (PC) with ABS (13-15), a study has been undertaken to characterize the morphology gradient through the thickness of an injection molded blend of PC with 10 weight percent ABS, and to find an explanation for the phase morphology that considers the processing

parameters.

## 2. EXPERIMENTAL

A blend with 10% by weight ABS and 90% by weight polycarbonate (PC) was provided by The Dow Chemical Company in the form of injection molded 5in (12.7cm) x 3in (7.6cm) x 1/8in (0.3cm) plaques. A tab was located at one end in the center of the width and a conventional rectangular edge gate fed this tab. The plaques were molded with an Arburg Model 300-210-700 injection molding machine with a screw rotational speed of 300rpm. The injection pressure was 55bar, the melt (barrel) temperature about 270°C and the mold temperature was 79.5°C. The total cycle time of 27.5sec consisted of a delayed injection time of 0.5sec, an injection time of 4sec, a packing time of 4sec, a cooling time of 18.0sec and a 1.0sec pause after mold opening.

The polymers were a commercial grade of polycarbonate (Calibre from The Dow Chemical Company) with melt flow index of 10 g/min (ASTM 1238 condition O) and a commercial ABS resin from The Dow Chemical Company reported by the manufacturer to be about 20% by weight acrylonitrile and 20% by weight butadiene rubber. Following a published

method (16), the ABS resin was dispersed in acetone to dissolve free SAN and the milky solution repeatedly centrifuged until a clear supernant liquid was obtained. The insoluble composite rubber particles were separated from the acetone-soluble fraction by decanting the clear liquid dried, and weighed.

The compositions of the soluble ABS and the SAN component were determined by infrared analysis. Films were cast from THF solution and the spectra obtained on a DigiLab Biorad FTS-60. The weight ratio of butadiene to styrene in ABS was determined from the absorbance ratio of bands at 968$cm^{-1}$ and 3077$cm^{-1}$ (17). When the styrene is above 75%, this ratio can also be obtained from the absorbance ratio of bands at 968$cm^{-1}$ and 1030$cm^{-1}$ (18). Both determinations were made for internal consistency. The relative weight fraction of acrylonitrile to styrene either in free SAN or in ABS was obtained from the absorbance ratio of the 2220$cm^{-1}$ and 755$cm^{-1}$ bands (19). Calibration curves were constructed from commercial resins of known composition. Analysis of the ABS resin showed it to be about 15% rubber by weight and 20% by weight acrylonitrile. Of the 85% of the ABS that was SAN, 79% was present as free SAN and 21% was associated with the rubber either as grafted SAN or as occluded SAN particles. The free SAN was estimated to be 25% acrylonitrile.

The number and weight average molecular weights of PC and the soluble SAN fraction of the ABS were measured with a Varian DS 651 GPC relative to polystyrene standards at 25°C using THF as the solvent. The weight average molecular weight of the SAN relative to polystyrene was about $1.4 \times 10^5$ with a polydispersity of 2.3, and that of PC was $5.6 \times 10^4$ with a polydispersity of 1.9.

Tensile specimens were cut to the ASTM-1708 geometry either parallel or perpendicular to the injection direction. A single edge notch (SEN) was machined at the midpoint of the gauge length, the notch was 0.037in (0.094cm) in depth with a 0.010in (0.025cm) notch radius and 45° flank angle. The specimens were cut and notched in such a way that the location of fracture was through the thickness at the center of the plaque. The notched tensile specimens were fractured in the Instron at -70°C with a crosshead speed of 229mm/min. The brittle cryogenic fracture surfaces were subsequently selectively etched by immersion in 30% by wight aqueous potassium hydroxide for approximately 5 hours, dried, coated with gold and examined in the JEM 35CF scanning electron microscope (SEM). Alternatively, some of the etched specimens were stained with a 1% by weight aqueous solution of osmium tetroxide at room temperature for two weeks, then coated with gold and examined in a JEOL 840A scanning electron microscope in the backscatter mode. One of the brittle fracture

surfaces that had been etched with aqueous KOH was subsequently etched with acetone to remove free SAN, then washed in water, dried, coated with gold and viewed in the SEM.

In some cases, the plaque was sectioned with a diamond wafering blade on the Isomet from the Buehler Company, then etched with aqueous KOH, washed with water, dried and coated with gold for viewing in the SEM. This procedure was used to examine the phase morphology in the tab of the injection molded plaque. The plane parallel to the mold-contacting surface was sectioned with the RMC MT-6000-XT cryogenic ultramicrotome.

Annealing experiments were carried out on rectangular specimen blocks cut from the center of the plaque with the wafering blade. The specimen block was positioned in a large DSC pan so that the surface cut through the thickness parallel to the injection direction contacted the bottom of the pan. In this way, the surface of interest was as close as possible to the DSC heating element and differences between the programmed temperature and the actual temperature experienced by the specimen were minimized as much as possible. Annealing was carried out in the Perkin Elmer DSC 7; the specimen was heated to the annealing temperature of 185°, 200° or 270°C at a heating rate of 200°C/min, held at temperature for

6 or 12 sec, then cooled to ambient temperature at a rate of 200°C/min. The surface of the specimen block that had contacted the bottom of the pan was etched with aqueous KOH, washed, dried and coated with gold for viewing in the SEM.

## 3. RESULTS AND DISCUSSION

### 3.1 Morphology

Brittle fracture surfaces both parallel and perpendicular to the injection direction were etched to remove the PC phase and viewed in the SEM to characterize the morphology gradient through the thickness of the plaque. Although the morphology probably varied to some extent along the length and width of the plaque, this was not examined and the midpoint of the plaque was chosen as a representative location. At the center of the plaque, the morphology appeared the same in both parallel and perpendicular directions, Figure 1a and 1b. When the PC was etched away , the ABS phase was revealed to discontinuous and to consist of two populations of spherical particles: a relatively small number of larger spheres approximately 1$\mu$m in diameter together with numerous small particles with a diameter of about 0.3$\mu$m.

In addition to the large and small particles, some string-like domains elongated in the injection direction and about 0.2$\mu$m in diameter were visible in the parallel view at a position 1.05mm from the edge of the 3mm thick plaque, Figure 1c. The string-like domains were not readily apparent in the perpendicular view from a similar location, Figure 1d. In this view, the ABS domains appeared very much as they did in the center of the plaque, cf Figure 1b, although there was occasionally the suggestion that small particle was actually the end of an elongated domain.

Midway between the edge and center of the plaque, at 0.84mm (not shown) and 0.67mm from the edge, the elongated domains were much more numerous in the parallel views and sometimes were attached to the large 1$\mu$m particles, Figure 1e. Fewer of the smaller 0.3$\mu$m particles were observed in this region, and they frequently appeared to be part of the string-like domains. The corresponding perpendicular view, Figure 1f, differed only subtly from those closer to the center of the plaque. Close examination showed that many of the small particles, which had the same diameter as the strings in the parallel view, were the protruding ends of elongated domains.

The small spherical particles were not observed in parallel views closer to the edge; at 0.53mm (not shown) and 0.45mm from the edge of

the plaque the morphology of the ABS phase consisted of densely packed string-like domains connecting the large spherical particles, Figure 1g. This "bead-and-string" morphology created ABS domains that were essentially continuous in the injection direction. Circular cross sections and protruding ends of strings were seen in the corresponding perpendicular view, Figure 1h. This view also showed star-like arrays with numerous strings emanating from the large 1$\mu$m particles; these appeared to produce interconnections among bead-and-string structures.

The bead-and-string structure was also observed near the edge but with subtle differences. Parallel views 0.20mm (not shown) and 0.13 mm from the edge were indistinguishable and showed that close to the edge the string-like domains were more discrete and less interconnected, Figure 1i. This was confirmed in the perpendicular view, Figure 1j, where on the average there were fewer strings attached to the large particles.

The ABS component was itself heterogeneous and consisted of free SAN and composite rubber particles with a grafted SAN shell and SAN sub-inclusions. The SEM backscatter image showed the large spheres to be selectively stained by $OsO_4$ which identified them as the rubber particles. In order to further differentiate the free SAN from the composite rubber particles, brittle fracture surfaces that had been etched with aqueous KOH

to remove PC were subsequently etched with acetone to remove the free SAN. Comparison of a parallel view from the center before the surface was etched with acetone, Figure 2a, with a view of the same region after etching with acetone, Figure 2b, showed that acetone removed the strings. This identified the small particles in the center part of the plaque and the string-like domains in the edge region as the free SAN component of the ABS phase.

The predominant feature of the morphology gradient through the thickness of the plaque was the change in the free SAN component from 0.3$\mu$m spheres in the center to strings connecting rubber particles in the bead-and-string structure nearer the edge. To illustrate the change in morphology through the thickness, the number density of SAN spheres was measured from the parallel micrographs at various positions, Figure 3. While the absolute numbers are not significant, they do show that while there were essentially no spherical particles near the edge, at about 0.5mm in from the edge the relative number density of free SAN particles began to increase rapidly and continued to increase to the center.

A model of the gradient morphology through the thickness of the plaque was developed, Figure 4. In the center, the morphology was isotropic in the parallel and perpendicular directions with the ABS phase

dispersed in the PC matrix as large composite rubber particles and smaller spherical SAN particles. Away from the center, a few string-like SAN domains elongated in the injection direction appeared, and about half the distance from the center to the edge, the morphology of the free SAN phase changed from predominantly spherical to predominantly string-like. The SAN strings connected the rubber particles to form an ABS bead-and-string structure was highly interconnected, although in a 0.2mm thick region at the edge of the plaque a subtle change occurred and the strings of the bead-and-string structure were more discrete with fewer interconnections.

## 3.2 Formation of Bead-and-String Structure

The shear rate dependent viscosity was estimated from methods described in the literature. The influence of acrylonitrile content on the flow curve of SAN is reportedly very slight (20); the shift factor for molecular weight from Casale et al(20) was used to obtain the viscosity at the reference temperature of 210°C, and with the temperature shift factor from Mendelson (21), which is reportedly independent of both molecular weight and acrylonitrile content, the rheological behavior at the injection temperature was determined. The flow curve of the PC component was estimated from the melt flow index using the parameters reported by Shevoy and Saini (22,23). The estimated viscosity ratio of free SAN to PC

at the injection temperature, 270°C, varied from 0.4 to 0.3 over the range of shear rates from 3 to $10^3$ $sec^{-1}$.

In a blend that was 90% PC and only 10% ABS would have been the dispersed phase. For purposes of discussing the phase deformation during melt flow, an ABS domain that consisted of a composite rubber particle with some free SAN was considered. The crosslinked rubber particle was not highly deformable, only the free SAN with a viscosity lower than that of the continuous PC phase would have been highly deformed by the flow field. No matter how complex the flow field was, it could be separated into elongational and shear components. Under elongational flow, with axial extensional forces in the flow direction and compressive lateral forces, the free SAN was drawn out into strings while cohesive forces prevented the strings from breaking-up. The molecular weight obtained for the free SAN component was in the range where theoretically a maximum in the extensibility of melt filaments was predicted (24). It is also known that a deformable sphere will extend in a shear flow field, and the theoretical description of the phenomenon is well advanced (25). The SAN/PC pair met the optimum conditions, in terms of viscosity ratio, that were described for extension of viscous drops into long threads (26).

The extension of SAN particles into long strings or threads was

anticipated from the general understanding or particle motions in shear and elongational flow, and indeed the viscosities of the PC and free SAN were in the optimum range for formation or the long strings. The unique feature when ABS was the dispersed phase was the attachment of the SAN strings to the rubber particles as the free SAN was drawn out. Miscibility with the grafted SAN provided adhesion to the rubber particles. Continuous "bead-and-string" structures of SAN "strings" connecting rubber "beads" could have formed if the original ABS domain contained more than one rubber particle or if several ABS domains coalesced during flow. Coalescence of a dispersed phase has been reported to occur under both elongational (27) and shear (28) flow conditions. This "bead-and-string" morphology created the possibility for the ABS phase to be co-continuous with PC in the flow direction.

### 3.3 Breakup of Bead-and-String Structure

The proposed bead-and-string melt morphology of the ABS phase was sustained by the flow field, when the flow conditions changed or flow ceased altogether, the bead-and-string morphology was affected. Although relaxation to a spherical shape was possible, viscous liquid such as SAN readjust their shape more slowly than less viscous fluid would, and instead can breakup into many drops following the growth of Rayleigh instabilities

(9-12). It has been emphasized that this mechanism of interfacial tension driven breakup can occur after flow has ceased only when the aspect ratio of the thread is very large (29).

A striking feature reported in the breakup of stationary fluid threads was the simultaneous disintegration at all points along the thread into a series of drops (30). Evidence that breakup of SAN strings followed the concepts developed in studies of lower viscosity fluids appeared in an etched surface, Figure 5. The micrographs show shapes that are very similar to the intermediate stages of breakup envisaged in the literature (30). Figure 5a shows a SAN string in an initial stage of breakup with undulations created by the instability, while Figure 5b contains several columns of uniform spheres about 0.3$\mu$m in diameter that formed when the string disintegrated but had not had time to disperse.

End-pinching behavior has been reported in fluid threads with bulbous ends (31). In this special case, the bulbous end broke off from the central portion of the thread due to capillary forces associated with curvature variations along the interface, rather than by a capillary wave instability (31,32). Because of the curvature at the conjunction of the SAN string from the rubber particle during relaxation in a separate process from breakup of the SAN string.

The range of flow conditions and cooling rates through the thickness of the plaque during the injection molding operation made it possible to find evidence for the various stages of end pinching and breakup in the micrographs. An example of the beginning of end-pinching with constriction at the point of union of a rubber particle and SAN string was seen in Figure 6a; in another example, the pointed end of the SAN string in Figure 6b suggested that it had just broken off from the nearby rubber particles; and in Figure 6c the appearance of the SAN strings suggested that they were at a stage after detachment when the pointed ends had relaxed to a bulbous shape and instability that would lead to breakup of the SAN string was beginning.

### 3.4 Effect of Annealing

Some evidence for bread-up of the bead-and-string structure after cessation of flow was obtained when the micrographs revealed instances of intermediate stages of break-up frozen into the injection molded plaque. The hypothesis that the bead-and-string structure was sustained by the flow field and was only retained after molding because rapid cooling did not permit sufficient time for relaxation was tested by observing the effect of annealing on the morphology. Figure 7 shows the changes near the edge, where the bead-and-string structure was retained in the injection molded

plaque, after annealing for a short period of time, nominally 12sec. The initial bead-and-string structure, Figure 7a, was only slightly altered after heating to 185°C by the appearance of a few small spherical SAN particles, Figure 7b; but after heating only 15°C higher, to 200°C, the bead-and-string structure had disappeared, Figure 7c, and instead of the long thin SAN strings there were numerous small spherical SAN particles while only remnants of thicker SAN strings remained. These were mostly separated from the rubber particles and often had bulbous ends and undulations in cross-section as if they were in the process of breaking up. A temperature of 270°C for nominally 12sec was sufficient for the bead-and-string to completely break-up into small spherical SAN particles, Figure 7d; in this instance only the linear arrangement of the SAN particles remained to show that they had originated from elongated strings.

The morphology of the annealed specimens was examined at other locations through the thickness. The regions where the morphology was examined were as close as possible to the heating element of the DSC so that the thermal history was as similar as possible for all locations. The morphology gradient through the thickness was completely removed by annealing at 270°C for nominally 6sec, the shortest holding time available on the DSC; under theses conditions, the bead-and-string structure broke up completely and spherical SAN particles were observed through the entire

thickness.

The bead-and-string structure broke up more slowly away from the edge. For example, 0.45mm inward from the edge of the specimens annealed at 185°C and 200°C for 12 sec, the appearance of a few spherical SAN particles was evidence for the beginning of breakup, but the bead-and-string structure did not bread up completely until the highest annealing temperature. The longer breakup time was attributed to the larger diameter of SAN strings at this location.

## 3.5 Origin of the Morphology Gradient

The melt morphology of the ABS phase as the blend entered the mold was determined to be the bead-and-string structure. This conclusion was based on SEM observations of etched material from the tab, which was assumed to have cooled rapidly enough to preserve the melt flow morphology in the gate. It was reasonable that dispersed ABS domains, formed in previous blending operations, would have elongated and coalesced into the bead-and-string structure in the high shear and elongational flow fields the melt experienced prior to entering the mold. The subsequent evolution to the final solid state structure was determined by the flow fields experienced by the melt during mold filling, and the cooling

rate during and after mold filling. Since injection molding is not a steady state operation, these were not known precisely and only a qualitative analysis was attempted.

In the case of non-isothermal flow, the velocity distribution through the thickness has an inflection point where the shear rate attains a maximum (1,33,34) while the shear rate is zero at the mold surface and at the center. The shear rate profile some distance behind the advancing front, Figure 8, was estimated from the approximate method described in the literature (1). In the region of higher shear rates, which occupied the largest portion of the thickness, the bead-and-string structure was probably retained during mold filling. Only near the center in the low shear rate region was the bead-and-string expected to breakup by the instability and end-pinching mechanisms during mold filling.

The center region was only a small part of the thickness, but because the velocity was highest, this region provided material to the advancing melt front where the fountain flow pattern developed (1). In the fountain pattern, elongational flow perpendicular to the injection direction carries material from the center to the mold surface where it solidifies rapidly to form the characteristic skin layer (1). It was thought likely that even though the ABS phase probably broke up into a dispersed particulate morphology

in the center during mold filling, the bead-and-string structure would reform under the elongational flow field at the melt front and subsequently be preserved in the skin layer that solidified upon contact with the cold mold surface. The schematic representation in Figure 9 illustrates the proposed formation of the bead-and-string structure at the melt front.

Indirect evidence to support this supposition was obtained by examining the morphology at the un-gated end of the mold where the melt front impinged and solidified rapidly when the mold was completely filled. In the center of the thickness at this location, the morphology of the free SAN phase consisted primarily of a dispersion of small particles, the expected product of bead-and-string breakup, together with a few SAN strings attached to rubber particles; while between the center and the edge, bead-and-string structures that could have formed by coalescence and extension of the spherical particles were observed, these were oriented normal to the mold-contacting surface along the flow lines at the front of the fountain flow.

Since the bead-and-string structure extended through the thickness approximately half the distance to the center, it was thought to be derived from both the elongation flow at the melt front and the shear flow behind the melt front. The region closest to the edge that derived from the

elongational flow at the melt front was discernable by the subtle change in the bead-and-string structure about 0.2mm from the edge. The calculated thickness of the skin layer that had solidified at the end of mold filling was in the range of 0.24 to 0.34mm (35-38), in good agreement with the observed dimension.

In the region between the skin layer that derived from the melt front, where solidification was rapid and the melt morphology was largely retained, and the center, where the low shear rate during mold filling and long cooling time after mold filling assured relaxation to the particulate morphology, the final solid state morphology was determined by the competition between the breakup rate and the cooling rate. A method in the literature was used to estimate the temperature gradient through the thickness of the melt at the conclusion of the mold filling stage and at various times thereafter during cooling (38). The melt diffusivity of PC was taken from the literature (39). In the calculations, it was assumed that at the end of mold filling the temperature varied from approximately the $T_g$ of PC, 150°C, at the skin layer to the temperature of the melt when it entered the mold, 270°C, at the center. In this way, it was estimated that the temperature in the center of the mold reached the $T_g$ of PC in about 12-13sec.

It was known from the isothermal annealing experiments that even

if the temperature exceeded the $T_g$ of PC at the end of mold filling, breakup might not have occurred during mold cooling. In particular, in the region where the temperature at the end of mold filling was on the order of 185°-200°C, the bead-and-string structure would not have broken up even if the temperature had remained constant for the approximately 12sec cooling time. Since the temperature in the mold in fact was continuously decreasing, it was even less likely that the bead-and-string structure would have had time to break up in this region. From the calculations, it was estimated that the 185°-200°C temperature range was achieved at the end of mold filling about 0.5mm inward from the edge. Examination of the morphology showed no evidence of breakup at this position.

Evidence of break-up, specifically the appearance of some spherical SAN particles, was only observed when the depth was greater than 0.5mm from the edge. The amount of breakup was expected to vary from relatively little at the 0.5mm position where the melt temperature was initially lower and less time was required to cool to 150°C , to almost complete breakup near the center where the temperature was initially highest and the cooling time longest. Thus a gradient was created through the thickness with various amounts of breakup by the instability and end-pinching mechanisms as seen in the micrographs (cf Figure 1). This gradient was also observed by the gradual increase in the number of SAN spheres from almost zero at

0.5mm to the very large number observed at the center of the plaque (cf Figure 3).

## 4. CONCLUSIONS

The phase morphology of a PC/ABS 90/10 blend in injection molded plaques was characterized. Examination of etched brittle fracture surfaces led to a description and explanation of the morphology gradient through the thickness. Specifically :

1. In the center of the plaque, the morphology was isotropic with the ABS phase dispersed in the PC matrix as large composite rubber particles and smaller spherical SAN particles. About half the distance from the center to the edge, the morphology of the free SAN changed from predominantly spherical to predominantly string-like. The SAN strings connected the rubber particles to form an oriented ABS bead-and-string structure that was essentially continuous in the injection direction.

2. The melt morphology of the ABS phase as the blend entered the mold was determined to be the bead-and-string structure. It was thought that this morphology was sustained during mold filling in regions of high

elongational and high shear flow.

3. The gradient in phase morphology was created by the competition between the relaxation rate of the bead-and-string structure and the cooling rate after mold filling. It was proposed that the bead-and-string structure was retained in the region where the melt experienced the highest elongational and shear flows during mold filling, and solidified most rapidly during cooling.

4. Near the center, where the shear rate was lowest and cooling time longest, it was proposed that the bead-and-string structure broke up by interfacial tension driven breakup and end-pinching mechanisms to produce the isotropic dispersion of 1$\mu$m composite rubber particles and 0.3$\mu$m free SAN particles.

(a) parallel to the injection direction, d = 1.5mm

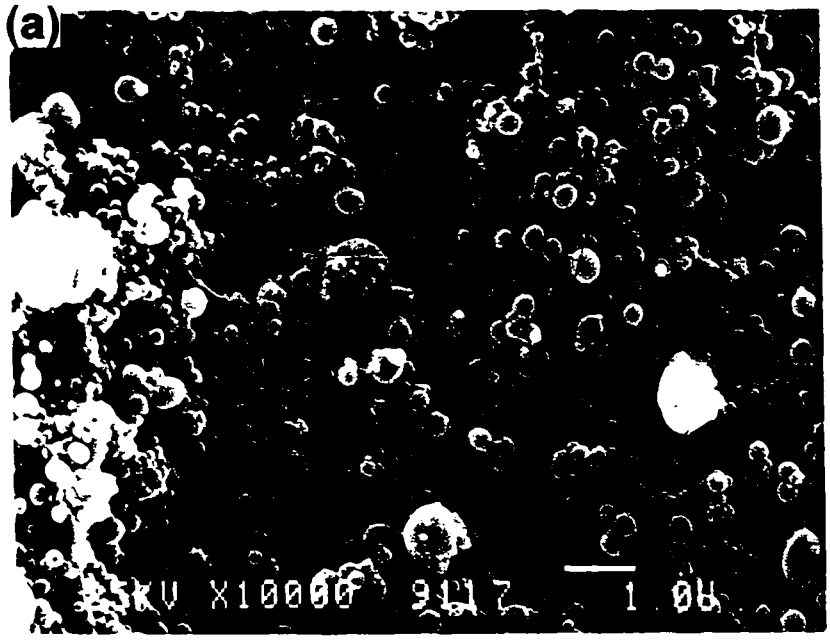


(b) perpendicular to the injection direction, d = 1.5mm

Figure 1. Scanning electron micrographs of the injection molded PC/ABS 90/10 blend at various positions through the thickness.
d : the distance from the edge of the 3mm plaque

(c) parallel to the injection direction, d = 1.1mm

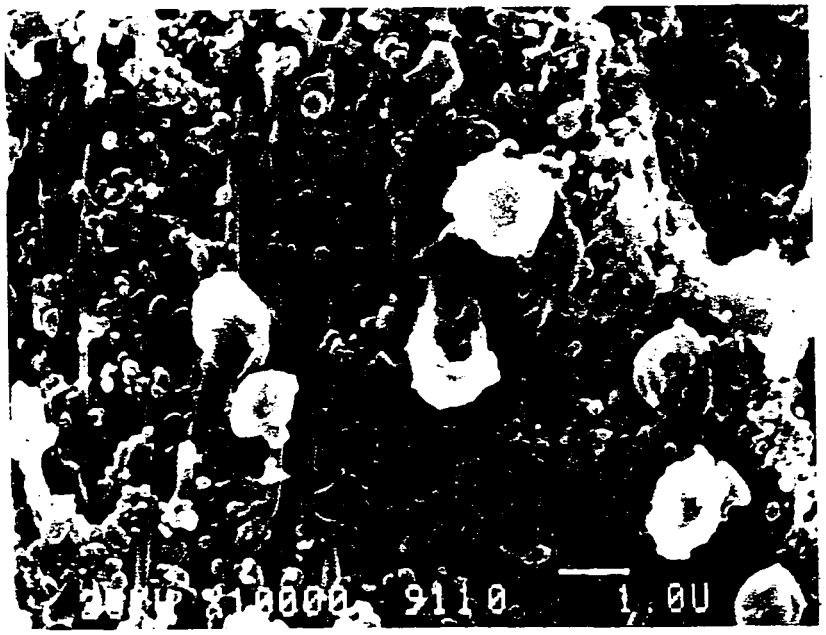

(d) perpendicular to the injection direction, d = 1.1mm

Figure 1. Scanning electron micrographs of the injection molded PC/ABS 90/10 blend at various positions through the thickness.
d : the distance from the edge of the 3mm plaque

(e) parallel to the injection direction, d = 0.67mm

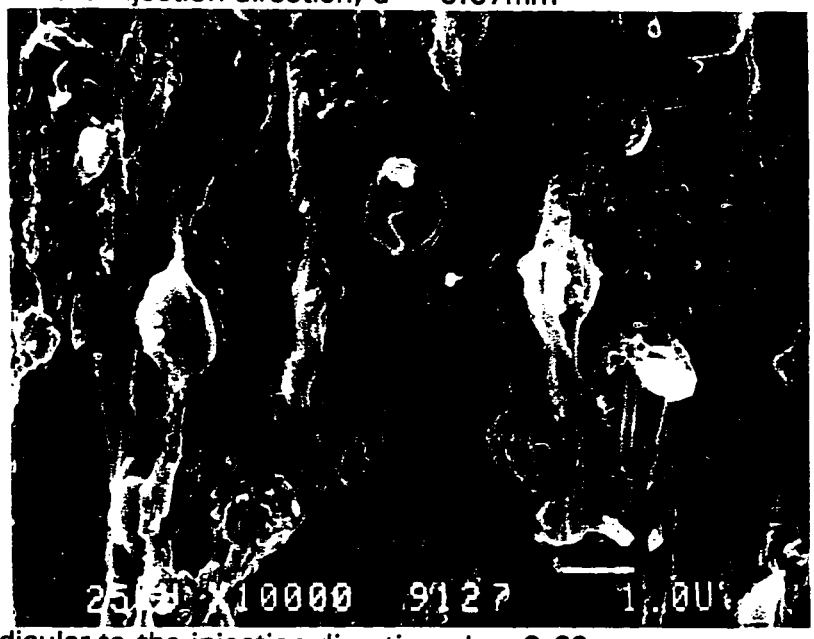


(f) perpendicular to the injection direction, d = 0.69mm

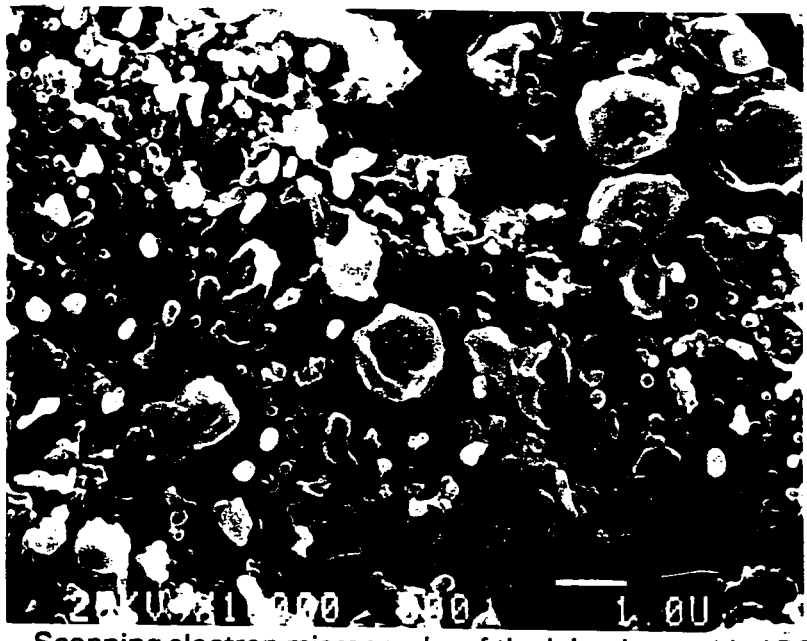

Figure 1. Scanning electron micrographs of the injection molded PC/ABS 90/10 blend at various positions through the thickness.
d : the distance from the edge of the 3mm plaque

(g) parallel to the injection direction, d = 0.45mm

(h) perpendicular to the injection direction, d = 0.45mm

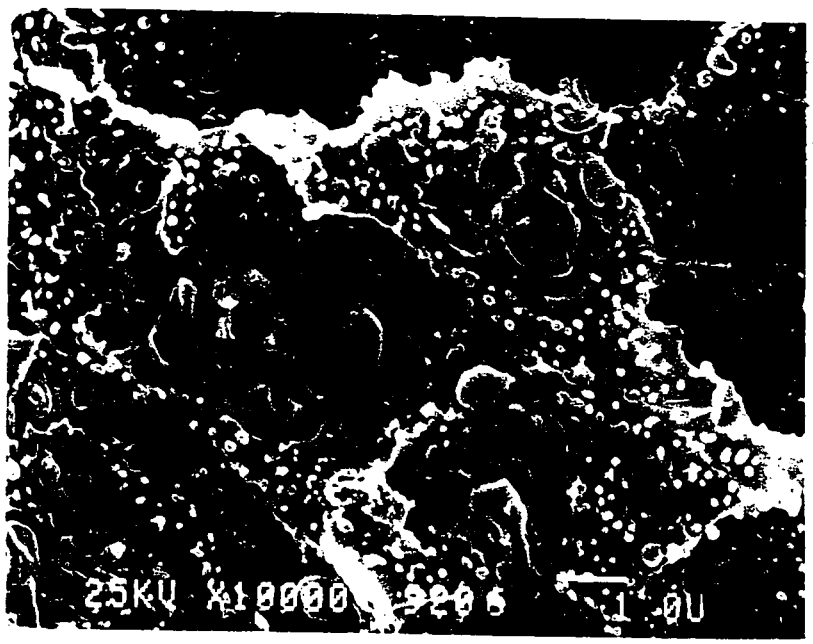

Figure 1. Scanning electron micrographs of the injection molded PC/ABS 90/10 blend at various positions through the thickness.
d : the distance from the edge of 3mm plaque

(i) parallel to the injection direction, d = 0.13mm

(j) perpendicular to the injection direction, d = 0.13mm

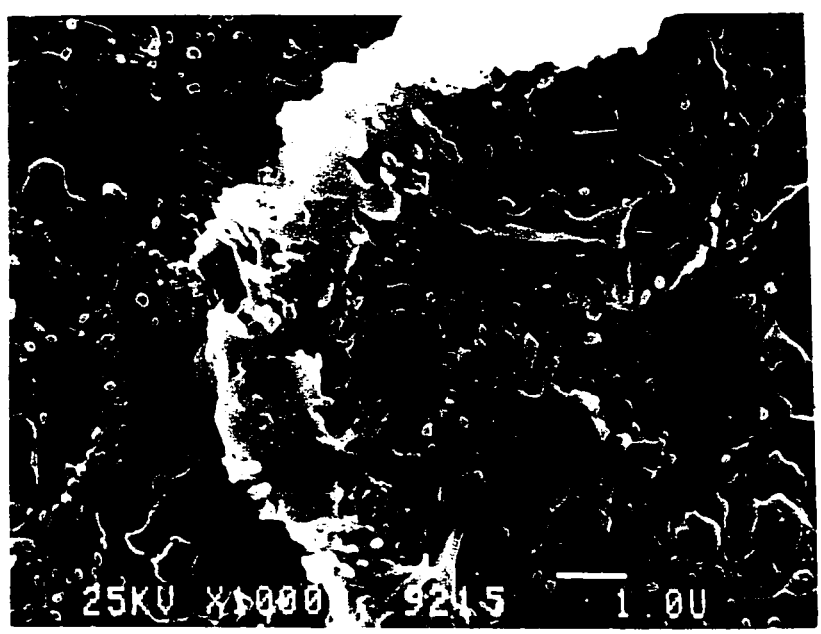


Figure 1. Scanning electron micrographs of the injection molded PC/ABS 90/10 blend at various positions through the thickness.
d : the distance from the edge of the 3mm plaque

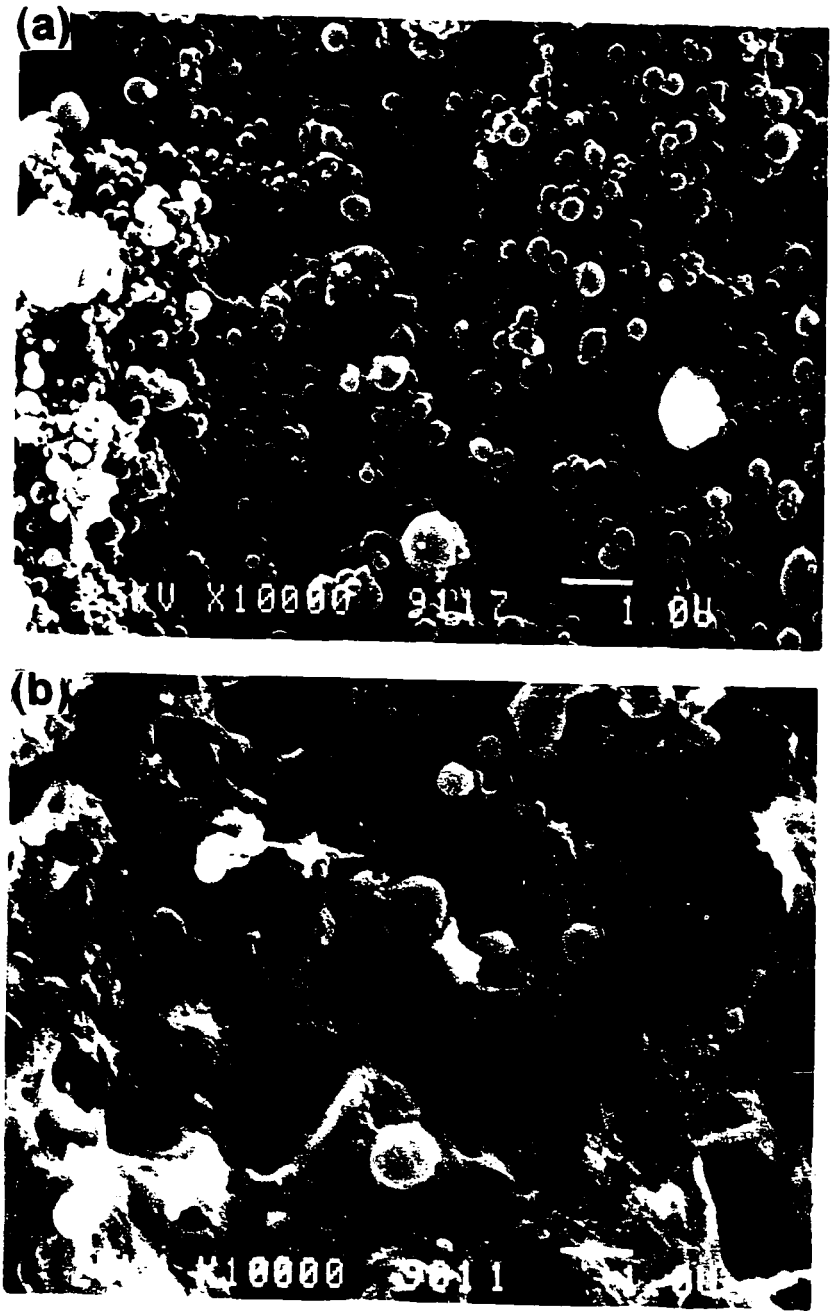


Figure 2. Views parallel to the injection direction near the center of the plaque. (a) etched with KOH to remove PC, and (b) etched with KOH and subsequently etched with acetone to remove free SAN

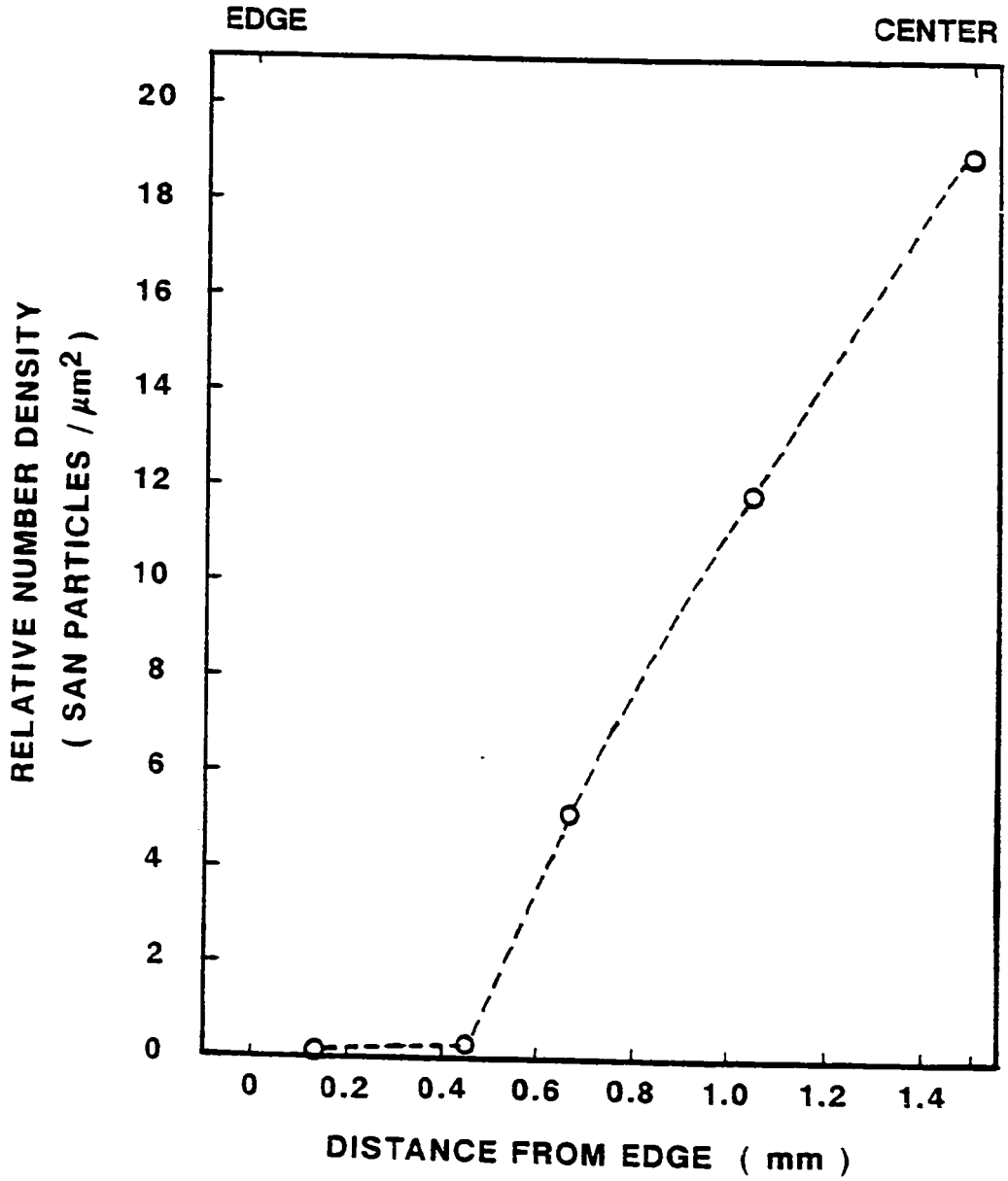


Figure 3. The relative number density of spherical SAN particles on micrographs of a parallel fracture surface at various positions through the thickness of the plaque.

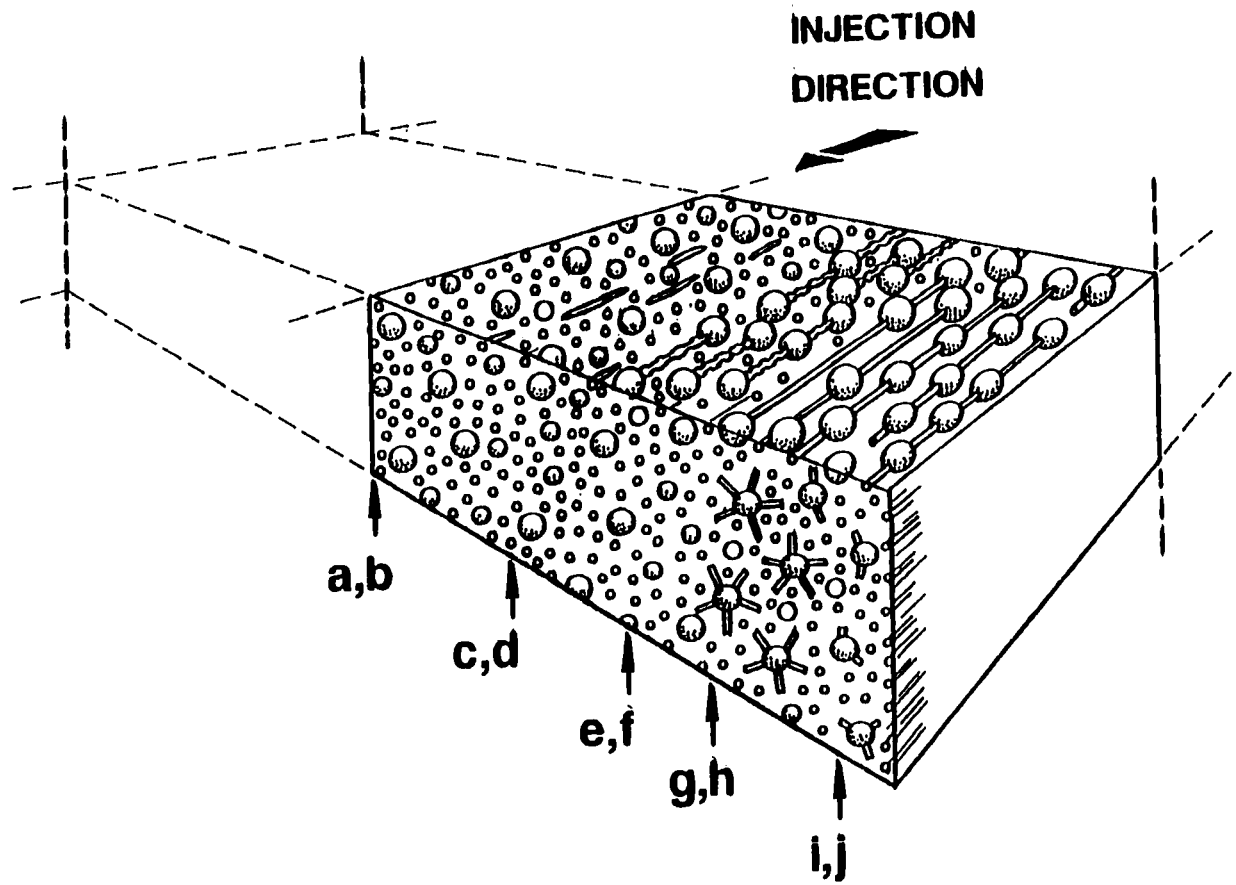


Figure 4. Schematic representation of the morphology of the injection molded PC/ABS 90/10 blend

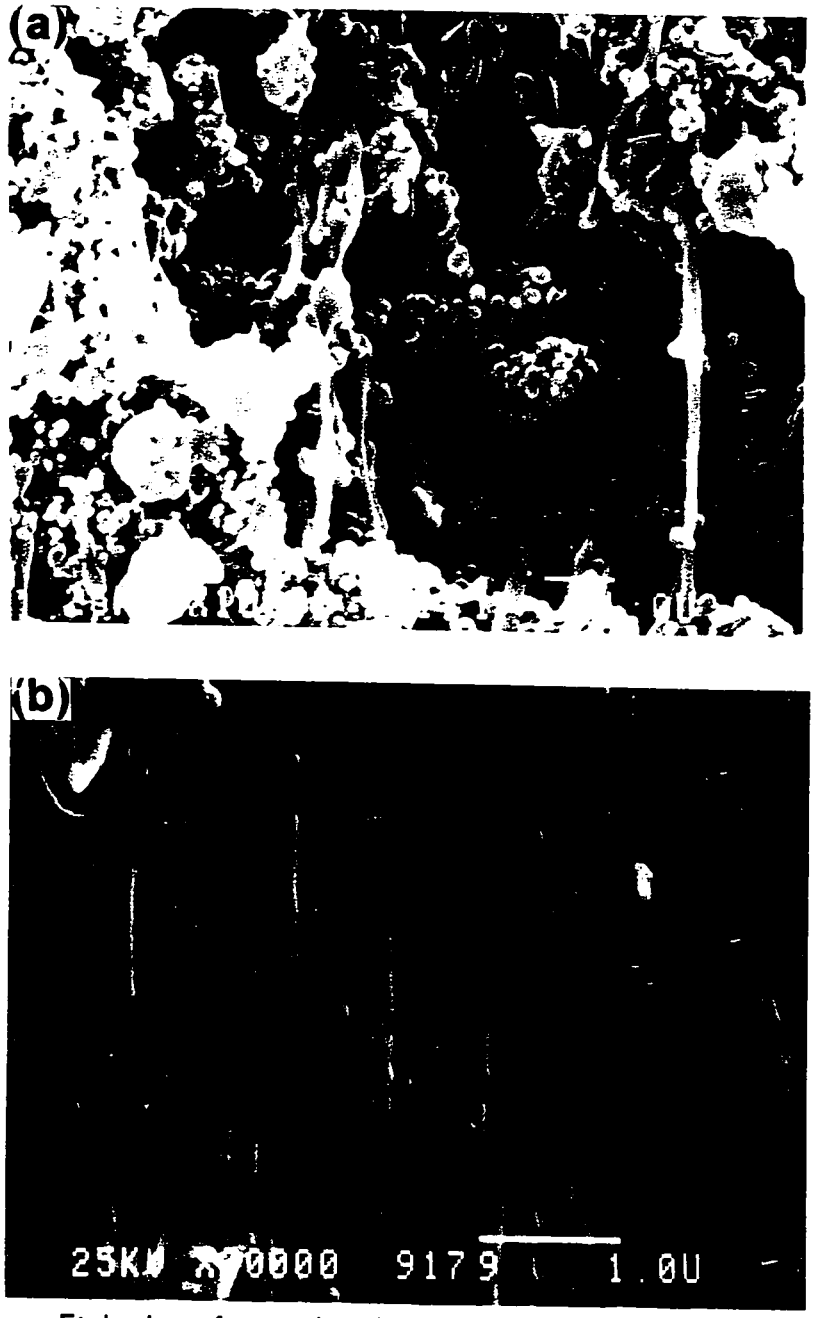


Figure 5. Etched surfaces showing SAN strings in various stages of breakup.(a) parallel to the injection direction 1.05mm from the edge, (b) parallel to the mold-contacting surface at a depth of 0.3mm

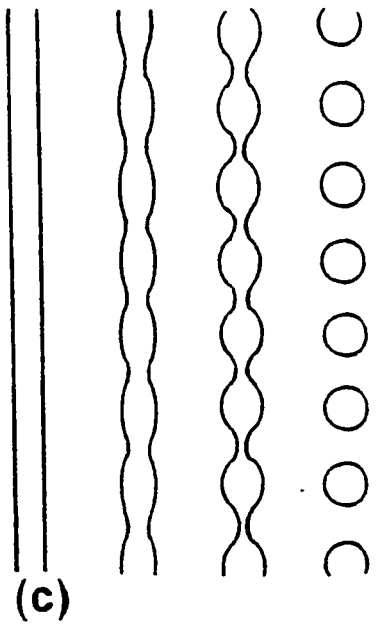


Figure 5. Etched surfaces showing SAN strings in various stages of breakup. (c) schematic representation

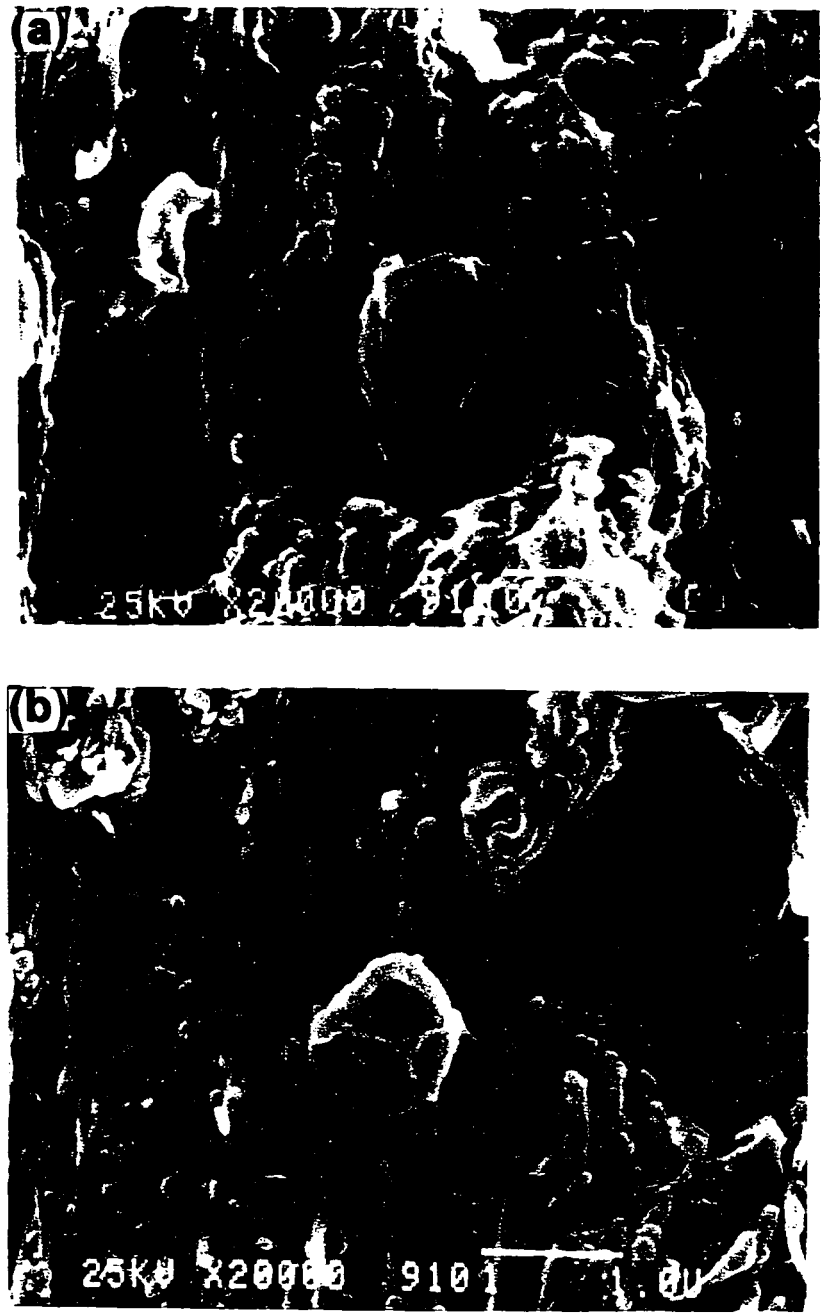


Figure 6. Etched surfaces showing various stages of end-pinching. (a) constriction at the junction of the rubber bead and SAN string, (b) the SAN string separated from the rubber bead

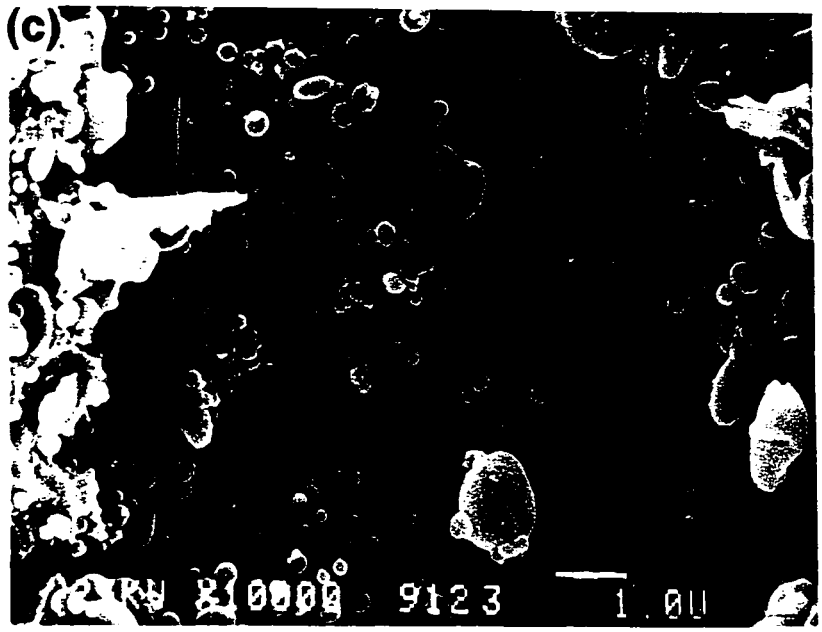


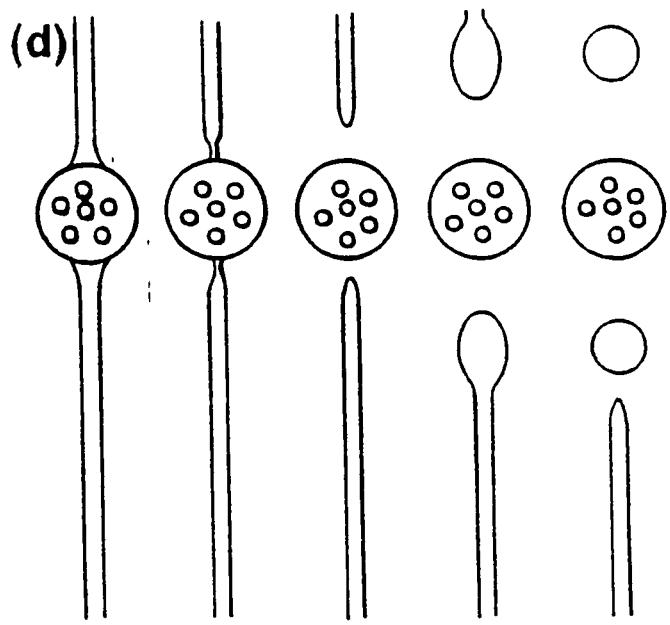


Figure 6. Etched surfaces showing various stages of end-pinching. (c) relaxation of the end of a separated SAN string into a bulbous shape, and (d) schematic representation.

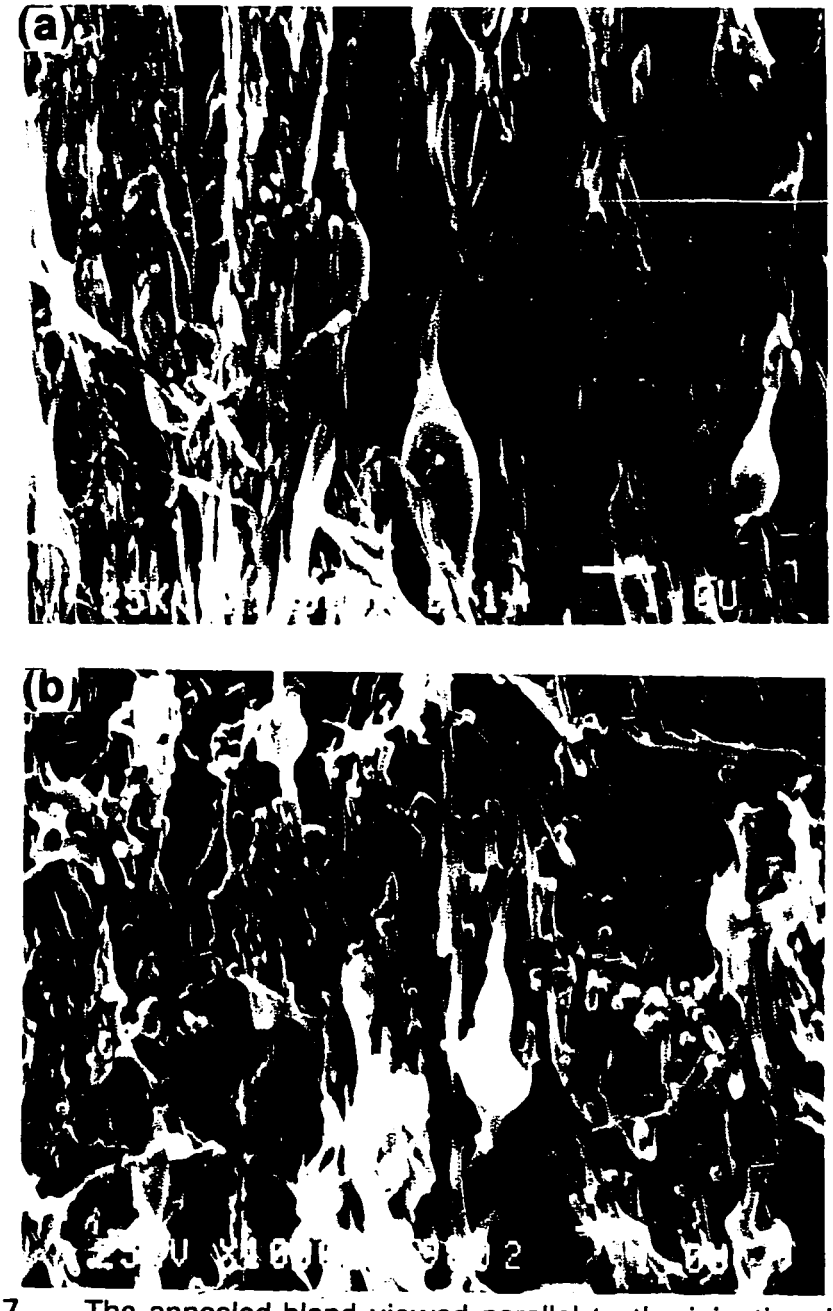


Figure 7. The annealed blend viewed parallel to the injection direction near the edge of the plaque; specimens were annealed for nominally 12sec and etched with aqueous KOH. (a) The unannealed control, (b) annealed at 185°C

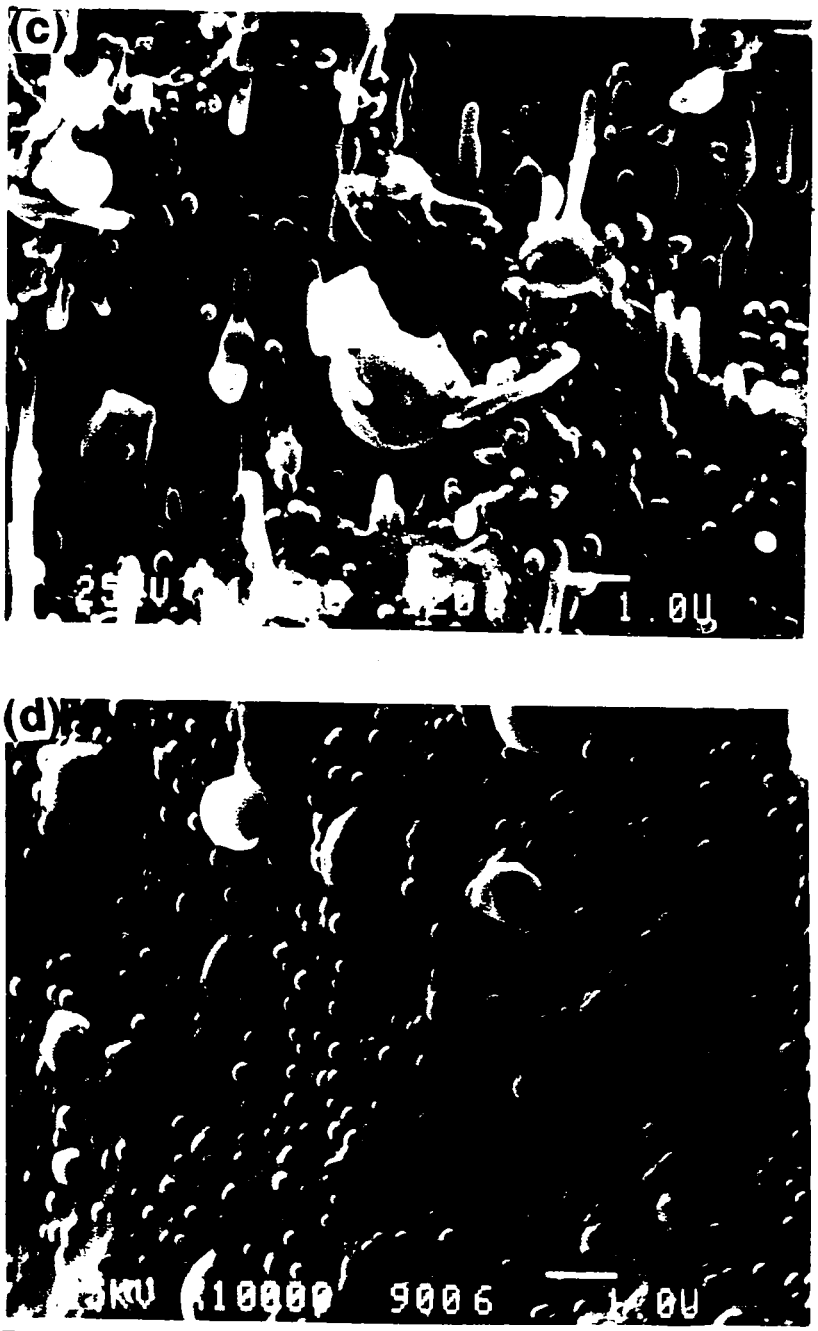


Figure 7. The annealed blend viewed parallel to the injection direction near the edge of the plaque; specimens were annealed for nominally 12sec and etched with aqueous KOH. (c) at 200°C, and (d) at 270°C

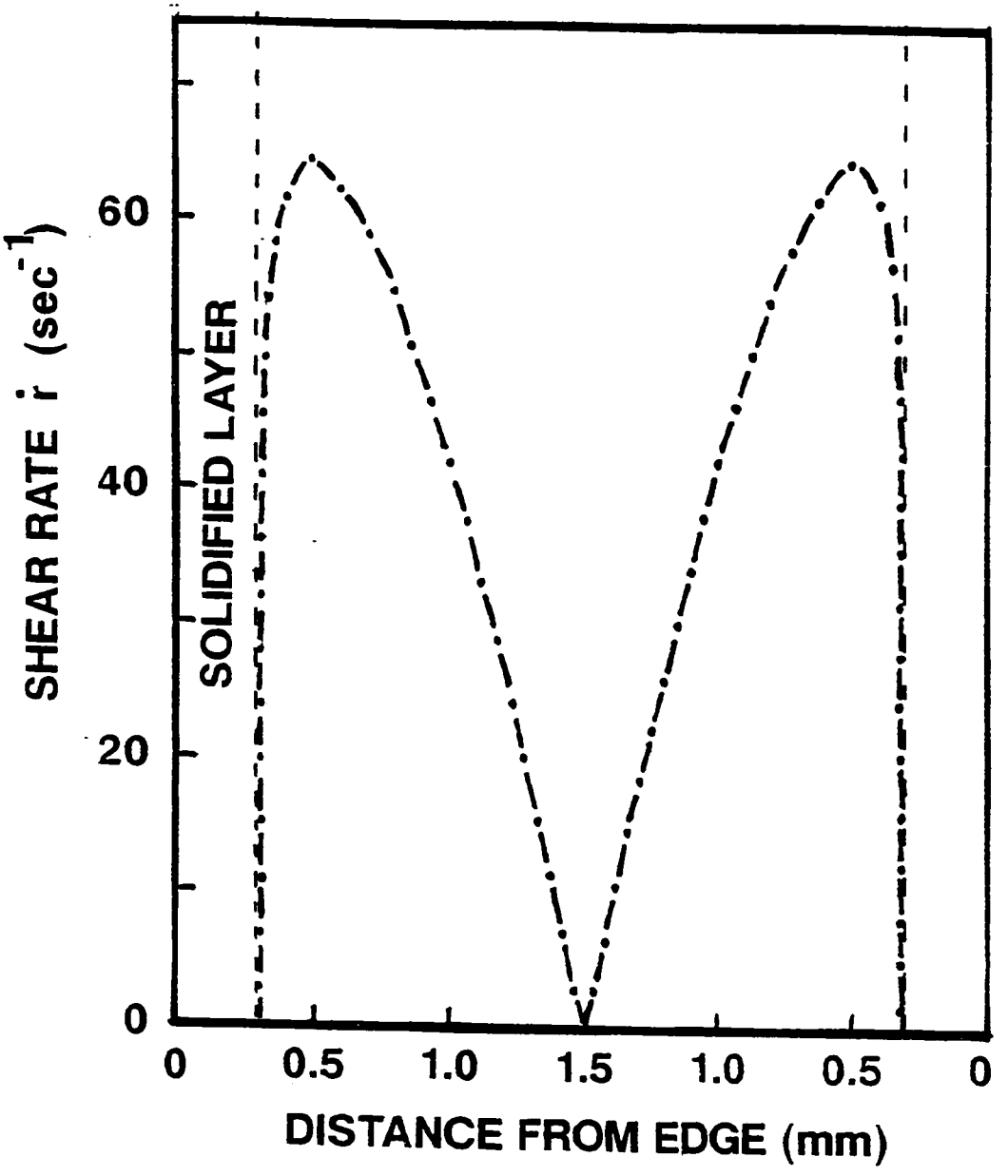


Figure 8. Shear rate profile through the thickness during mold filling, estimated for the PC/ABS 90/10 blend (1).

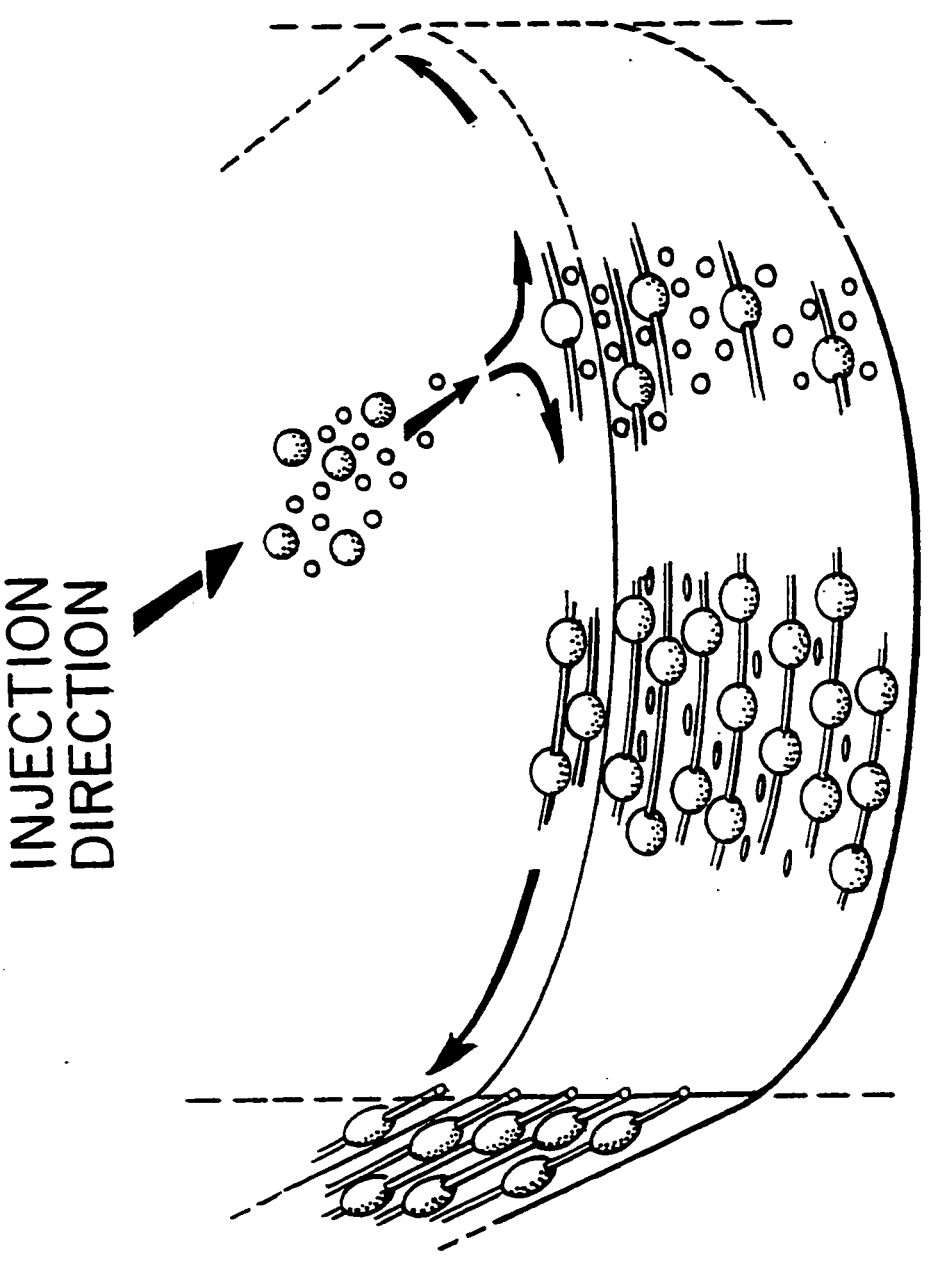


Figure 9. Schematic representation showing the formation of the bead-and-string structure at the melt front.

# CHAPTER 2

## PHASE MORPHOLOGY OF INJECTION MOLDED PC/ABS BLENDS

### 1. INTRODUCTION

Blending to achieve a microheterogeneous mixture of two or more polymers is a well-known method used to improve mechanical, environmental and rheological properties of polymers. Since in these blends the identity of the components is preserved, performance characteristics depend on size and shape of the component phases. The morphology in turn depends on interfacial and rheological properties of the components (1-4), but often to a similar extent on the processing conditions (5-7).

Injection molding is one of the most important processing techniques by which blends are fabricated into plastic parts; the morphological anisotropy characteristic of injection molded blends is primarily the result of orientation of phases along the complex melt flow lines during mold filling, which include the "fountain flow" pattern at the melt front (8). In this case, a very thin region of material at the mold surface experiences elongational flow at the front of the fountain flow pattern and creates an oriented surface skin. Most of the material has a melt morphology determined

initially by shear and elongational flow fields experienced prior to entering the mold followed in the mold filling stage by shear flow behind the front of the fountain flow pattern. The shear rate profile through the thickness can create a gradient in the melt morphology. How much of the melt morphology is retained after cessation of flow depends on the cooling rate which determines the amount of relaxation that occurs before solidification of the melt.

The mode of dispersion also depends on the interfacial properties of the components. In some cases, the interfacial energy between two unmodified polymers is sufficiently low that dispersion does not require a "compatibilizing" agent and can be achieved by simply melt mixing the two polymers (9-12). Polycarbonate (PC) blended with ABS is as example of a system that is compatible in the pratical sence that, when melt blended, the components are well-dispersed with sufficient interfacial adhesion to realize significant property enhancement. In this study, similar injection molding conditions were used to prepare blends of PC and ABS that spanned the entire composition range in increments of 10 weight percent. The morphology of injection molded pieces was characterized and subsequently described with the focus on processing-induced features that related to blend composition.

## 2. EXPERIMENTAL

Blends of ABS and polycarbonate were provided by The Dow Chemical Company in the form of 5in (12.7cm) x 3in (7.6cm) x 1/8in (0.3cm) injection molded plaques. Samples were provided across the entire composition range in 10 wt. percent increments, and the compositions are indicated as the weight percents PC/ABS. The ABS and PC resins were described previously (13). For injection molding, the melt temperature was 270°C for the PC-rich blends and 250°C for the ABS-rich blends, otherwise the molding conditions were the same as described previously (13).

Tensile specimens were cut to the ASTM-1708 geometry either parallel or perpendicular to the injection direction. A single edge notch (SEN) was machined at the midpoint of the gauge length, the notch was 0.037in (0.094cm) in depth with a 0.010in (0.025cm) notch radius and 45° flank angle, The specimens were cut and notched in such a way that the location of the fracture surfaces would correspond to the midpoint of the plaque. The notched tensile specimens were fractured in the Instron at -70°C with a crosshead speed of 229mm/min. The cryogenic fracture surfaces were subsequently selectively etched by immersion in 30% by weight aqueous potassium hydroxide for 2 to 5 hours to remove the PC phase , then washed in water for 2 hours, dried, coated with gold and

examined in the JEM 35CF scanning electron microscope (SEM) (13). Alternatively, some of the etched specimens were stained with a 1 wt. percent aqueous solution of osmium tetroxide at room temperature for 1 week, then coated with gold and examined in a JEOL 840A scanning electron microscope in the backscatter mode. Two of the blends, PC/ABS 50/50 and 30/70, were annealed in the DSC nominally for 12sec at 250°C and then etched. The procedures were the same as described previously (13).

## 3. RESULTS and DISCUSSION

The morphology of PC/ABS blends was examined across the entire composition range. In all cases, the morphology gradient produced by the flow pattern through the thickness of the plaque was characterized. Although the morphology probably also varied to some extent along the length and width of the plaque, this was not examined, and the midpoint of the plaque was chosen as a representative location to compare the morphologies of the various compositions. Brittle fracture surfaces both parallel and perpendicular to the injection direction were etched to remove the PC phase and viewed in the SEM. The micrographs used to illustrate the various morphologies were at the same magnification, 6000x, in order

to emphasize the changes that occurred as the composition was varied.

## 3.1. PC-Rich Compositions

### 3.1.1. PC/ABS 90/10

Near the edge of the PC/ABS 90/10 composition, the ABS phase had the "bead-and-string" structure described previously (13). Rubber particles connected by SAN strings about 0.1 to 0.3$\mu$m in diameter and oriented in the injection direction created ABS bead-and-string domains that were essentially continuous in the injection direction, Figure 1a. Circular cross-sections and protruding ends of fractured SAN strings about 0.2$\mu$m in diameter were seen in the perpendicular fracture surface, Figure 1b. This view also showed star-like arrays with several SAN strings emanating from a rubber particle; these appeared to produce connections between bead-and-string structures. Near the center of the plaque, the morphology appeared the same in both parallel and perpendicular directions. The ABS phase that remained when the PC was etched away consisted of two populations of dispersed spheres, Figure 1c. The larger 1$\mu$m spheres were single rubber particles with grafted SAN, while the free SAN was dispersed as the smaller 0.3$\mu$m spheres. Identification of the small spheres was confirmed when they were selectively removed by etching with acetone, a solvent for SAN,

and the rubber particles were identified with the large spheres when SEM backscatter images showed the large spheres to be selectively stained by $OsO_4$ (13).

The gradient in morphology through the thickness of the PC/ABS 90/10 composition was determined by examining entire etched brittle fracture surfaces in both the parallel and perpendicular directions, and is shown schematically in Figure 1d. In the center, large rubber particles and smaller free SAN particles were randomly dispersed in the PC matrix. Somewhat away from the center, occasional rod-shaped SAN domains elongated in the injection direction appeared; closer to the edge, the SAN domains became longer and thinner and were frequently connected to rubber particles. This oriented bead-and-string structure was the dominant morphology of the ABS phase near the edge.

The gradient in morphology through the thickness was illustrated by determining the number density of SAN spheres on parallel micrographs from various positions. While the absolute numbers are not significant, the relative number density of free SAN particles plotted in Figure 2 shows that there were essentially no spherical particles near the edge, while at about 0.5mm in from the edge the number of free SAN particles began to increase rapidly and continued to increase to the center.

Formation of the bead-and-string structure during injection molding of PC/ABS 90/10 blend was described in a previous publication (13). Briefly, formation of the ABS bead-and-string morphology was thought to occur prior to entering the mold where the melt was subjected to elongational and shear flow, and in the mold where the flow pattern was fountain flow. The crosslinked rubber particles were not very deformable; however, since the viscosity of free SAN was lower than that of PC (13), the free SAN would have been highly extended under elongational or shear flow conditions while miscibility with the grafted SAN would have provided adhesion to the rubber particles. Where the shear or elongational flow stresses were minimal, as during mold filling in the center of the mold behind the fountain flow front, or when mold filling was completed, the highly drawn out SAN strings would have had an opportunity to relax. The extent of relaxation would have depended on the shear rate profile through the thickness of the plaque, which determined the amount of elongation in the melt, and the cooling rate after mold filling, which controlled the amount of melt relaxation before solidification. Close to the mold contacting surface, the melt would have solidified rapidly and the solid state morphology would most closely have resembled the melt morphology. In the center of the plaque the low shear rate during mold filling and longer cooling time after mold filling would have favored relaxation of the bead-and-string morphology. Instead of relaxing to a composite ABS domain,

Rayleigh instabilities, i.e. disturbances in the cross-section of the very long, thin SAN string, caused it to break up into a series of spherical SAN particles. In the center of the plaque, the SAN spheres separated from the rubber particles and possessing a diameter on the same size scale as the diameter of the SAN strings argued for the breakup mechanism in this region.

### 3.1.2. PC/ABS 70/30

The bead-and-string structure was also observed near the edge of the plaque when the blend composition was PC/ABS 70/30. In the view parallel to the injection direction, Figure 3a, the bead-and-string structure was more dense than in the 90/10 composition and although the SAN strings had approximately the same diameter, about 0.2$\mu$m, there appeared to be numerous interconnections between nearby bead-and-string structures. The perpendicular view contained many broken ends of SAN strings, Figure 3b, and additionally, some small areas of coalescence were seen. The interconnections and coalescence of the bead-and-string structure were more apparent in a higher magnification view perpendicular to the injection direction, Figure 3c. The rubber particle in the center of the micrograph had numerous SAN strings attached that interconnected with other SAN stings and nearby rubber particles. Just beside it, a group of SAN strings, seen in

the micrograph as a cluster of broken ends, all appeared to emanate from a coalesced region.

The morphology of the ABS phase in the center of the plaque consisted of dispersed rubber particles and smaller particles of free SAN. Compared to the 90/10 composition, the particles were more numerous, and in addition, some irregularly shaped ABS domains that contained more than one rubber particle were in evidence, Figure 3d. Perpendicular views of the ABS morphology in the center of the plaque were indistinguishable from Figure 3d; PC was clearly the continuous phase in this region of the plaque.

Coalescence of bead-and-string domains near the edge is shown schematically in Figure 3d. While the SAN is represented as being predominantly string-like in this region, as was apparent from the parallel views and the numerous broken ends in the perpendicular micrographs, the schematic drawing shows the initial stage in the formation of sheet-like ABS domains by coalescence and interconnection of bead-and-string structures. The process of coalescence by which a sheet-like morphology evolved from the bead-and-string structures as they became more densely arrayed was most apparent in cross-section, that is, in the perpendicular micrographs. Here, in addition to the ends of individual strings, elongated domains created

by coalescence of several strings were visible. Some coalescence of SAN strings was also apparent in the parallel direction, coalescence in this view showed interconnections which gave the ABS phase a degree of continuity in the thickness direction.

The melt had an opportunity to relax in the center of the mold during cooling. Melt relaxation by the breakup mechanism required long thin SAN strings, and the presence of numerous small 0.25$\mu$m SAN particles in the center region was an indication that despite the interconnections, many SAN strings or segments of strings were long enough to break up by the growth of Rayleigh instabilities. On the other hand, there were also larger composite ABS domains in the center with several rubber particles such as might have formed by the relaxation of an interconnected or partially coalesced bead-and-string structure.

## 3.2. Intermediate Blend Compositions

### 3.2.1. PC/ABS 60/40

The morphology of the PC/ABS 60/40 blend composition, when viewed near the edge parallel to the injection direction, appeared very similar to the 70/30 composition with the ABS phase forming interconnected bead-

and-string structures, Figure 4a. However, perpendicular to the injection direction, a typical view showed only occasional ends of SAN strings, Figure 4b: instead, the morphology of the ABS domains in the perpendicular view was very similar to that in the view parallel to the injection direction. Taken together, the two edge views, Figures 4a and 4b, suggested a stratified, sheet-like ABS morphology that could have formed by lateral coalescence of the interconnected ABS bead-and-string domains. The formation of such a sheet-like domain by coalescence of numerous SAN strings was seen end-on in a higher magnification perpendicular view, Figure 4c.

In the center, the PC phase of the 60/40 composition was continuous with numerous dispersed rubber particles and free SAN spheres, Figure 4d; however, in addition, large irregularly shaped ABS domains were also present. These were highly branched and somewhat more extended in the injection direction than through the thickness. They created regions in which the ABS phase was co-continuous with PC. The morphology of the PC/ABS 60/40 blend as shown schematically in Figure 4e was significantly different from that of the 70/30 blend both near the edge, where the morphology of the 60/40 blend was clearly stratified rather than predominantly the linear bead-and-string structure, and in the center, where there were regions of co-continuity of the phases in the 60/40 blend while the ABS phase clearly formed only inclusions in the 70/30 composition.

### 3.2.2. PC/ABS 50/50

The morphology of the 50/50 composition was examined in some detail as being representative of the intermediate composition range, 60/40 to 40/60. Etched brittle fracture surfaces of the PC/ABS 50/50 composition at four positions, Figure 5, illustrate the gradient in morphology through the thickness both parallel and perpendicular to the injection direction. Close to the edge, a view of the morphology parallel to the injection direction, Figure 5a, showed coalesced sheet-like ABS domains extended in the injection direction. Only occasionally could an isolated segment of the bead-and-string structure be found in the parallel micrographs.

Perpendicular to the flow, only a few broken ends of SAN strings were visible, Figure 5b; these had the same diameter, about 0.2$\mu$m , as strings in the bead-and-string structure of the 90/10 composition. The predominant feature of the ABS phase in the perpendicular view was the elongated domain morphology that caused the perpendicular view to closely resemble the parallel view in appearance, and revealed that the ABS domain morphology was sheet-like near the edge. Upon careful examination, the ABS domains appeared more coalesced in the parallel view while in the perpendicular view evidence remained of the bead-and-string structure. In particular, many of the ABS domains had numerous strings attached. This

suggested that during flow the bead-and-string structures became stratified and the interconnected SAN strings coalesced laterally to create the elongated appearance in the perpendicular direction. The PC domains were identified by the elongated holes that separated the ABS domains in both the parallel and perpendicular directions. Although the holes were somewhat more elongated in the perpendicular view, the PC phase also took on a sheet-like morphology near the edge of the plaque.

About 0.84mm inward from the edge, the ABS domains lost some of the sheet-like appearance, Figure 5c, especially in the perpendicular view, Figure 5d, and the holes that identified the PC domains were less extended in the injection direction. These were changes that might have occurred if the sheet morphology had just begun to relax before solidification; there was still evidence that this morphology derived from the bead-and-string structure, for example the occasional broken ends of SAN strings in the perpendicular view.

The morphology changed considerably at a depth of 1.27mm, Figure 5e and 5f. The thin SAN strings observed near the edge were absent, and the stratified morphology was replaced by a thicker, interconnected ABS domain morphology that was continuous. The PC phase may also have been continuous. The micrographs showed irregular elongated holes as well

as circular holes created when the PC was etched away. While these holes could have indicated discrete domains, they could also have been connected to create a continuous interpenetrating PC phase. Parallel and perpendicular views were similar. In lower magnification views it was apparent that both parallel and perpendicular to the injection direction the PC and ABS domains were more extended in the plane of the plaque than in the thickness direction.

Further changes in the morphology from a depth of 1.27mm, Figure 5e and 5f, to the center, 5g and 5h, were only slight. Both ABS and PC domains were somewhat thicker in the center and directionality of the morphology was less apparent. Both parallel and perpendicular views near the center showed numerous small SAN spheres remaining in the holes where the PC was etched out. These spheres were the same size, about 0.2$\mu$m in diameter, as the SAN spheres observed in the PC-rich blends.

One approach to quantifying the coarseness of a phase morphology uses the Chalkley method to estimate the volume to surface ratio from micrographs (14, 15). A line of length l is placed randomly on an SEM micrograph and the number of hits, $N_h$, defined as the number of times th end fell inside the phase of interest, in this case a PC domain, and the number of cuts, $N_c$, the number of times the line crossed an interface, are

determined. The Chalkley parameter C then gives the ratio of volume to surface according to

$$C = l N_c / 4N_c$$

and the reciprocal Chalkley parameter $C^{-1}$ is an estimation of the average surface per unit volume. The reciprocal Chalkley parameter for the PC phase was determined from the parallel views of the morphology at various locations through the thickness with $l = 10\mu m$, and when plotted as a function of location, Figure 6, clearly revealed the change in morphology through the thickness. The reciprocal Chalkley parameter was largest the edge where the thin sheet-like domains created a large surface to volume ratio. It decreased from a value of 11 at the edge to 2.5 in the center with the most of the decrease occurring about midway to the center at the position where the change form thin sheet-like domains to thicker interconnected ABS domains with a lower surface to volume ratio was noted in the micrographs.

A schematic model of the gradient morphology through the thickness of the PC/ABS 50/50 blend was developed, Figure 7. The stratified, sheet-like morphology observed close to the mold surface where solidification would have occurred most rapidly was thought to most closely represent

the morphology in the flowing melt. The phase-separation of ABS itself gave an additional aspect of complexity to the morphology of the ABS phase in blends with PC. Taking the basic morphology of the ABS phase during melt flow to be the bead-and-string structure, the sheet-like morphology of the 50/50 blend was viewed as the result of increasing interconnection, coalescence and stratification of the bead-and-string structure as the blend composition became richer in ABS. While the melt morphology was preserved to an extent by rapid cooling near the edge, considerable relaxation occurred in approximately the center half of the thickness. Two mechanisms for relaxation of the ABS phase appeared to create the morphology in the center region of the 50/50 blend composition. In PC-rich regions of the melt where the bead-and-string was not highly interconnected, break-up of long thin SAN strings created the 0.3$\mu$m SAN particles that were observed only at the two positions closest to the center. However in regions where the bead-and-string structure was more coalesced, recovery into thick ABS domains would have been favored. The thick continuous or semi-continuous ABS domains first appeared in the center of the plaque when the ABS morphology at the edge was predominantly interconnected and stratified.

Previously, it was demonstrated that relaxation of the bead-and-string structure created the small SAN spheres by the Rayleigh instability

mechanism when intermediated stages of breakup were observed after the bead-and-string structure was annealed for short periods of time in the DSC.(13) Relaxation of the interconnected, stratified ABS morphology was examined in the same way. After the initial interconnected, stratified morphology near the edge, Figure 8a, was heated to 250°C for only about 12 sec, the stratification was much less apparent, Figure 8b, while the ABS domains had become thicker and appeared to be sufficiently interconnected that the ABS phase was continuous. Occasionally, thin SAN strings in various stages of breakup could also be seen in the micrographs of the annealed blend (arrows in Figure 8b), attesting to the role of both relaxation mechanisms in creating the morphology in the center region of the intermediate blend compositions.

### 3.2.3. PC/ABS 40/60

Near the edge of the 40/60 composition the interconnected ABS bead-and-string structures were densely arrayed and interspersed with elongated PC domains, Figure 9a. Viewed in the parallel direction near the edge, the only noticeable change through the intermediate composition range, PC/ABS 60/40 to 40/60, was progressively more coalescence of the ABS bead-and-string structure. Particularly in the perpendicular view, Figure 9b, there was evidence that a network of SAN strings had coalesced to

create the stratified morphology, but overall the views parallel and perpendicular to the injection direction were very similar. The similarity in the parallel and perpendicular views near the edge, and the stratified, sheet-like morphology these revealed, were distinguishing features that differentiated the intermediate blend compositions from the PC-rich compositions.

In the center of the plaque the ABS phase was continuous, Figure 9c. The morphology appeared the same in both parallel and perpendicular directions with irregularly shaped PC domains identified by the holes. In this view the PC phase did not appear to be co-continuous with the ABS although in places the PC domains were interconnected over short distances. Most of the holes left when the PC was etched away contained spherical SAN particles about 0.2$\mu$m in diameter. The presence of SAN inclusions in the PC domains probably resulted from the breakup of isolated SAN strings in PC-rich regions of the melt, although it has also been suggested that composite domains can exist in the flowing melt (16). The morphology of the PC/ABS 40/60 blend is shown schematically in Figure 9d. The continuous or semi-continuous nature of the ABS phase in the center was thought to result from relaxation of the stratified morphology in the melt and was a distinguishing feature of the intermediate composition range.

## 3.3. ABS-Rich Blend Compositions

### 3.3.1. PC/ABS 30/70

The holes near the edge of etched brittle fracture surfaces of the PC/ABS 30/70 composition revealed PC domains about 1$\mu$m in diameter and elongated in the injection direction, Figure 10a. Perpendicular to the injection direction, Figure 10b, the holes were circular with a diameter corresponding to the width of the elongated holes in the parallel view. Sometimes, especially close to the edge, the holes in the perpendicular view were somewhat elongated suggesting that the PC domains were sheet-like as well as rod-shaped in this region. In the center, Figure 10c, the morphology was isotropic with spherical holes about 1$\mu$m or less in diameter. The schematic model of the phase morphology, Figure 10d, showed the more-or-less isotropic morphology in the center with spherical PC domains 1$\mu$m and less in diameter dispersed in the ABS matrix, while toward the edge the PC domains became elongated in the injection direction and took on a rod or sheet-like shape.

The length to width ratio of the PC domains, Figure 11, showed the change in shape through the thickness. The gradient in aspect ratio depended on the flow profile through the thickness, which determined the

amount of elongation in the melt, and the cooling rate after mold filling, which controlled the amount of melt relaxation. Since the melt viscosity of PC was greater than that of free SAN (13), the PC domains were not as highly extended in the melt as the SAN was when ABS was the dispersed phase. Specifically the PC domains were not so highly extended that they would have become unstable and broken up during relaxation as the SAN did. Instead, when elongational or shear flow ceased, the elongated PC domains would have relaxed to a spherical shape(17). This was confirmed when the elongated domain morphology near the edge, Figure 12a, was replaced by a dispersion of spherical PC domain after the blend was annealed for nominally 12sec at 250°C, Figure 12b.

### 3.3.2. PC/ABS 10/90

The morphology of the PC/ABS 10/90 composition was similar to that of the 30/70 composition except that the elongated PC domains near the edge were shorter and thinner, Figure 13a, and the spherical domains in the center were smaller, Figure 13b. The ABS-rich blends presented a conventional situation with regard to blend morphology. The decrease in domain size with deceasing concentration of the dispersed component, in this case the spherical PC domains in the center decreased from an average diameter of 0.4$\mu$m in PC/ABS 30/70 to 0.15$\mu$m in 10/90, has been well

documented(18).

## 3.4. Effects of Composition

A common feature of the injection molded plaques of all the PC/ABS blend compositions was the identification from the morphology gradient through the thickness of two fairly distinct zones. An edge zone extended approximately half the distance to the center; here the morphology was strongly influenced by flow conditions during mold filling with domain morphologies that were highly extended in the injection direction. A second zone that comprised the center half of the thickness showed minimal effects of mold filling flow, here the domain morphology possessed little or no directional variation and had an overall appearance that has been described in the literature as relaxed or coarsened. Because the morphologies of 7 blend compositions spanning the entire composition range were characterized in some detail, it was possible to identify qualitatively systematic effects of composition on morphology of the edge and center zones.

When the edge views parallel to the injection direction were compared across the composition range ( Figures 1a, 3a, 4a, 5a, 9a, 10a and 13a) the domains were highly elongated in the injection direction and changed

gradually as the blend became richer in ABS from isolated ABS bead-and-string structures with some interconnections in PC/ABS 90/10 (Figure 1a) to stratified, coalesced bead-and-string domains of the PC/ABS 50/50 composition (Figure 5a) to finally elongated PC domains in a completely coalesced ABS phase, PC/ABS 10/90 (Figure 13a). The views perpendicular to the injection direction were more revealing of the morphological changes that occurred in the edge zone with composition (Figure 1b, 3b, 4b, 5b, 9b, 10b and 13b). In the PC-rich blends, PC/ABS 90/10 and 70/30, free SAN was dispersed primarily as strings connecting rubber particles. This was inferred from the preponderance of circular cross-sections and broken ends of SAN strings in the perpendicular views of these compositions, only small areas where SAN strings had coalesced were observed. Coalescence of SAN strings into domains that persisted for large distances in the perpendicular view, with few cross-sections of SAN strings visible, was a major difference between the morphologies of the 70/30 and 60/40 compositions. AS the blend was made increasingly rich in ABS, the coalesced, stratified ABS domains in the perpendicular view gradually thickened until ABS became the continuous phase in the ABS-rich blends.

The melt morphology during mold filling was only stable in flow, and the extent to which it was preserved near the edge was due to rapid cooling and solidification in this region of the mold. In the center, considerable

relaxation occurred either because of the slower cooling rate in this region and/or because the melt morphology in this region was subjected to lower shear stresses during mold filling. It has been seen that the bead-and-string structure relaxed by growth of Rayleigh instabilities to a dispersion of individual rubber particles and SAN spheres. This was the primary relaxation mechanism in PC-rich blends and created a morphology in the center where PC was the continuous phase. The bread-up mechanism required long thin SAN strings. Even in the intermediate composition range, breakup of occasional SAN strings in PC-rich regions of the melt was probably the reason the PC domains in the center contained some dispersed SAN spheres.

A second relaxation mode occurred when the stratified ABS morphology replaced the interconnected bead-and-string structure near the edge. When the bead-and-string structure coalesced and became stratified in the melt, relaxation into thick ABS domains replaced the break-up mechanism. Accordingly, the appearance of thick semi-continuous or continuous ABS domains in place of dispersed rubber and SAN particles in the center coincided with the appearance of a stratified morphology near the edge, as revealed by the perpendicular edge views. This transition occurred at a blend composition of PC/ABS 60/40, and the second mode of relaxation predominated in all the intermediate compositions where the

stratified, sheet-like ABS morphology was observed near the edge.

When the blend became richer in ABS, PC/ABS 30/70 and 10/90, dispersed PC domains were not so highly extended that they would have become unstable and broken up as the ABS bead-and-string structure did in the PC-rich blends. Consequently, only relaxation of extended PC domains was observed in the ABS-rich blends, and the morphology in the center showed a gradual change from co-continuous ABS and PC phases to continuous ABS phase with dispersed PC as the composition changed from PC/ABS 50/50 to 10/90.

## 4. CONCLUSIONS

The morphology gradient of PC/ABS blends in injection molded plaques was characterized over the entire composition range. Examination of etched brittle fracture surfaces in the SEM through the thickness of the plaques led to the identification of three composition ranges based on the morphological features.

1. The PC-rich blends consisted of the composition range PC/ABS 90/10 to 70/30. The ABS phase formed bead-and-string structures near the

edge of the plaque that were essentially continuous in the injection direction; with increasing ABS content, the bead-and-string structures became more densely arrayed and more interconnected. In the center, PC was the continuous phase with ABS dispersed as individual rubber particles about 1$\mu$m in diameter and smaller 0.3$\mu$m particles of free SAN. When the ABS content was in the higher end of the range, some consolidated ABS domains were also observed.

2. There was a transition in the morphology between the PC/ABS 70/30 and 60/40 compositions. Intermediate compositions, 60/40 to 40/60, were characterized near the edge by an interconnected, coalesced ABS bead-and-string structure that with the PC phase formed a stratified sheet-like morphology. In the center, the ABS phase appeared to be continuous. The PC phase was thought to be co-continuous in the 60/40 composition, but formed a dispersed phase with SAN inclusions in the 40/60 composition.

3. The ABS-rich blends in the composition range PC/ABS 30/70 to 10/90 had a very conventional blend morphology with PC domains dispersed in the continuous ABS phase. The PC domains were elongated in the injection direction near the edge and were spherical in the center of

the plaque. The PC domains became smaller as the fraction of PC in the blend decreased.

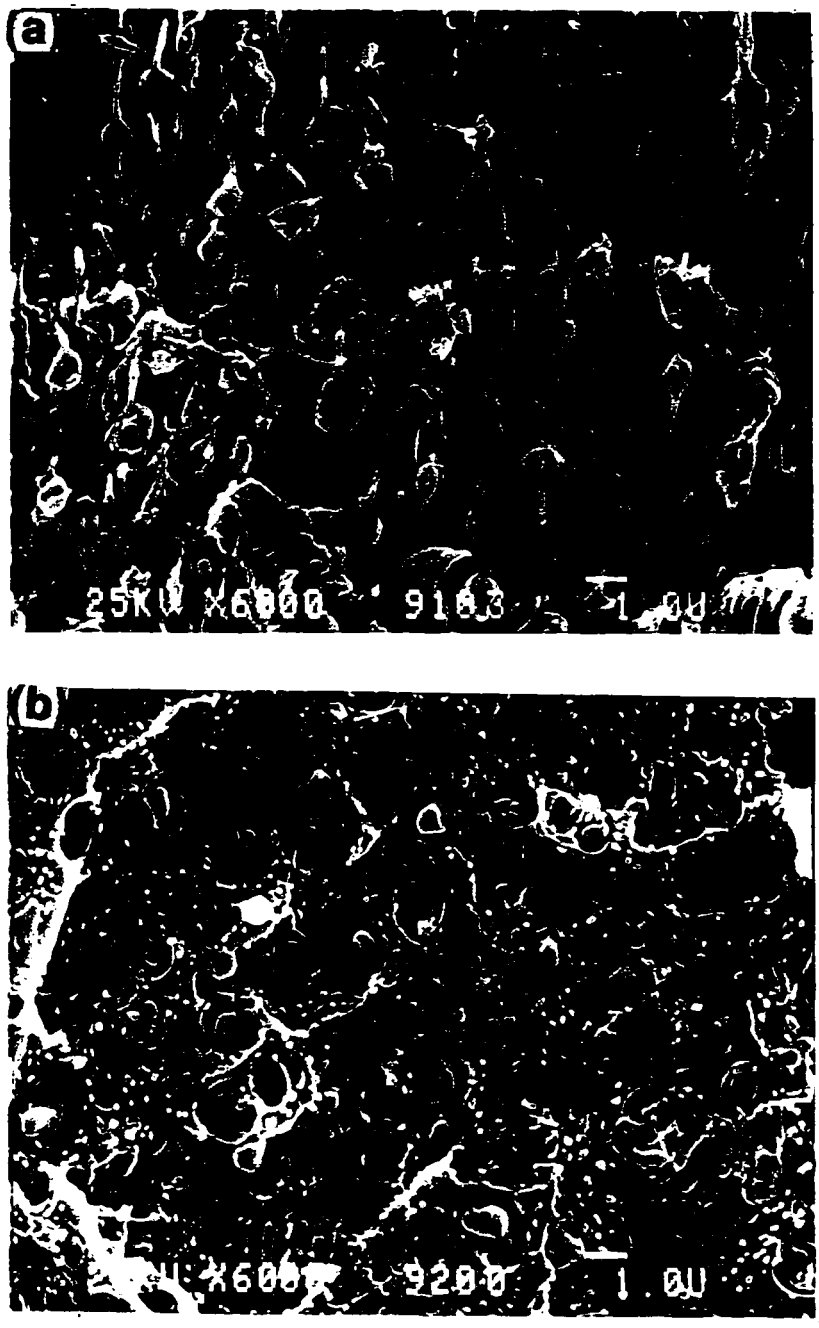


Figure 1. Scanning electron micrographs of injection molded PC/ABS 90/10 blend near the edge. (a) parallel to the injection direction d = 0.13mm (b) perpendicular to the injection direction, d = 0.13mm. d:distance from the edge of the 3mm thick plaque

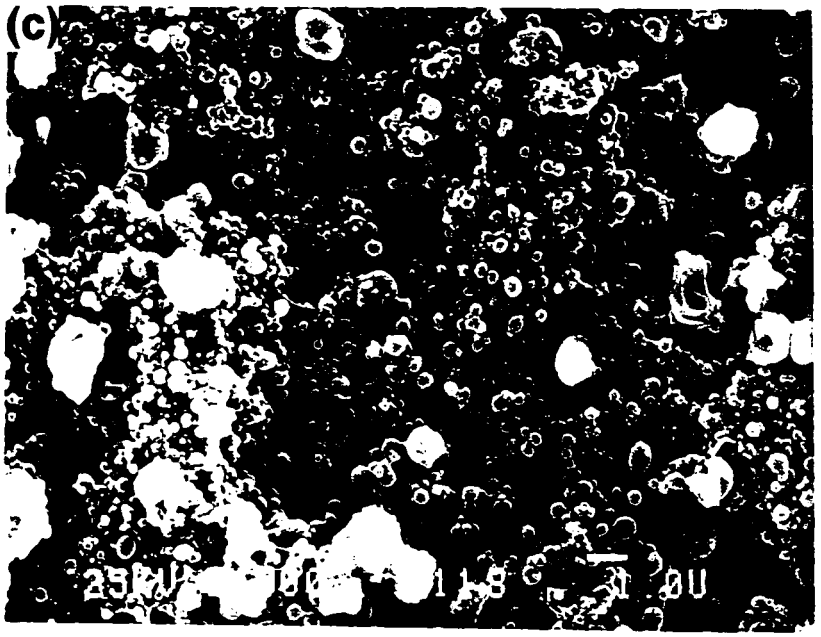


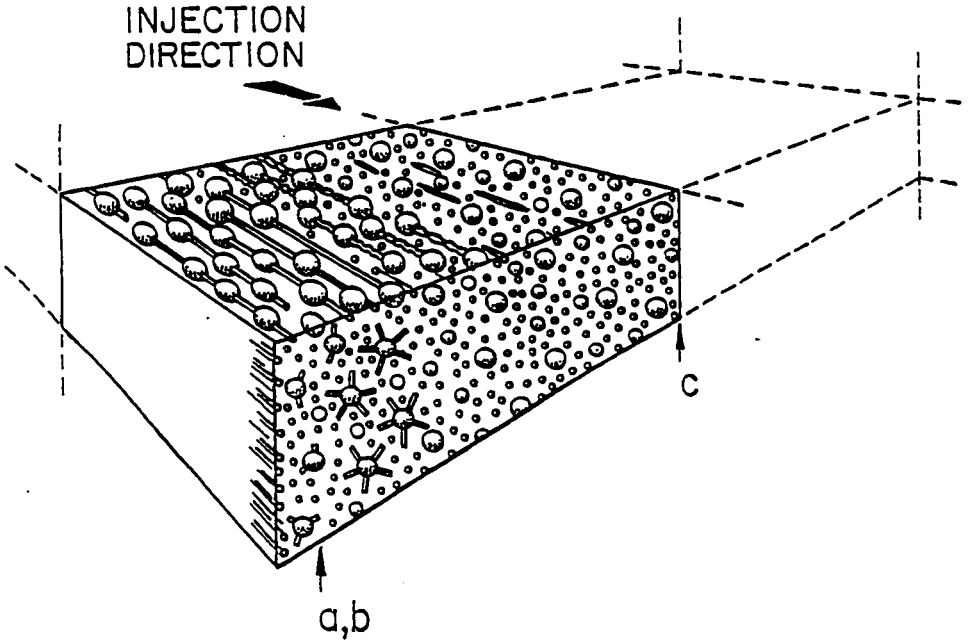


Figure 1. Scanning electron micrographs of injection molded PC/ABS 90/10 blend. (c) parallel to the injection direction at the center; and (d) schematic representation of the morphology through the thickness.

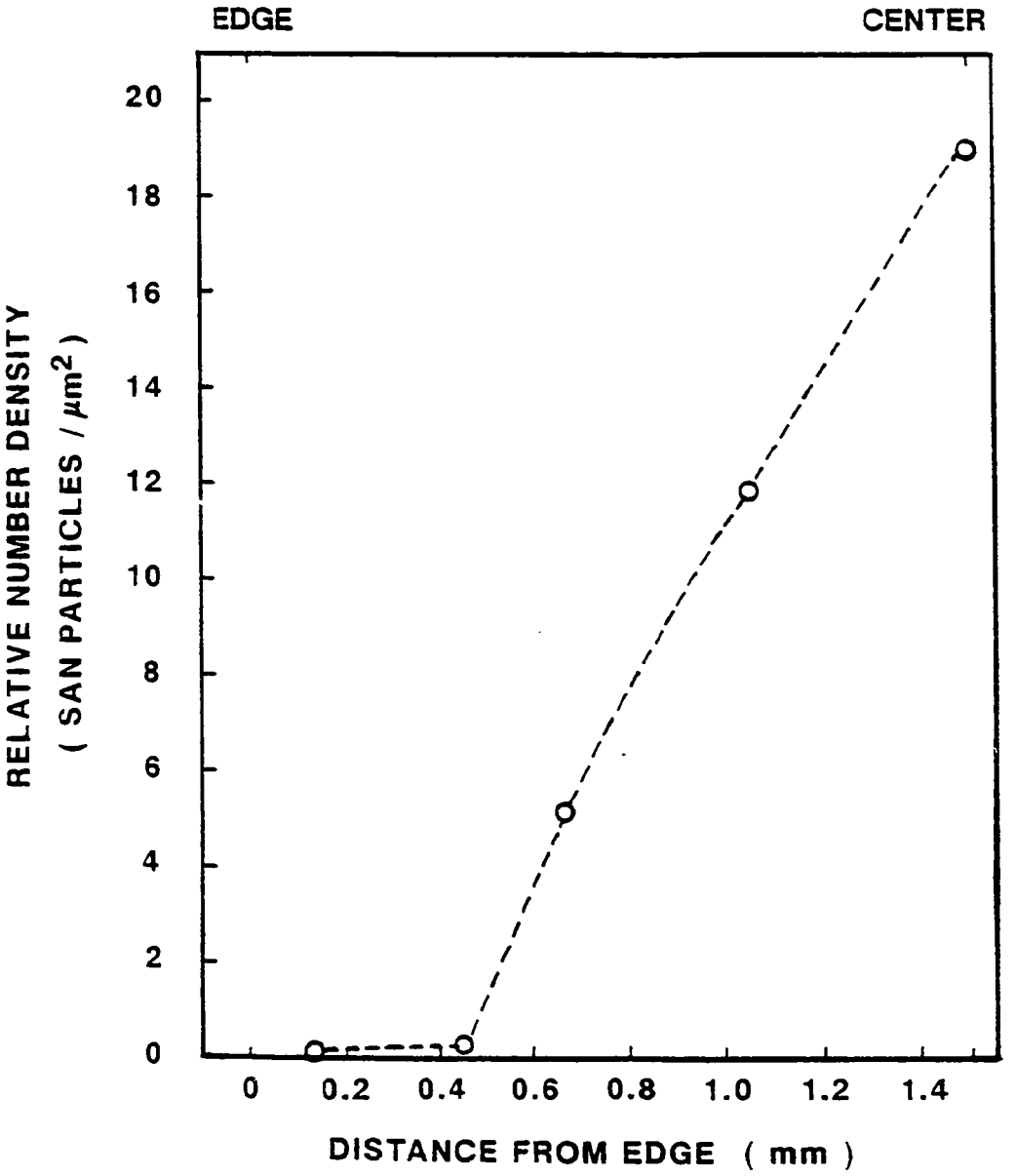


Figure 2. The relative number density of SAN particles on micrographs of a PC/ABS 90/10 parallel fracture surface at various positions through the thickness.

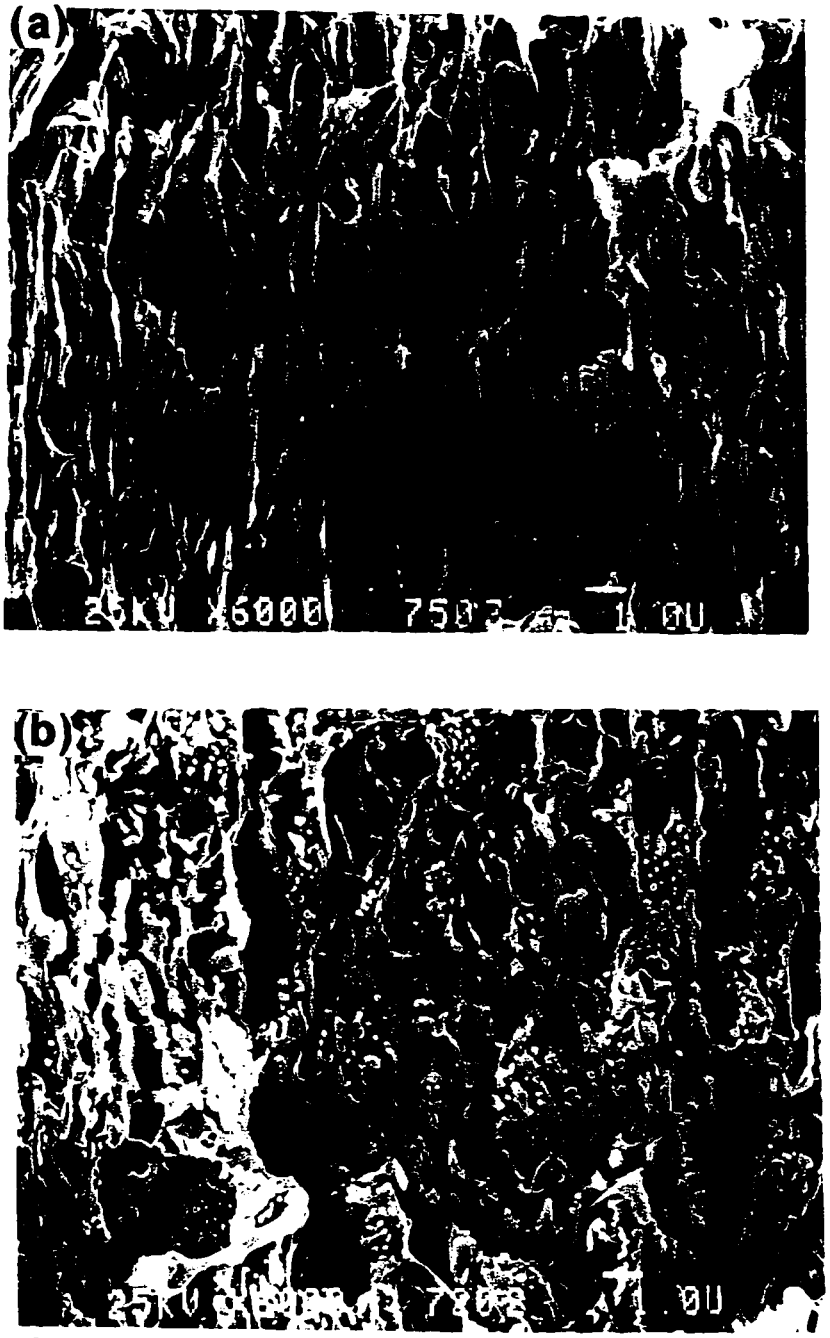


Figure 3. Scanning electron micrographs of injection molded PC/ABS 70/30 blend near the edge.(a) parallel to the injection direction, d=0.18mm (b) perpendicular to the injection direction, d=0.22mm. d:distance from the edge of the 3mm thick plaque

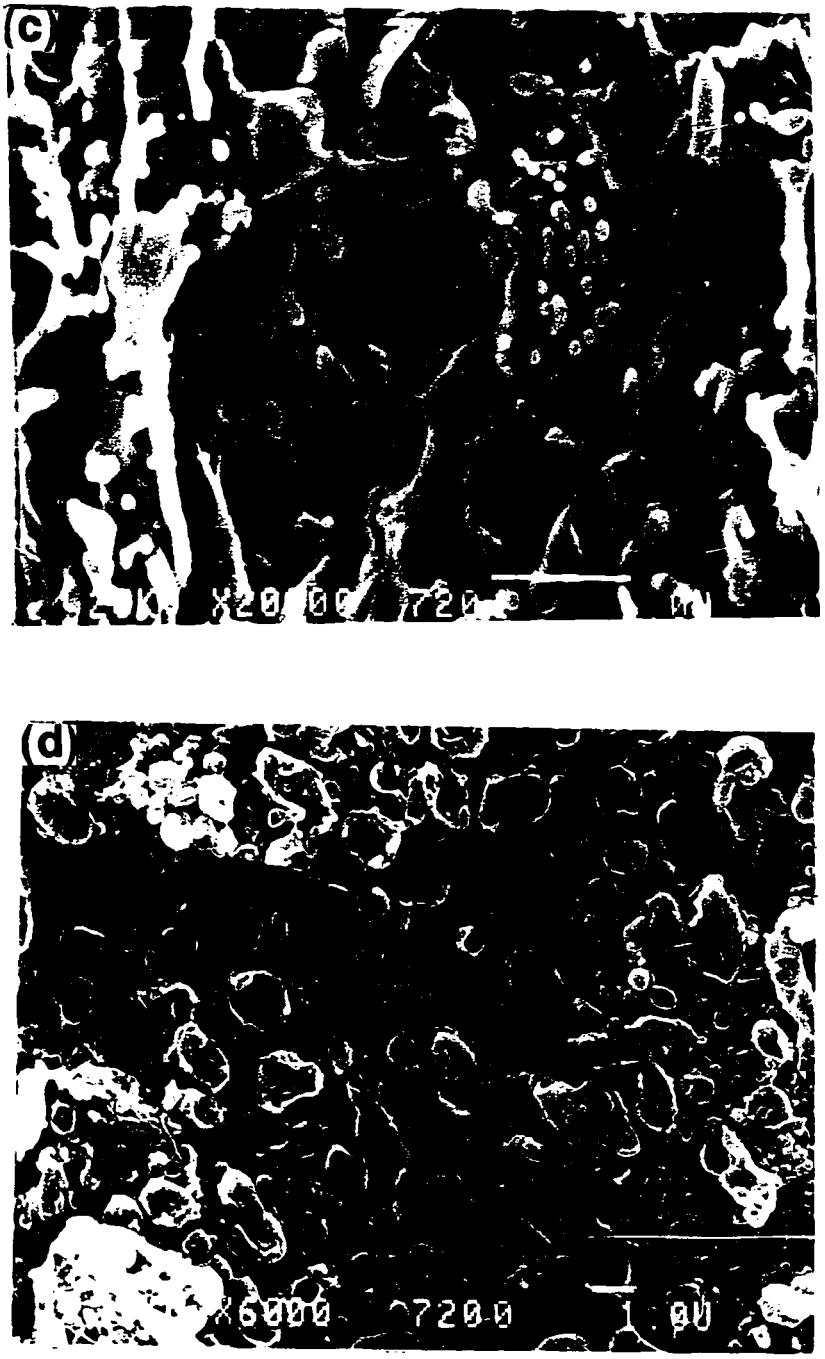


Figure 3. Scanning electron micrographs of injection molded PC/ABS 70/30 blend. (c) a higher magnification of (b), (d) parallel to the injection at the center

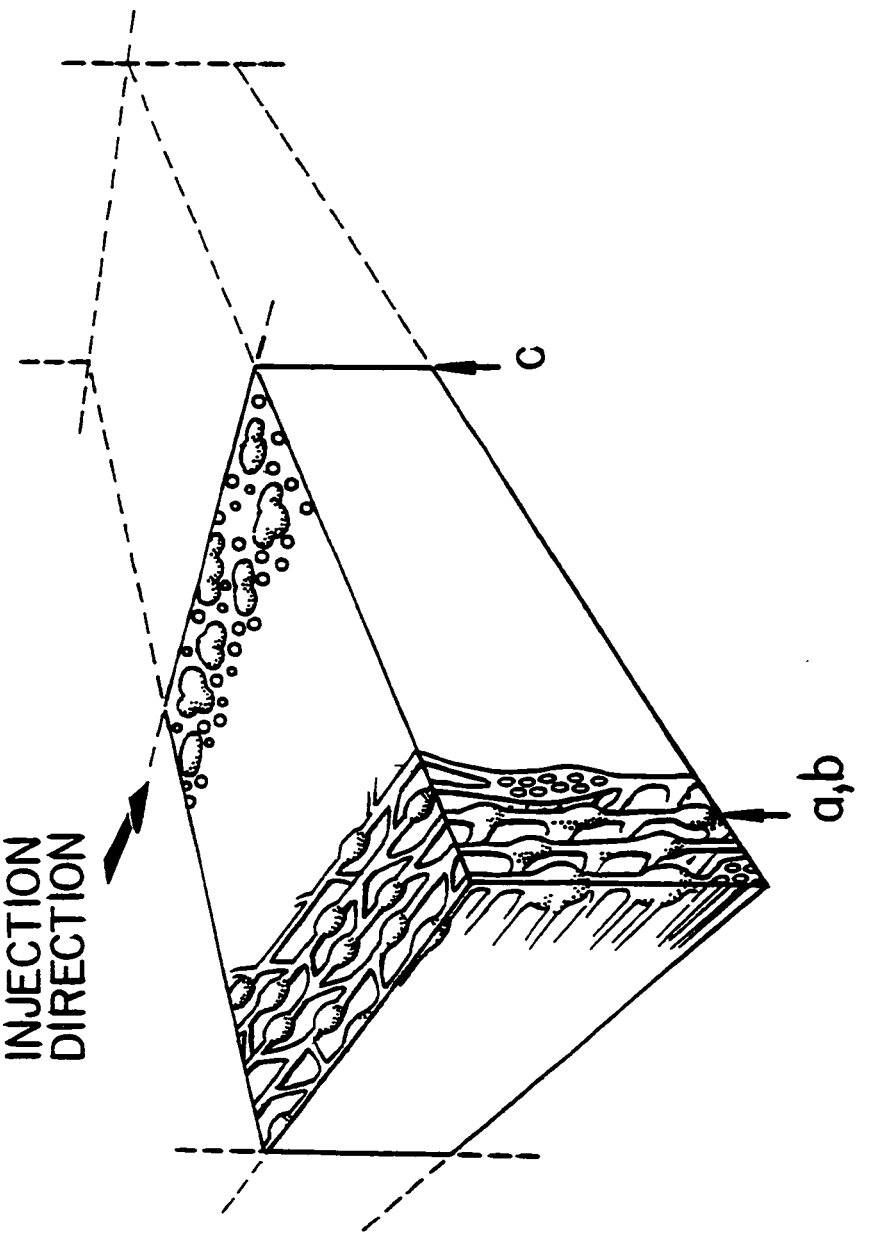


Figure 3. (e) Schematic representation of the morphology through the thickness

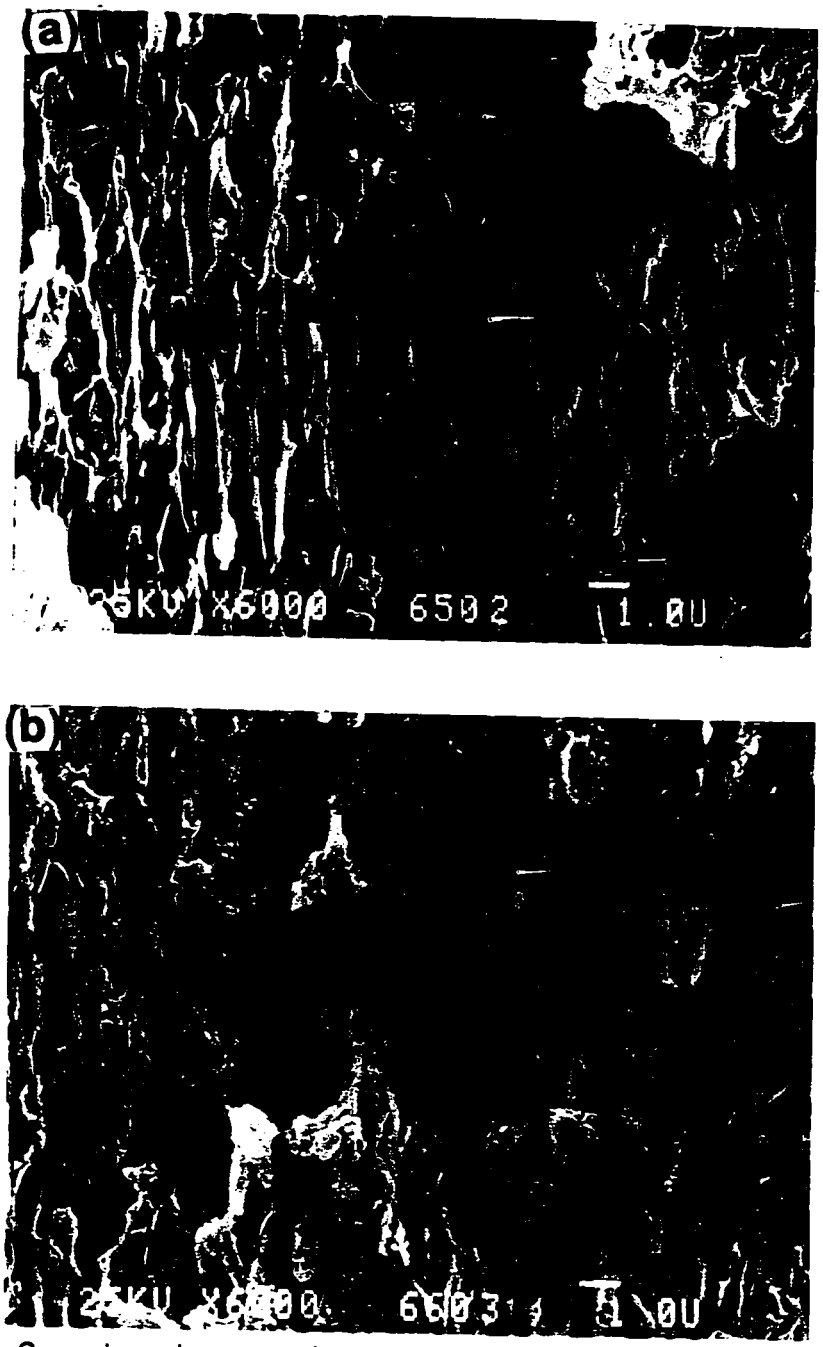


Figure 4. Scanning electron micrographs of injection molded PC/ABS 60/40 blend near the edge (a) parallel to the injection direction, d = 0.19mm (b) perpendicular to the injection direction, d = 0.21mm. d : distance from the edge

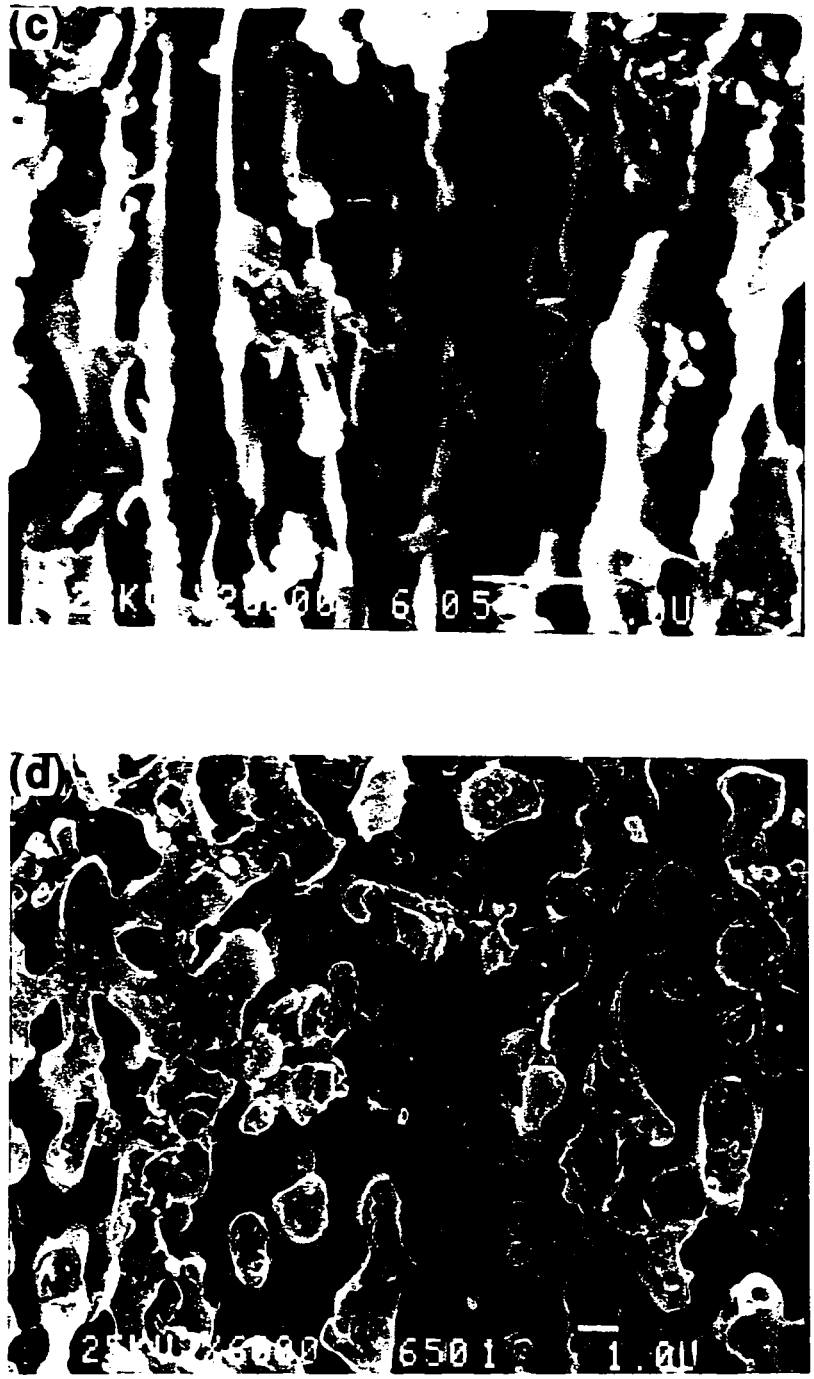


Figure 4. Scanning electron micrographs of injection molded PC/ABS 60/40 blend (c) a higher magnification of (b); (d) parallel to the injection direction at the center

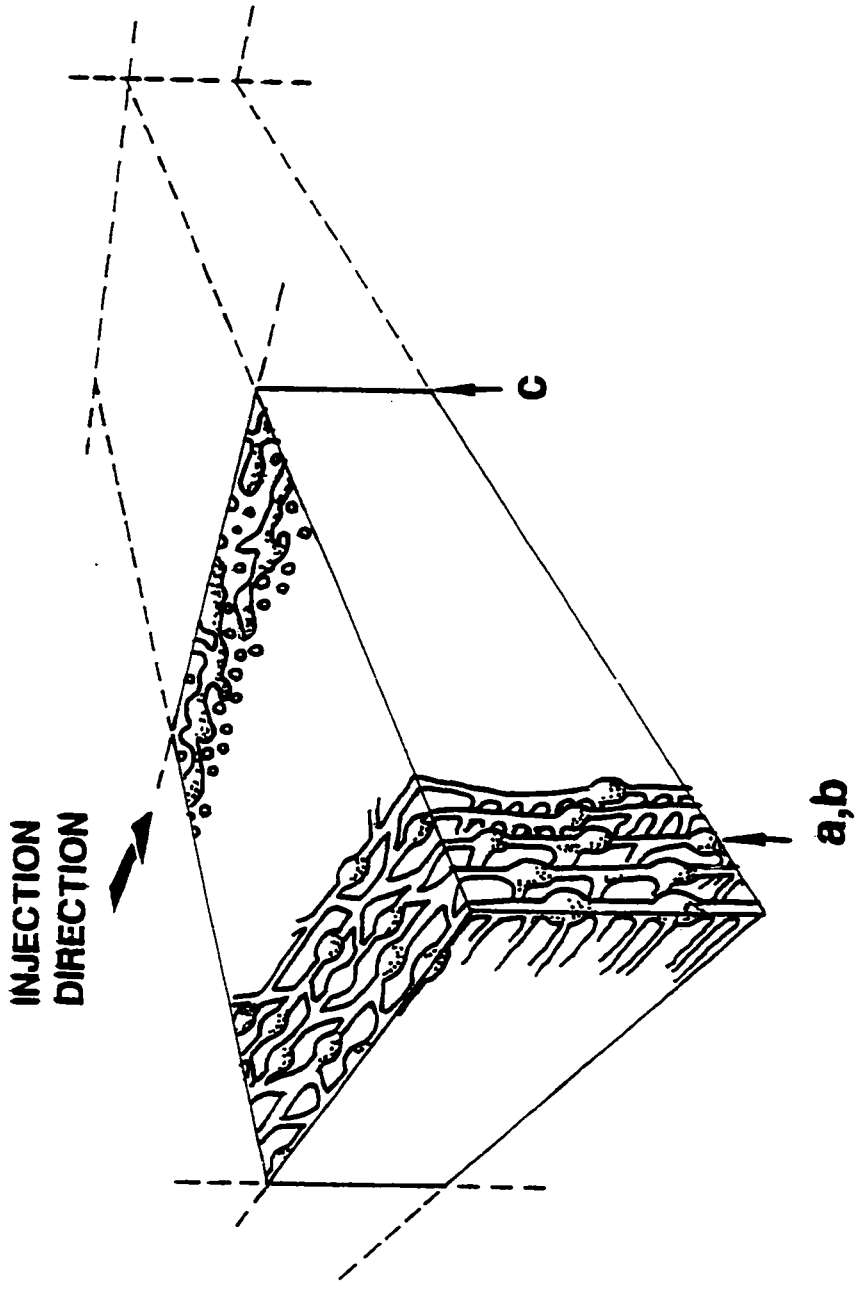


Figure 4. (e) Schematic representation of the morphology through the thickness

(a) parallel to the injection direction, d = 0.26mm

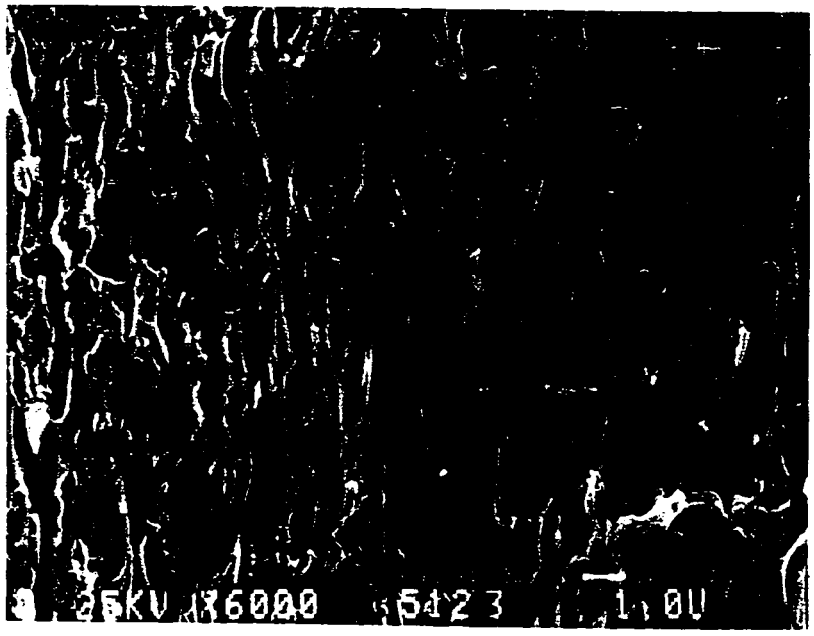

(b) perpendicular to the injection direction, d = 0.21mm

Figure 5. Scanning electron micrographs of injection molded PC/ABS 50/50 blend at various positions through the thickness, d : distance from the edge of the 3mm thick plaque

(c) parallel to the injection direction, d = 0.84mm

(d) perpendicular to the injection direction, d = 0.84mm

Figure 5. Scanning electron micrographs of injection molded PC/ABS 50/50 blend at various positions through the thickness

(e) parallel to the injection direction, d = 1.27mm

(f) perpendicular to the injection direction, d = 1.29mm

Figure 5. Scanning electron micrographs of injection molded PC/ABS 50/50 blend at various positions through the thickness

(g) parallel to the injection direction, d = 1.5 mm

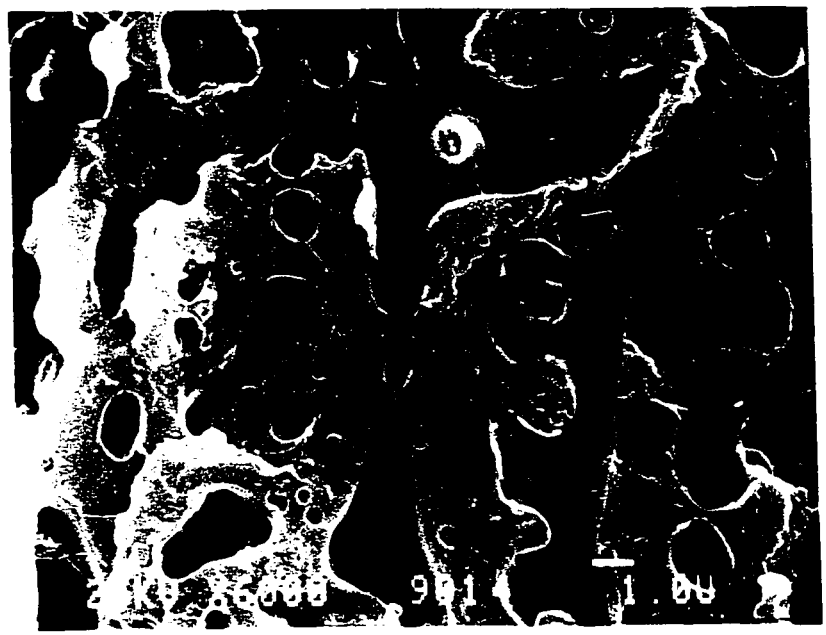

(h) perpendicular to the injection direction, d = 1.5mm

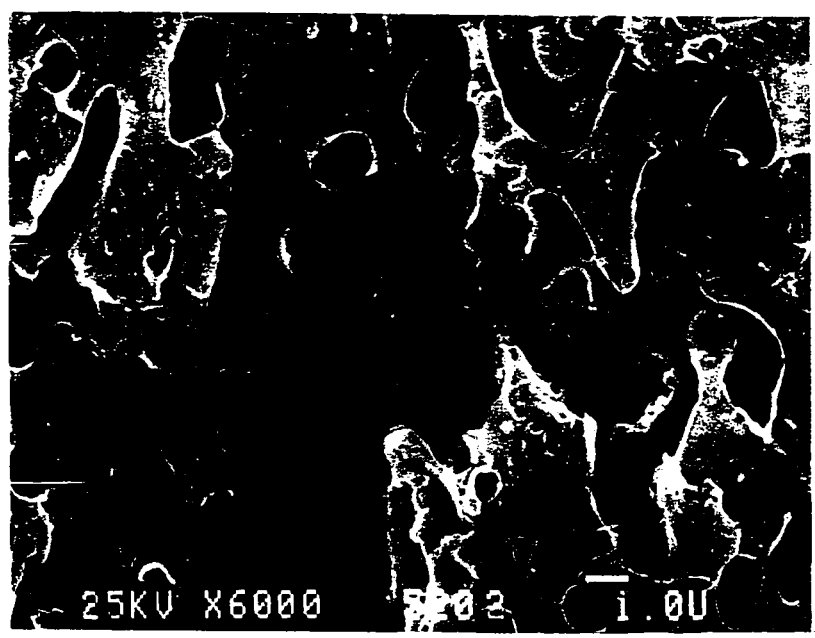


Figure 5. Scanning electron micrographs of injection molded PC/ABS 50/50 blend at various positions through the thickness

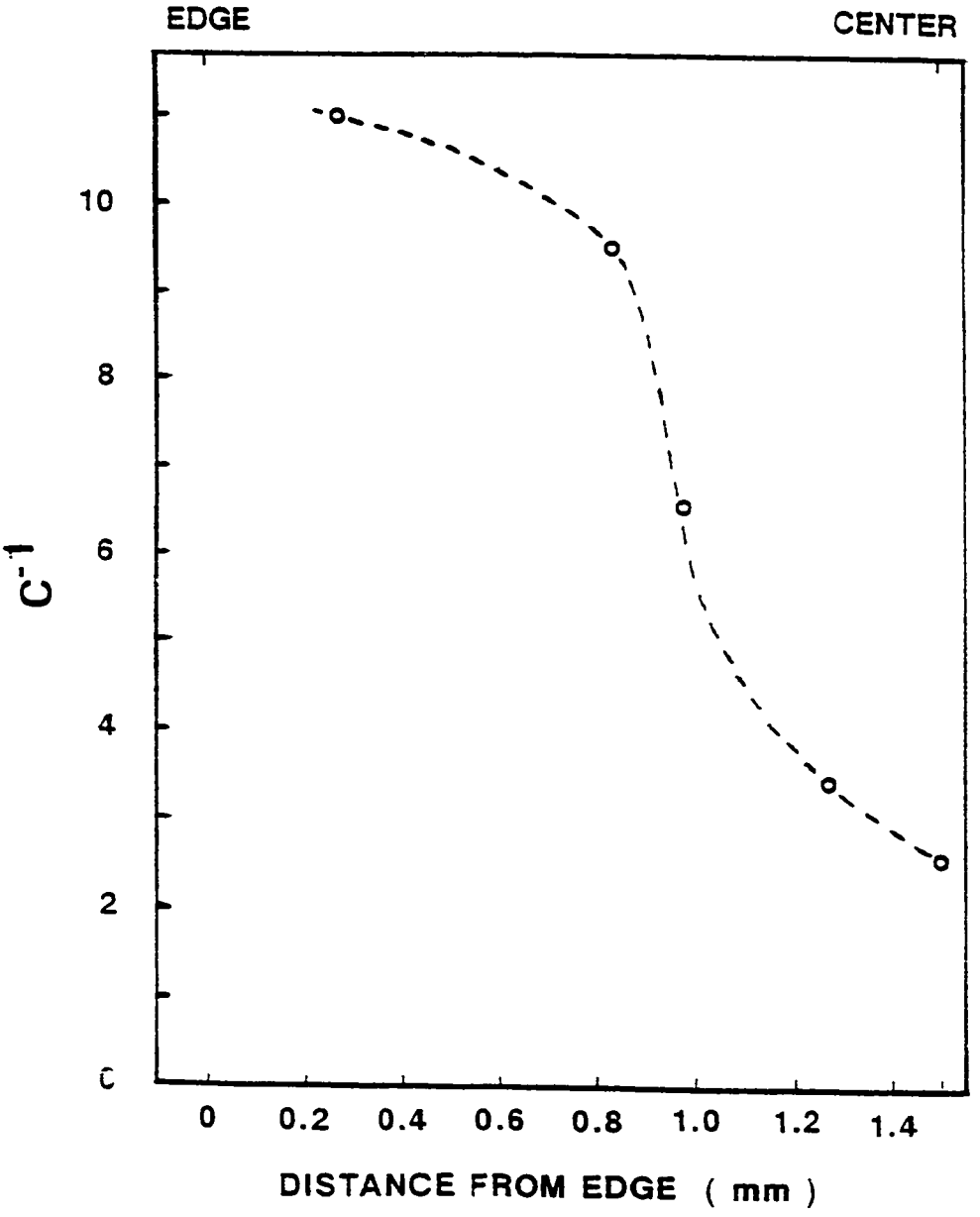


Figure 6. The reciprocal Chalkley parameter $C^{-1}$ through the thickness of the PC/ABS 50/50 blend.

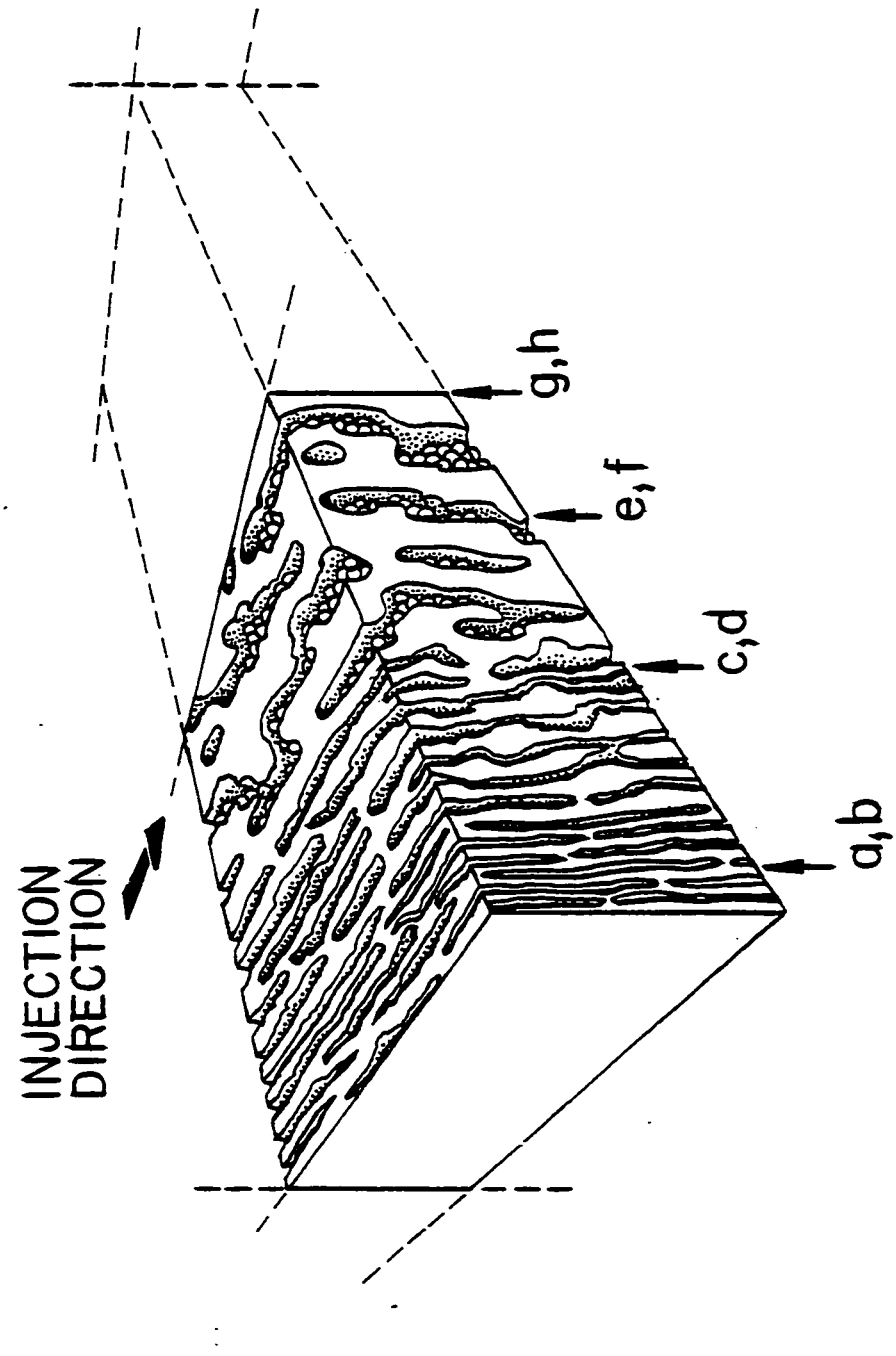


Figure 7. Schematic representation of the morphology of the PC/ABS 50/50 blend

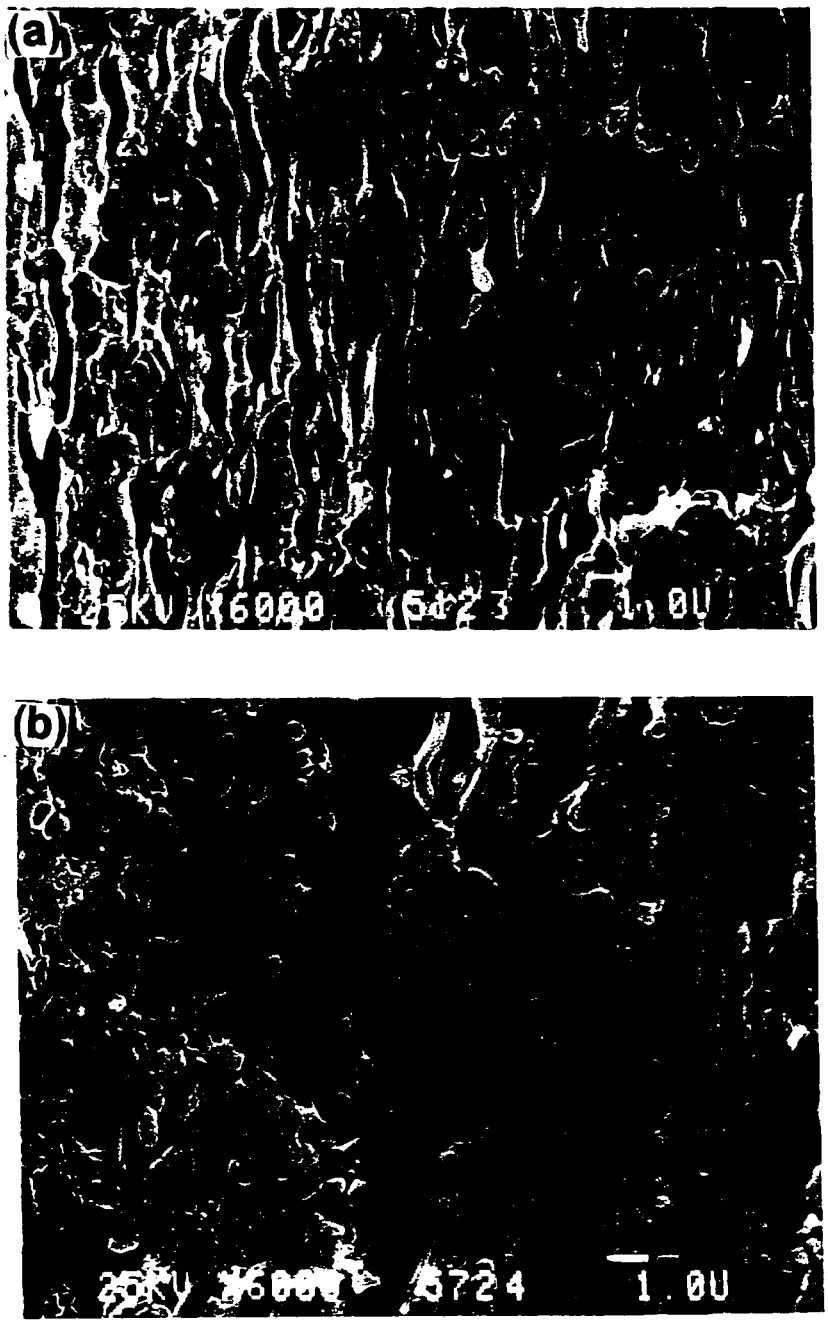


Figure 8. The annealed PC/ABS 50/50 blend viewed parallel to the injection direction near the edge. (a)The unannealed control; and (b)annealed for nominally 12sec at 250°C

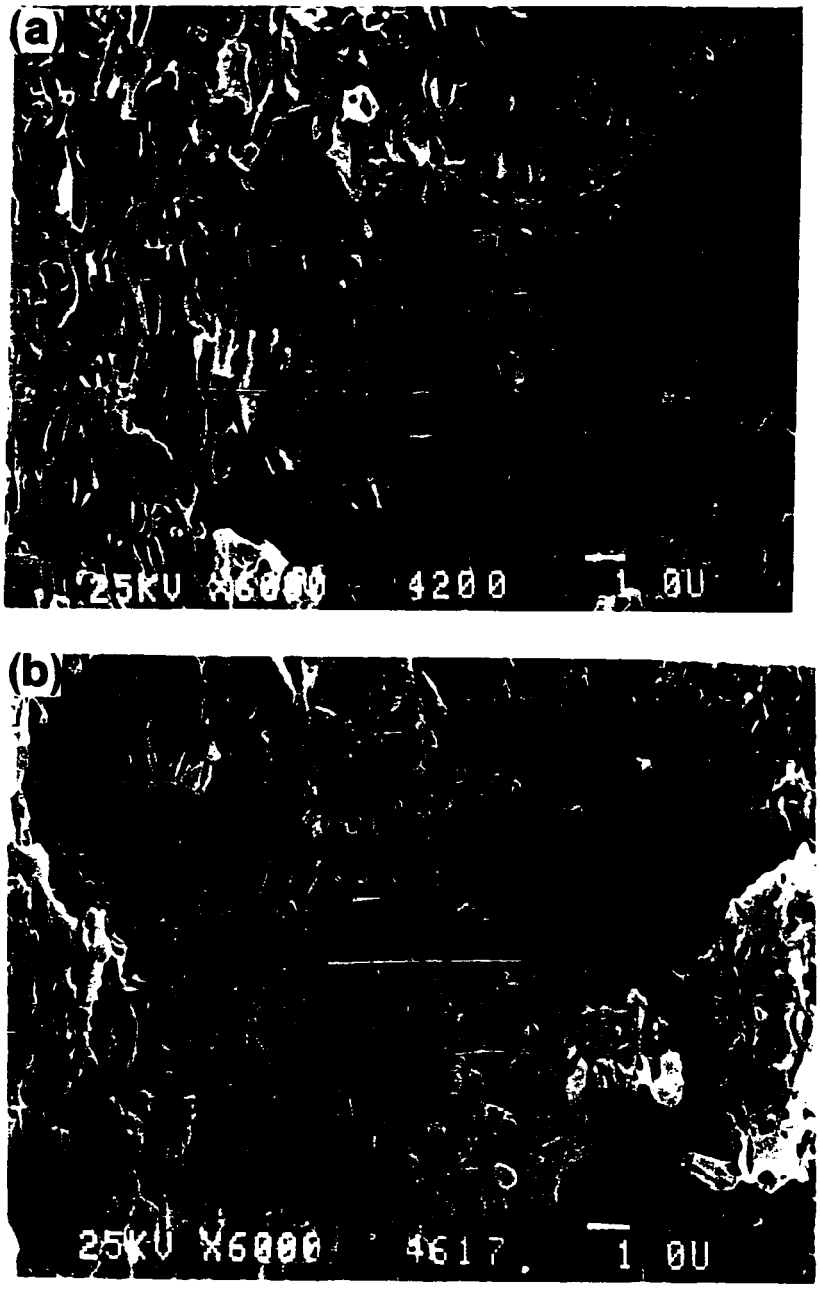


Figure 9. Scanning electron micrographs of injection molded PC/ABS 40/60 blend near the edge. (a)parallel to the injection direction, d = 0.16mm; (b) perpendicular to the injection direction, d = 0.14mm, d:distance from the edge of the 3mm thick plaque

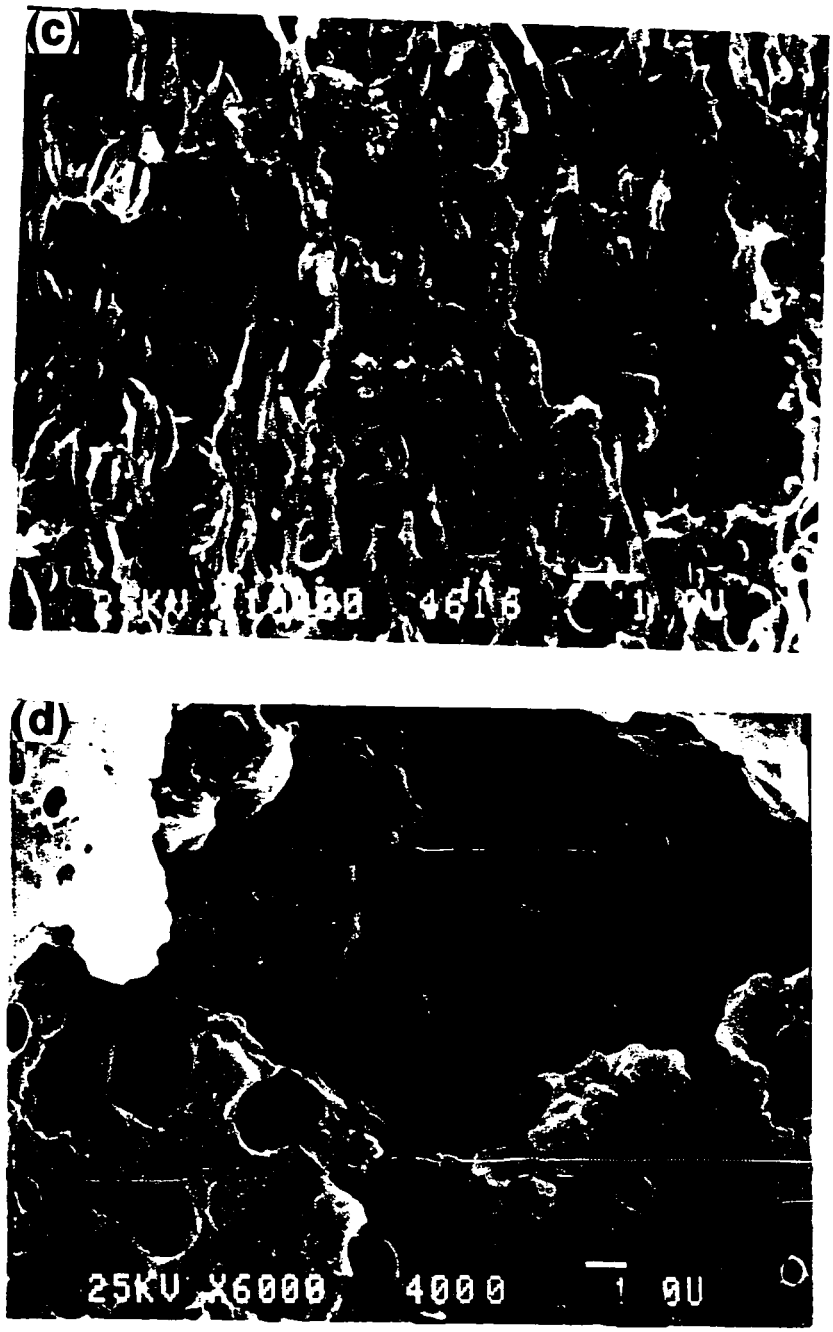


Figure 9. Scanning electron micrographs of injection molded PC/ABS 40/60 blend.(c) a higher magnification of (b), (d) parallel to the injection direction at the center

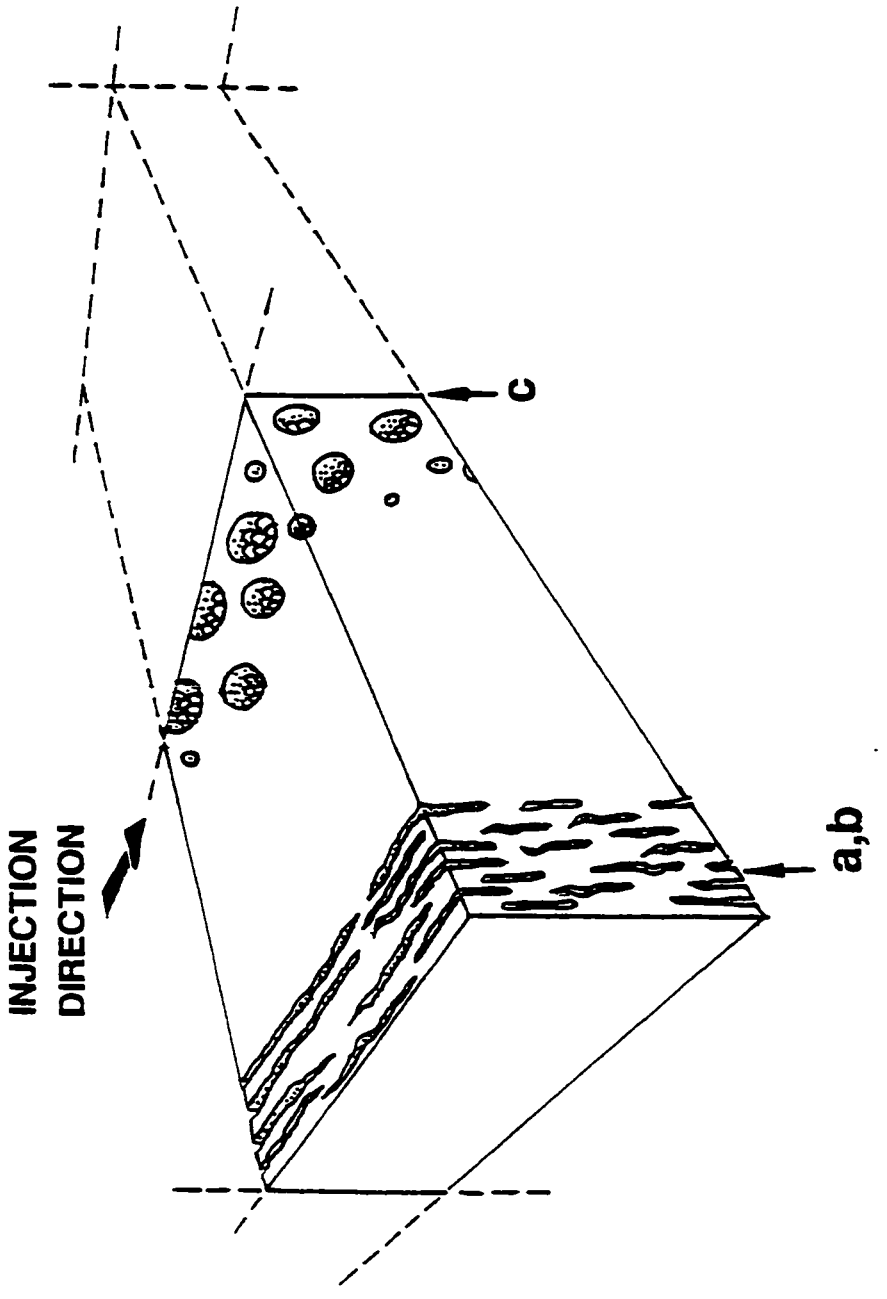


Figure 9. (e) Schematic representation of the morphology through the thickness

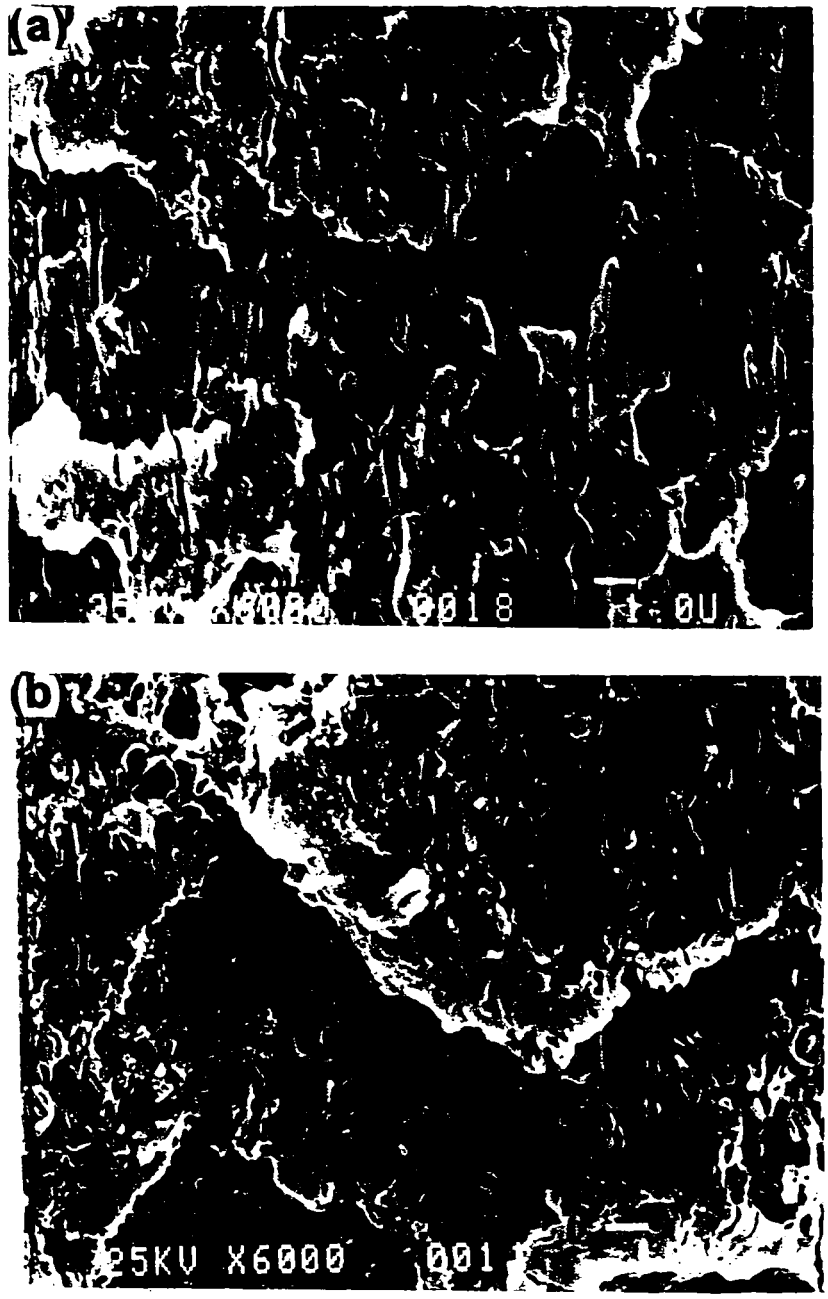


Figure 10. Scanning electron micrographs of injection molded PC/ABS 30/70 blend near the edge,(a)parallel to the injection direction, d=0.12mm (b)perpendicular to the injection direction, d=0.11mm, d:distance from the edge of the 3mm thick plaque

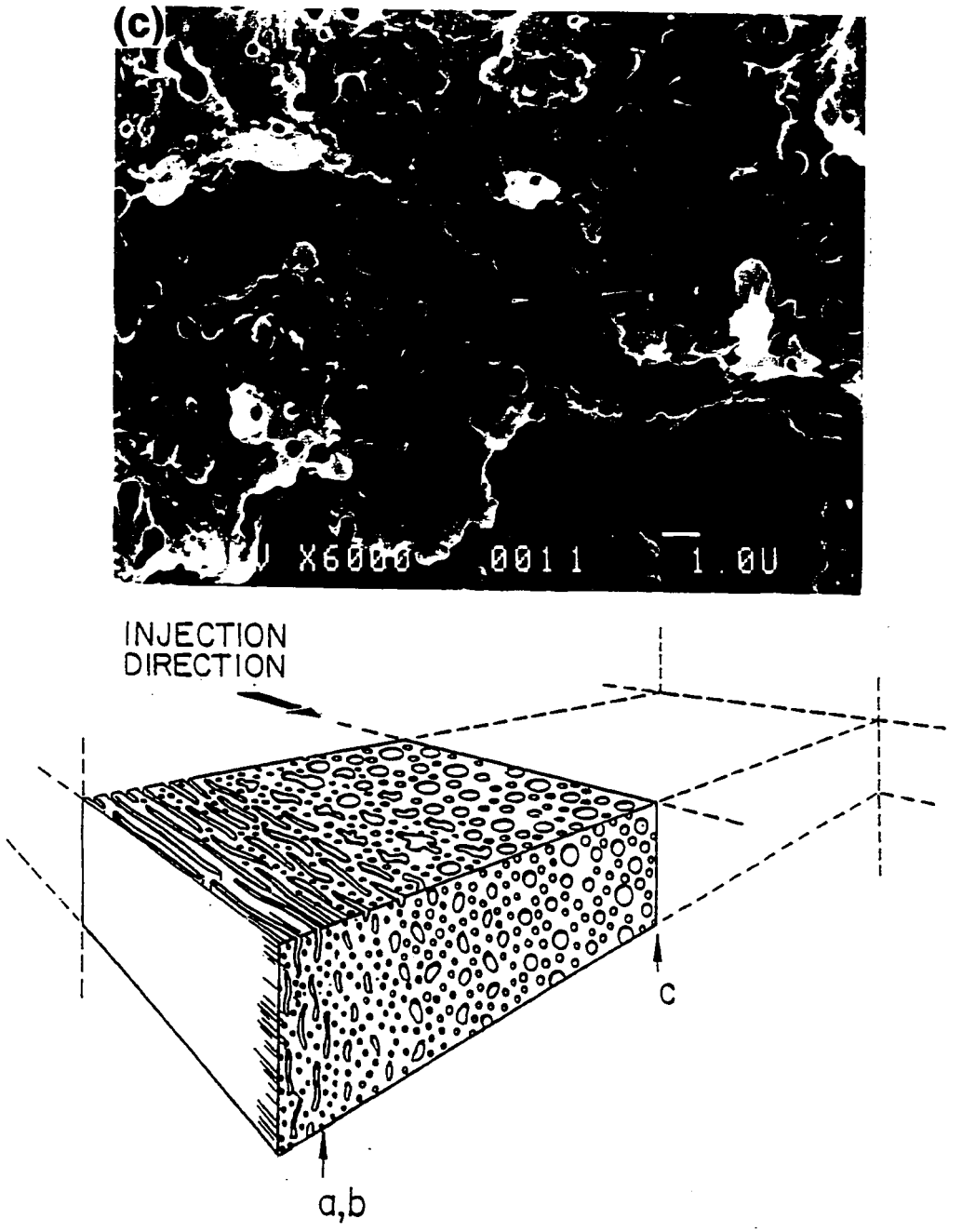


Figure 10. Scanning electron micrographs of injection molded PC/ABS 30/70 blend (c) parallel to the injection direction at the center; and (d)schematic representation of the morphology through the thickness

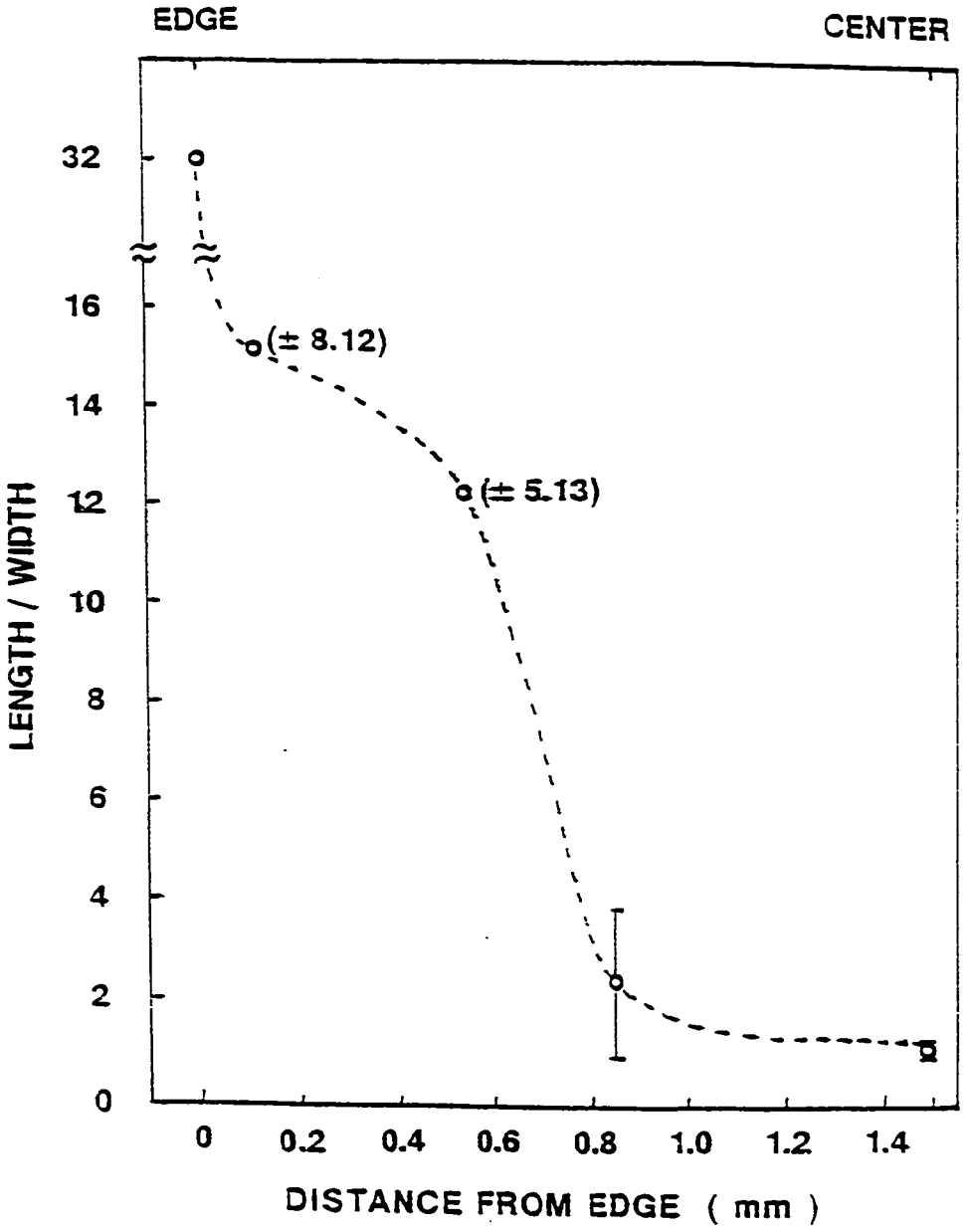


Figure 11. The length to width ratio of the PC domains through the thickness of the PC/ABS 30/70 blend

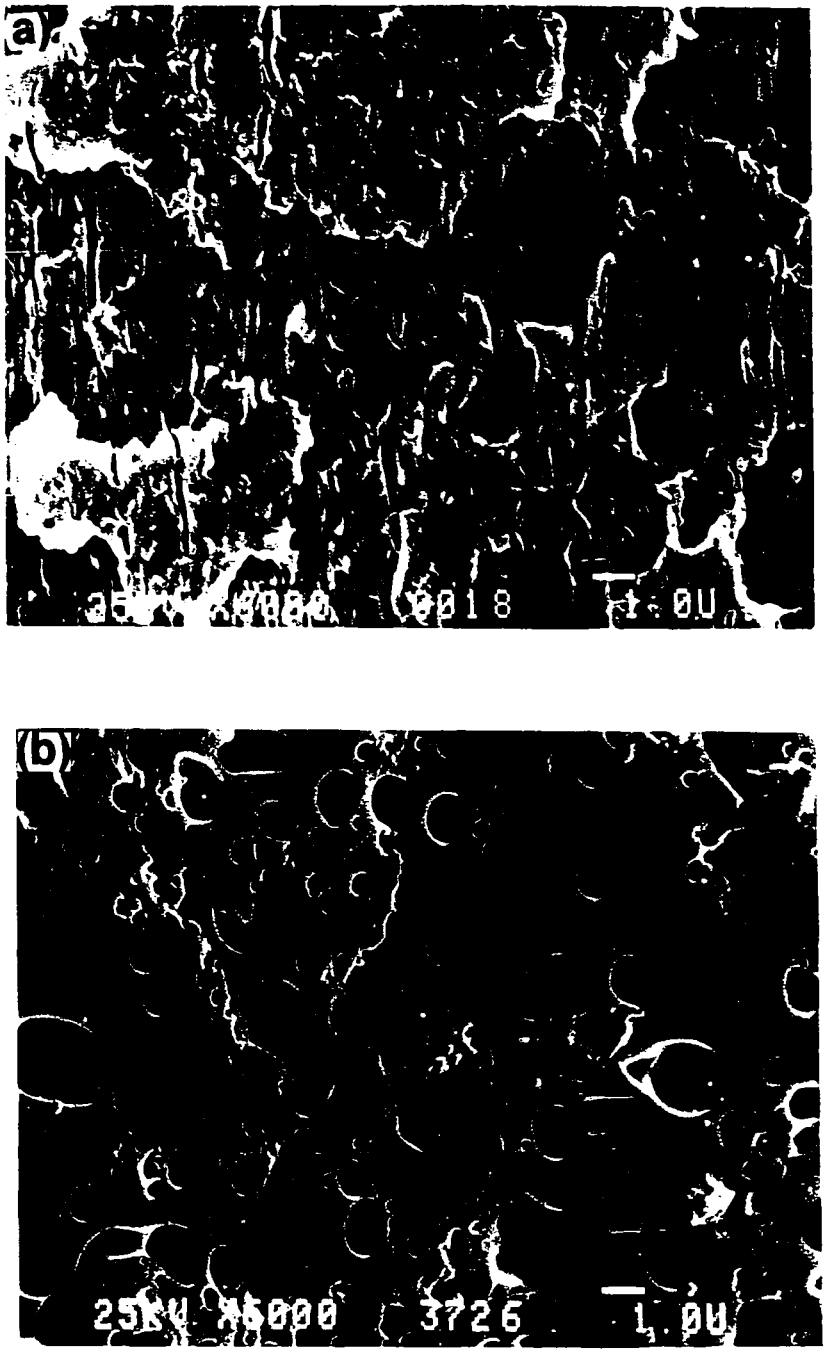


Figure 12. The annealed PC/ABS 30/70 blend viewed parallel to the injection direction near the edge. (a) The unannealed control; and (b) annealed for nominally 12sec at 250°C

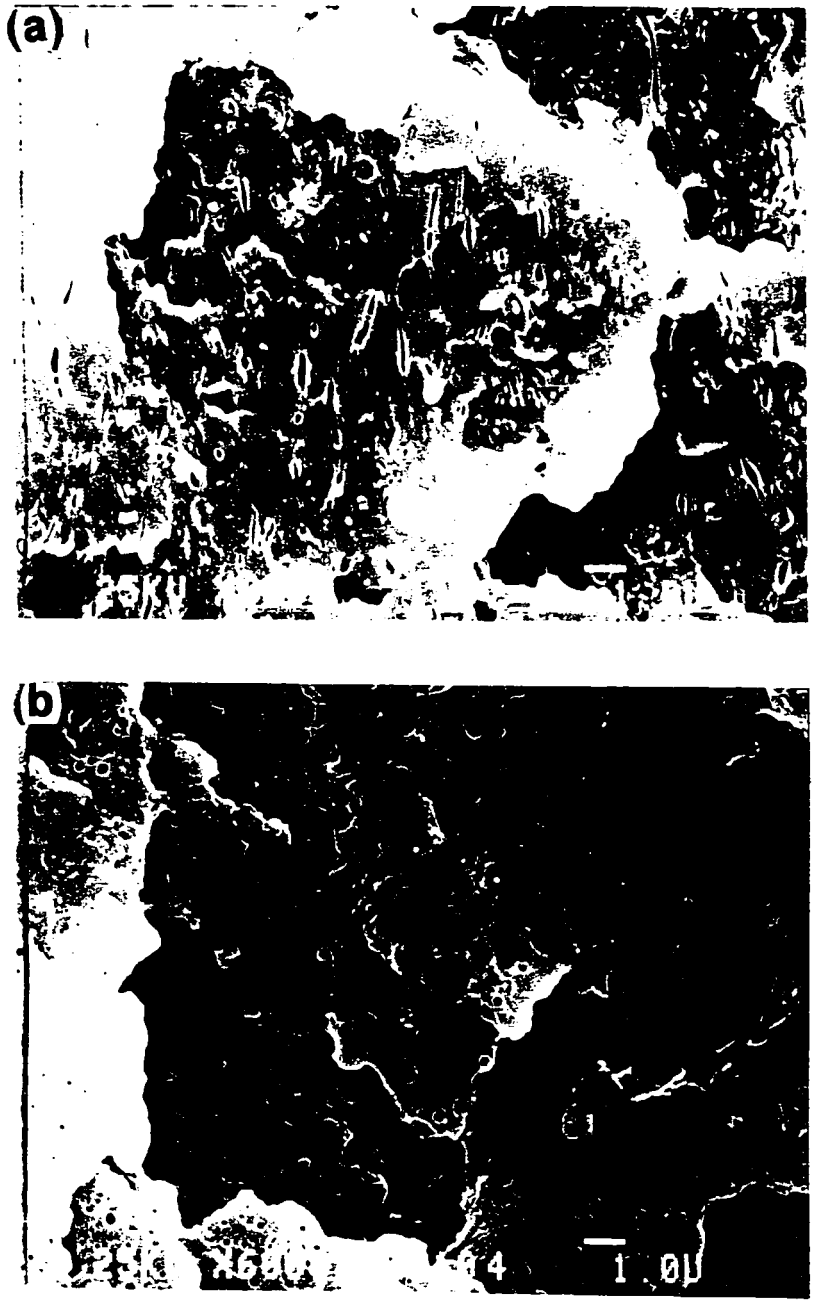


Figure 13. Scanning electron micrographs of injection molded PC/ABS 10/90 blend. Parallel to the injection direction (a) near the edge, d = 0.15mm (b) at the center. d: distance from the edge of the 3mm thick plaque

## CHAPTER 3

# FRACTOGRAPHY OF INJECTION MOLDED POLYCARBONATE/ABS BLENDS

## 1. INTRODUCTION

Frequently, studies of the deformation mechanisms that precede and control ultimate failure of polymers are conducted on very thin films. With thicknesses on the micron size scale, deformation of thin films is readily observed in situ in the optical or electron microscope. In this case, the stress state approximates plane stress; however, most applications involve thick shapes where the stress state is mostly plane strain. Stress state is an important factor in the ductile to brittle transition; in general, a material is more inclined to fail in a brittle manner when the stress state is closer to plane strain.

Deformation and fracture of injection molded shapes are further complicated by the possibility for a processing-induced morphology gradient through the thickness. This is particularly of concern with phase separated polymer blends because domain size and shape under non-steady state flow conditions are strongly dependent on rheological differences and interfacial tension. Additionally, the size scale of the domain morphology of phase-

separated polymer blends is frequently in the range that produces maximum light scattering and optical opacity with the consequence that failure phenomena can not be readily observed in thick sheets by conventional optical microscope techniques.

Fractography is widely used in post-failure analysis of metals and other opaque materials where it is possible to identify from the appearance of the fracture surface where the fracture originated, how it propagated and whether it was ductile or brittle. In the literature, a variety of ductile fracture modes have been described for polymeric and non-polymeric materials from the characteristic features of the fracture surface(1,2). Shear tearing is a well-known plane stress fracture mode in metals and polymers. In the presence of phase heterogeneities, cavitation inside or at the interface of the second phase may also occur. With sufficient degree of triaxiality, fracture can initiate with "pop-in" in the center. The tunneling pop-in crack relieves the triaxiality and permits plane stress shear lips to form near the edges. This creates a characteristic valley in the center of one fracture surface and a corresponding ridge on the other(3,4). "Herringbone" fracture is a plane strain mode characterized by discontinuous crack growth. Repeated interception of the main crack with a series of secondary cracks results in a fish bone appearance(5-7). Sometimes plane stress shear lips flank the herringbone pattern.

Blends of polycarbonate (PC) and ABS in all ratios can be injection molded or extruded as thick parts. Previously, the flow-induced morphology gradient through the thickness of injection molded plaques of these blends was described(8,9). It is anticipated that the blends will exhibit an unusual variety of fracture modes because of the complex domain morphology, and the fact that the two constituent polymers exhibit different types of fracture. Ductile failure of polycarbonate occurs by a shear tearing mode, and brittle failure by crazing(10,11), the ductile-to-brittle transition is strongly dependent on notch geometry, thickness and other testing and material variables(12,13). Mixed mode pop-in fracture of polycarbonate has also been observed(14). Rubber-toughened styrenic polymers typically fail by multiple crazing, but it is well-known that the quantitative effectiveness of the rubber depends on several important factors including particle size and the phase structure within the rubber particle(15). In the case of an ABS with rubber particles in the 1$\mu$m size range that contain occluded plastic, failure occurs by multiple crazing of the glassy matrix accompanied by cavitation within the composite rubber particles(16). In spite of the commercial success of PC/ABS blends, no comprehensive investigation of the fracture behavior has been reported. In the present study, the ductile-to-brittle transition was characterized, and the relationship between morphology and fracture behavior was investigated over the entire composition range in increments of 10 weight percent.

## 2. EXPERIMENTAL

Blends of ABS and polycarbonate (PC) were provided by The Dow Chemical Company in the form of 5in (12.7 cm) x 3in (7.6 cm) x 1/8in (0.3 cm) injection molded plaques. Samples were provided across the entire composition range in 10 weight percent increments, and the compositions are indicated as the weight percents PC/ABS. The ABS and PC resins were described previously(8), as were the injection molding conditions (9). Tensile specimens were cut to the ASTM-D 1708 geometry parallel or perpendicular to the injection direction. A single edge notch (SEN) was machined at the midpoint of the gauge length, the notch was 0.037in. (0.094 cm) in depth with a 0.01 in (0.025 cm) notch radius and 45° flank angle. Sections 1mm in thickness from the edge and center regions were cut on the Isomet with a diamond wafering blade from the Buehler Company.

Tensile tests were carried out in an Instron machine. The crosshead speed was 229 mm/min. and the test temperature was varied from -70°C to 25°C. Fracture surfaces were examined with an Olympus Model SZK stereoscan optical microscope or an Olympus Model BH in the reflection

mode, then coated with gold and viewed in a JEM 35CF scanning electron microscope (SEM). Some of the fracture surfaces were selectively etched by immersion in 30% by weight aqueous potassium hydroxide for 2 to 5 hours to remove the PC phase, then washed in water for 2 hours, dried, coated with gold and examined in the JEM 35CF scanning electron microscope(8).

## 3. RESULTS and DISCUSSION

### 3.1. Ductile Fracture Modes

Ductile fracture surfaces of ABS and all the blends, obtained at room temperature with a crosshead speed of 229 mm/min, were completely stress whitened while that of PC was transparent. In addition, except for PC, a stress whitened deformation zone extended 2-3 mm above and below the fracture plane. Representative stereoscan optical micrographs of ductile fracture surfaces are shown in Figure 1. On the fracture surfaces of PC, PC/ABS 90/10 and 70/30 (Figure 1a and 1b) tear lines with characteristic sucking-in of the edges were indicative of plane stress shear fracture. Denser tear lines are observed for the PC/ABS 70/30 blend than for PC/ABS 90/10 and PC. Stress whitening on fracture surfaces of the blends but not

on PC showed that voiding occurred during shear deformation and fracture. This stress whitening was the major difference between the fracture surfaces of PC and the two blends.

Sucking-in characteristic of plane stress shear fracture can also be observed on the edges of the PC/ABS 50/50 composition (Figure 1c). However the center region shows a valley on one fracture surface and a corresponding ridge on the other surface. This central portion is called plane strain pop-in(4). It results when a crack relieves the triaxial stress condition at the center and tunnels inside while external ligaments are still intact. When the latter subsequently fracture in plane stress, shear lips form on the edges and create characteristic sucking-in at the edges.

Sucking-in was not observed on the edges of PC/ABS 30/70 and 10/90 blends. The fracture surfaces of these compositions (Figure 1d) showed a characteristic spine and rib pattern called herringbone or chevron fracture with narrow shear lips on the edges. The shear region accounts for about 35% of the fracture surface of the PC/ABS 30/70 blend and about 20% of the PC/ABS 10/90. Although the herringbone pattern is often considered to be indicative of brittleness, a considerable amount of plastic deformation occurs in formation of the ridges(6). Materials that are still more brittle do not exhibit the herringbone. In this study, the herringbone

pattern was classified as a ductile fracture mode.

Herringbone fracture occurred when the main crack repeatedly interacted with secondary cracks. The discontinuous fracture proceeded by initiation of secondary cracks along the centerline in front of the primary crack so that impingement of the expanding crack front created the characteristic radiating ridges. Since the two cracks grew in slightly different planes, a tearing ridge formed where they intersected. In order for the two crack fronts to interact, it was necessary for the secondary crack to grow radially at approximately the same speed as the primary crack; if it had grown more slowly, it would have been overtaken by the primary crack and the pattern of a closed ellipse would have been overtaken by the primary crack; if it had grown more slowly, it would have been overtaken by the primary crack and the pattern of a closed ellipse would have appeared on the fracture surface.

The fracture surface of ABS shows stress whitening with square edges (Figure 1e) suggestive of macroscopic plane strain conditions, although it has been emphasized that when the deformation mechanism is cavitation, plane stress conditions may prevail at the microscopic level which has the effect of promoting ductile fracture while minimizing thickness effects(17). This was confirmed in higher magnification views of

the ABS fracture surface which showed a typical multiple craze breakdown pattern(18).

The fracture surfaces described in the preceding paragraphs showed a gradual progression in the macroscopic fracture mode from shear fracture of PC in the plane stress condition to plane strain craze fracture of ABS. When ABS was blended with PC, both shear and cavitational mechanisms become possible so that the highest PC blends fracture in the plane stress shear mode of PC, but macroscopic shear deformation in this case was accompanied by cavitation and stress whitening. As the ABS content increased, mixed mode fracture occurred; in the center the plane strain condition with cavitation produced pop-in, and then herringbone features as the ABS content increased further, while shear lips at the edges were the result of plane stress shear fracture. The plane strain center region accounted for an increasing amount of the fracture surface as the ABS content increased while the shear lips became narrower and finally with ABS were no longer observable.

## 3.2. Ductile-to-Brittle Transition

Fracture surfaces of specimens tested at lower temperatures were examined to determine the ductile-to-brittle transition. Above -20°C all PC

fracture surfaces showed the ductile tearing lines observed at room temperature. However between -20°C and -60°C some specimens showed ductile fracture while others tested at the same temperature showed brittle fracture. This bimodal behavior reflected the high notch sensitivity of PC. A brittle fracture surface (Figure 2) showed the typical craze breakdown pattern with a mirror region closest to the notch followed by mackerel and hackle regions which have been described in the literature (19-22). In the mirror region the crack propagates slowly through the center of the craze. As the velocity increases the crack jumps along the interface between crazed and uncrazed material which creates the mackerel pattern. When the crack velocity exceeds that of the growing craze the crack tip catches up with the craze tip and further crack growth occurs by nucleation of small bundles of crazes in the stress field of the crack tip and propagation through this craze zone. Repetition of the process results in the hackle surface. No sucking-in of the sides was discernible, which indicated the plane strain condition has been imposed, although sometimes the craze fracture surface showed narrow shear lips.

The blends did not exhibit the bimodal fracture behavior of PC in the ductile-to-brittle transition. In all cases the fracture surfaces were characterized by a highly stress whitened region near the notch which resembled the room temperature ductile fracture surface followed by a

featureless less stress whitened region further from the notch. The featureless brittle region increased in length as the testing temperature was lowered. The specimen-to-specimen consistency of the observations indicated that blending with ABS considerably reduced the notch sensitivity.

Figure 3 summarizes the ductile-to-brittle transition temperatures for specimens tested with a crosshead speed of 229 mm/min at 5 to 10°C temperature intervals. For PC this is the highest temperature where bimodal fracture behavior was observed; for the blends the transition temperature was defined as the highest temperature where a brittle region was observed on the fracture surface. On the S-shaped curve the PC/ABS 70/30 and 60/40 blends were the most ductile and were more ductile than PC under these testing conditions, while the 30/70 and 10/90 blends were the most brittle. No ductile-to-brittle transition was observed with ABS; stress-whitening and the multiple craze breakdown pattern were observed on the fracture surface over the entire temperature range examined.

Fracture surfaces of blends from the ductile-to-brittle transition are shown in Figure 4. For PC/ABS 90/10 at -40°C the ductile region near the notch resembled the room temperature fracture surface with prominent tear lines and sucking-in of the edges (Figure 4a). In addition to ductile tearing lines, parabolic marking on the ductile region of PC/ABS 80/20 and 70/30

fracture surfaces (Figure 4b) resulted when the main fracture front intersected secondary cracks initiated ahead of and above or below the main crack front (23). Some of the other more ductile blends, PC/ABS 60/40 and 50/50, showed pop-in with shear lips in the ductile region near the notch similar to the room temperature pop-in except that the center crack was wider at -50°C (Figure 4c) than at room temperature. The most brittle blends, PC/ABS 30/70 and 10/90, are those that show the herringbone pattern at room temperature. The herringbone pattern in the ductile region at -25°C(Figure 4d) was the same as that at room temperature at the magnification used to obtain these micrographs. The only blend that produced a completely brittle fracture surface at -70°C, the lowest temperature used in the study, was the PC/ABS 10/90 composition. ABS exhibited stress whitening over the entire fracture surface even at -70°C.

### 3.3. PC-Rich Compositions

Polycarbonate was the continuous phase of blend compositions PC/ABS 90/10 to 70/30. The domain morphology in the center half of the thickness was a more or less isotropic dispersion of 1$\mu$m rubber particles and 0.3$\mu$m SAN particles (9). Sometimes, in the 70/30 blend, the rubber domains contained more than one rubber particle, but these domains did not exceed several microns in size, The blend morphology was observed

undeformed when the brittle region of the fracture surface in Figure 4a was examined at higher magnification in the SEM.

Deformation of the dispersed morphology of the 90/10 blend was observed when the ductile shear tearing region of the fracture surface in Figure 4a was examined at higher magnification. In the center of the thickness, cavitated rubber particles were observed, Figure 5a. It was determined that fracture had propagated through the center of the cavitated rubber particles when the matching fracture surface was found to contain the other part of the cavitated rubber particle, Figure 5b. There was no indication of failure at the interface between rubber domains and the PC matrix. Cavitation also occurred at the SAN particles in the ductile region of the fracture surface. In this case, the PC deformed plastically around the SAN particles with separation of the PC/SAN interface. When the matching fracture surfaces in Figure 5a and b were compared, holes that contained SAN particles on one fracture surface matched up with empty holes on the other. The SAN spheres appeared to be undeformed.

The cavitation mechanism is commonly encountered in blends with a particulate dispersed phase on the micron size scale, particularly in the center of a thick piece where triaxiality is highest. Adhesion between PC and grafted SAN (24) encouraged cavitation of the low modulus rubber

particles rather than separation of the interface; while the response to the smaller, higher modulus SAN particles was interfacial failure. Both kinds of voiding relieved the notch sensitivity of PC, and bimodal fracture behavior that was characteristic of PC in the ductile-to-brittle transition region was subsequently eliminated. Blending the least amount of ABS, 10%. was sufficient to remove the notch sensitivity; increasing the amount of ABS to 30% improved the toughness by increasing the number density of dispersed particles.

Near the edge, the morphology consisted of a bead-and-string structure with rubber particles connected in the injection direction by elongated SAN strings. The region of the ductile fracture surface where the morphology was bead-and-string was characterized by cavitated rubber particles, Figure 5c, similar to those observed in the center. Near the edge the free SAN formed more-or-less continuous 0.2$\mu$m strings that were oriented in the injection direction and perpendicular to the crack growth direction. Although the free SAN strings did not promote cavitation of the PC, the cavitation mechanism was less critical near the edge where the condition was closer to plane stress than in the center. Instead, the free SAN strings functioned somewhat like reinforcing fibers, and when the matching fracture surface to Figure 5c was etched to remove the PC, fractured SAN strings re-oriented along the tear direction of PC could be

seen, Figure 5d.

### 3.4. Intermediate Compositions

Blend compositions in the PC/ABS 60/40 to 40/60 range had co-continuous or almost co-continuous morphologies(9). In the center, thick ABS domains appeared to be continuous, while the PC phase was thought to vary from co-continuous in the 60/40 blend to dispersed with SAN inclusions in the 40/60 composition. The morphology of these compositions near the edge was characterized by an interconnected, coalesced ABS bead-and-string structure that with the PC phase formed a stratified, sheet-like morphology.

The ductile fracture mode in these compositions was plane strain pop-in in the center with plane stress shear lips at the edges. Deformation in the pop-in region was examined more closely on a fracture surface of the 50/50 composition like that in Figure 4c where there was a pop-in region near the notch and a featureless brittle region distant from the notch. The positions on the fracture surface that were examined are indicated in Figure 6b, a sketch of the fracture surface in Figure 4c. In the brittle region, Figure 6b, the domain morphology was clearly revealed by the slight separation of the phases; both phases fractured in a brittle manner since there was no

evidence of cavitation in the ABS phase nor pull-out of the PC. Near the tip of the pop-in, Figure 6c, numerous voids in the ABS phase indicated the locations of cavitated rubber particles. Compared to Figure 6b, the PC domains in Figure 6c appeared only slightly deformed. Within the pop-in region, however, the PC domains were highly pulled out and most appeared to have fractured by tearing, Figure 6d.

In these intermediate compositions, the ABS domains were large enough to craze. The sequence of micrographs in Figure 6 suggested that plane strain pop-in proceeded initially by crazing of SAN and cavitation of the rubber particles. When the growing craze encountered a PC domain, it created a local stress concentration (25), shown schematically in Figure 7a. If the crack speed was high enough, as at the tip of the pop-in zone, the PC fractured in a brittle manner in response to the stress concentration. However if the crack speed was somewhat slower, the PC responded by local drawing, as shown schematically in Figure 7b. A key factor in this model was the continuous nature of the PC domains. Because of this, the PC domains remained load bearing during crack propagation even though drawing and thinning of PC caused local interfacial failure, Figure 7c. The decreasing ductility as the composition changed from PC/ABS 60/40 to 40/60 reflected a gradual loss in continuity of the PC phase.

When cavitation and subsequently initiation and growth of a center crack relieved the triaxial stress condition at the center, extension of the intact external ligaments was possible before they fractured in plane stress to create the shear lips. Crazing probably was not the predominate deformation mode in the edge region which was characterized by a highly interconnected ABS bead-and-string structure that together with sheet-like PC domains formed a highly stratified morphology; higher magnification scanning electron micrographs of the shear lips showed ghat this region deformed by profuse cavitation of the rubber particles together with drawing and thinning of the sheet-like PC domains, Figure 6d.

The morphology of the injection molded PC/ABS blends was characterized by relatively well-defined center and edge regions, and the thickness of the center region of the morphology approximately coincided with the plane strain pop-in region on the fracture surface. It was therefore not immediately obvious whether the pop-in fracture mode was primarily the result of the stress state or whether the morphology caused the center region to be intrinsically less ductile than the edge region.

Some insight was obtained when 1mm thick sections from the edge and center were notched and tested in an identical manner as specimens cut from the entire 3mm thickness. These experiments were carried out at

room temperature and a fairly low crosshead speed, 0.1 mm/min. The stress-displacement curves were essentially the same for the three specimens, but while the fracture surface of the thick specimen showed typical plane strain pop-in in the center, Figure 8a, the fracture surfaces in Figure 8b and c show that the 1mm sections from both the edge and center of the plaque fractured by plane stress shear tearing. Sucking-in or shear thinning at the fracture site to 40% and 60%, respectively, of the original thickness was observed with the 1mm specimens. In comparison, shear thinning of the fractured 3mm specimen was much less. to about 90% of the thickness, and was accounted for in the shear lips. This experiment suggested that the center region was intrinsically only slightly less ductile than the edge region when the direction of crack propagation was perpendicular to the injection direction, and therefore the formation of a center tunneling crack that created the pop-in feature was primarily due to the triaxial stress state in the center of the thicker specimens.

The anisotropic properties of the flow-induced layered morphology of the edge region were revealed when the direction of crack propagation was parallel to the injection direction. Although this study focussed on fracture behavior of specimens machined parallel to the injection direction, so that the direction of crack propagation was perpendicular to the injection direction, a few experiments were carried out with the orthogonal

orientation. The 50/50 blend was much less ductile in this orientation; the surface of a specimen machined perpendicular to the injection direction and fractured at -10°C with a cross head speed of 229 mm/min, Figure 9, showed a stress-whitened ductile region near the notch and a more brittle region further from the notch. The pop-in region near the notch formed when a center crack relieved the triaxial stress; however in this case the appearance of additional crack initiation sites near the edge revealed that the external ligaments did not remain intact. Under these testing conditions, the edge cracks grew fast enough to overtake the center crack and coalesced to form the more brittle region further from the notch. Crack initiation near the edge would occur if the layered morphology were exceptionally weak in the transverse direction.

### 3.5. ABS-Rich Compositions

ABS was the continuous phase in blend compositions PC/ABS 30/70 to 10/90. The morphology was more-or-less isotropic in the center region of the injection molded plaques with spherical PC domains 1$\mu$m or less in diameter dispersed in the ABS matrix. The particle size became smaller as the amount of PC was decreased, so the PC domains were smaller in 10/90 than in 30/70. This is qualitatively different from the other end of the composition spectrum; when ABS was the dispersed phase, a change in

composition was reflected more in a change in number density of particles than in particle size. This had to do with different mechanisms of particle formation; specifically, particulate domains of SAN formed by breakup of the flow-induced bead-and-string structure while particulate PC domains formed in the conventional manner during melt blending (8,9). Toward the edge, the PC domains were elongated in the injection direction. This morphology was observed in higher magnification micrographs of the brittle region of the fracture surface in Figure 4d.

Examination of the morphology in the multiple crack initiation region that formed the center ridge of the herringbone, Figure 10a, revealed profuse cavitation of the rubber particles, Figure 10b, as well as cavitation of the matrix around the PC domains. Figure 10c. The plastically deformed matrix was not adhered to the PC particles which retained their more or less spherical shape. The radial ridges of the herringbone away from the initiation zone consisted of obliquely slanted peaks characteristic of shear of tear failure, Figure 10d. The cavitated rubber particles and the PC domains were generally obscured by the pulled out matrix in these areas.

When ABS was the matrix, the initial deformation preceding ductile fracture was cavitation of the rubber particles and craze formation in the SAN. As with the 50/50 blend, impingement of the growing craze on a PC

domain created a stress concentration as shown schematically in Figure 11a. However, in the ABS-rich blends the PC domains were not continuous and the entire load carried by the PC domains was transferred across the interface from the ABS phase. It appeared from the evidence on the ductile fracture surfaces, specifically the presence of voids containing undeformed spherical PC particles, that adhesion was not good enough to support drawing of the PC domains, and instead the interface failed during craze growth, Figure 11b. Crack propagation through the void created by interfacial failure is shown schematically in Figure 11c. Initiation of secondary cracks from voids such as this would account for the multiple crack initiation that was characteristic of the herringbone fracture in ABS-rich blends, and also the deleterious effect of the PC phase that caused the ABS-rich compositions to be the more brittle than the other blends.

A herringbone pattern was also observed with PC/ABS 30/70 specimens machined perpendicular to the injection direction so that the crack grew parallel to the injection direction; however instead of the ridges of the herringbone pointing toward the notch, in this case the ridges pointed away to form a reverse herringbone pattern, Figure 12. Multiple crack initiation in the center where triaxiality was highest created the herringbone pattern; the reverse herringbone formed by a similar mechanism but with multiple crack initiation near the edges. Since fracture would not have

initiated at this unusual site in an isotropic material, it was apparent that the anisotropic morphology caused the edge region of the injection molded ABS-rich blends to be exceptionally weak in the transverse direction.

## 4. CONCLUSIONS

Post-failure analysis of fracture surfaces was used to characterize the ductile failure mode and the brittle-to-ductile transition of injection molded blends of polycarbonate and ABS over the entire composition range. Correlation of failure behavior with phase morphology led to the following conclusions:

1. Macroscopically, three ductile fracture modes were identified: PC-rich blends fractured by plane stress shear tearing; intermediate compositions fractured by mixed mode pop-in; and herringbone fracture was observed with ABS-rich blends

2.The three fracture modes correlated with three ranges in the phase morphology: shear tearing was observed in the composition range PC/ABS 90/10 to 70/30 where PC was the continuous phase; the pop-in mode occurred when the composition was in the range PC/ABS 60/40 to 40/60

and the phases were co-continuous or almost co-continuous; and herringbone fracture was observed in blend compositions PC/ABS 30/70 to 10/90 where ABS was the continuous phase.

3. An S-shaped relationship was observed between the ductile-to-brittle transition temperature and the composition with PC/ABS 70/30 and 60/40 the most ductile compositions and PC/ABS 30/70 and 10/90 the most brittle.

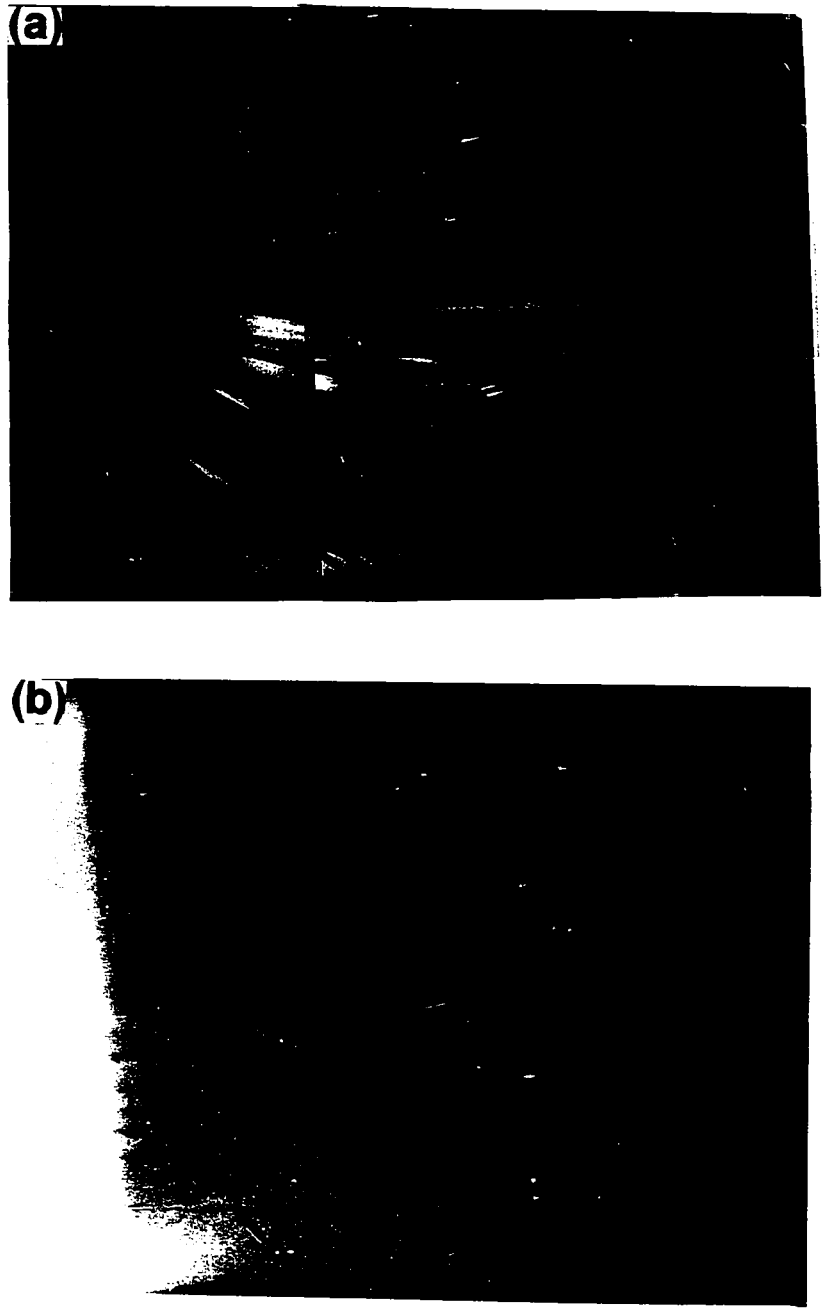


Figure 1. Ductile fracture surfaces obtained at room temperature with a crosshead speed of 229 mm/min as viewed in the stereoscan optical microscope. (a)PC (reflected dark field OM), (b)PC/ABS 70/30

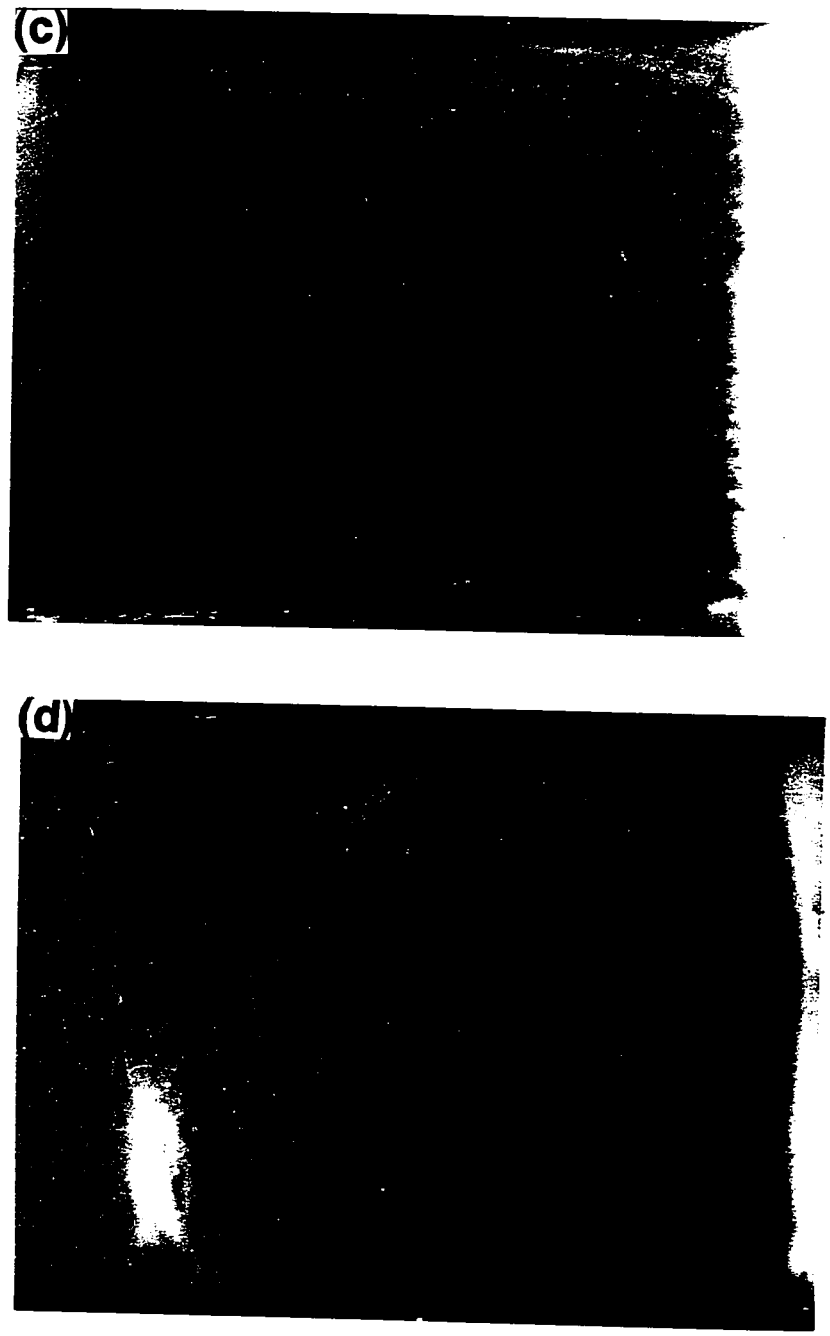


Figure 1. Ductile fracture surfaces obtained at room temperature with a crosshead speed of 229 mm/min as viewed in the stereoscan optical microscope, (c)50/50, (d)30/70

Figure 1. Ductile fracture surfaces obtained at room temperature with a crosshead speed of 229 mm/min as viewed in the stereoscan optical microscope. (e)ABS

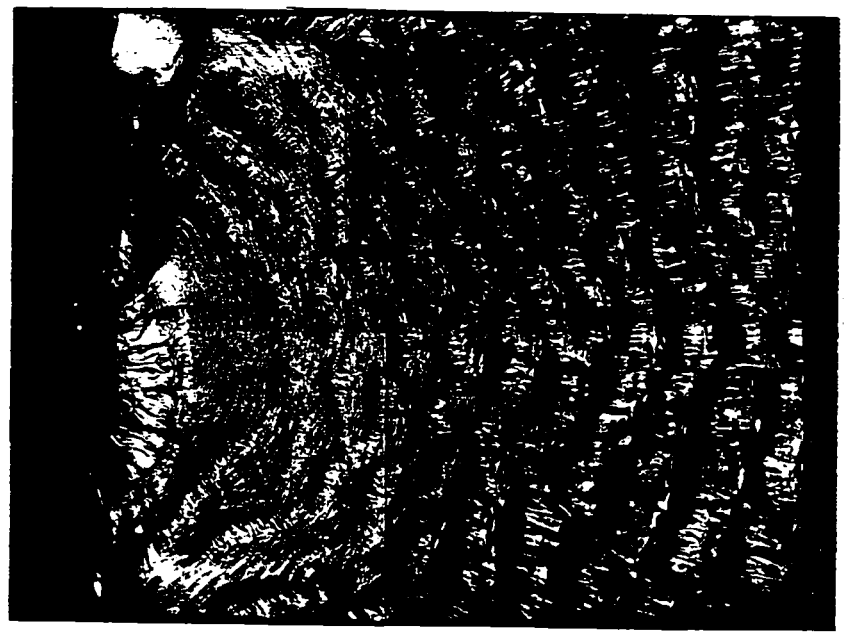

Figure 2. Brittle fracture surface of PC obtained at -20°C and a crosshead speed of 229mm/min as viewed in the optical microscope with reflected light

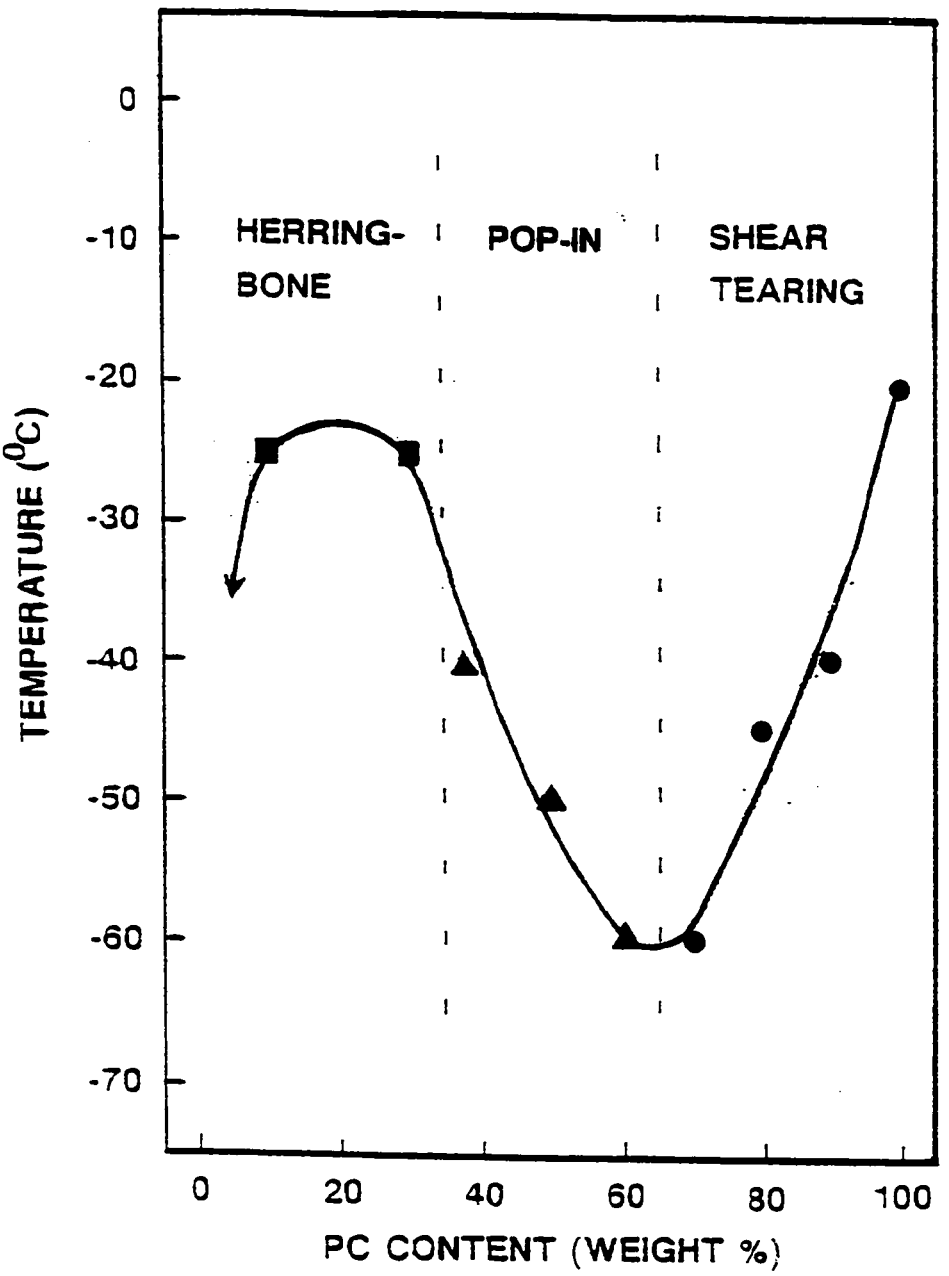


Figure 3. The ductile-to-brittle transition of PC/ABS blends for a crosshead speed of 229 mm/min.

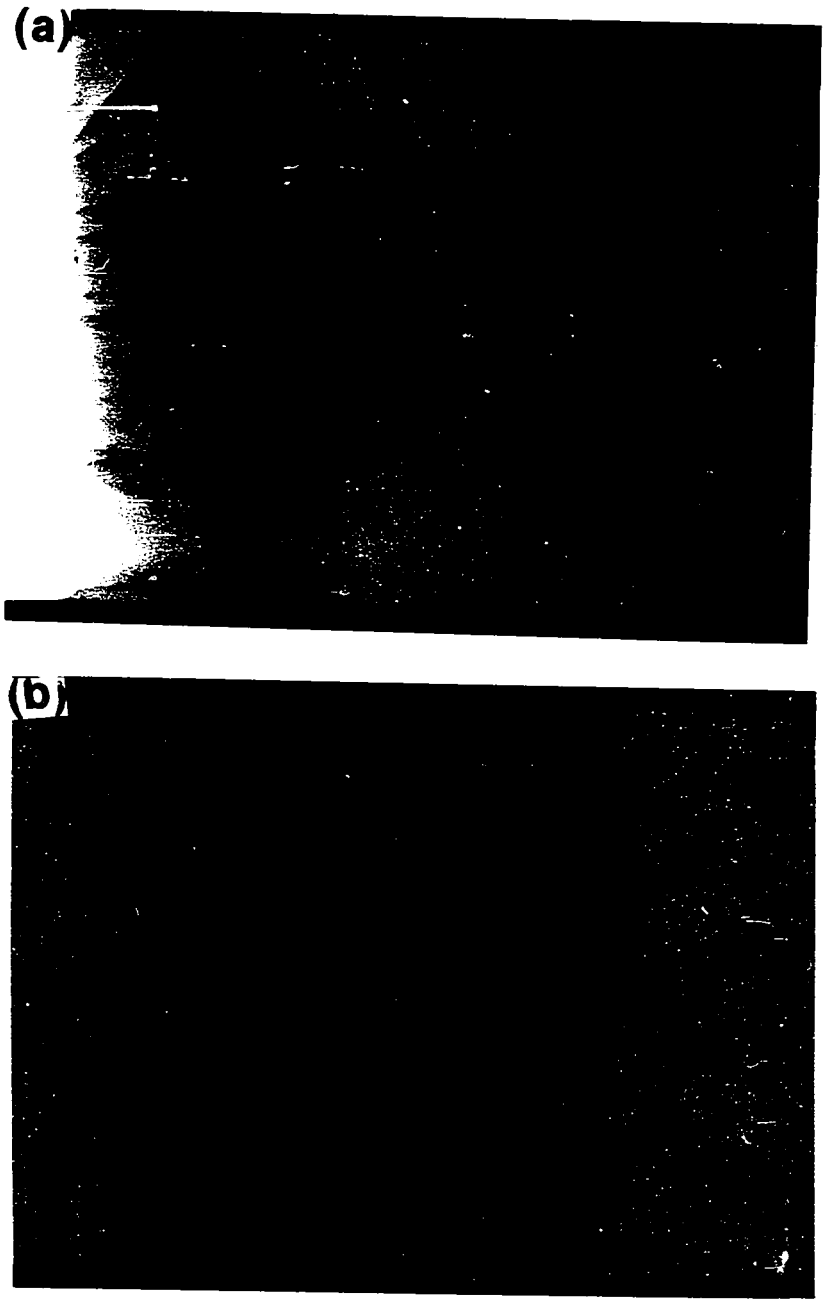


Figure 4. Fracture surfaces in the ductile-to-brittle transition region with a crosshead speed of 229 mm/min as viewed in the stereoscan optical microscope.(a)PC/ABS 90/10 at -40°C (b)70/30 at -40°C

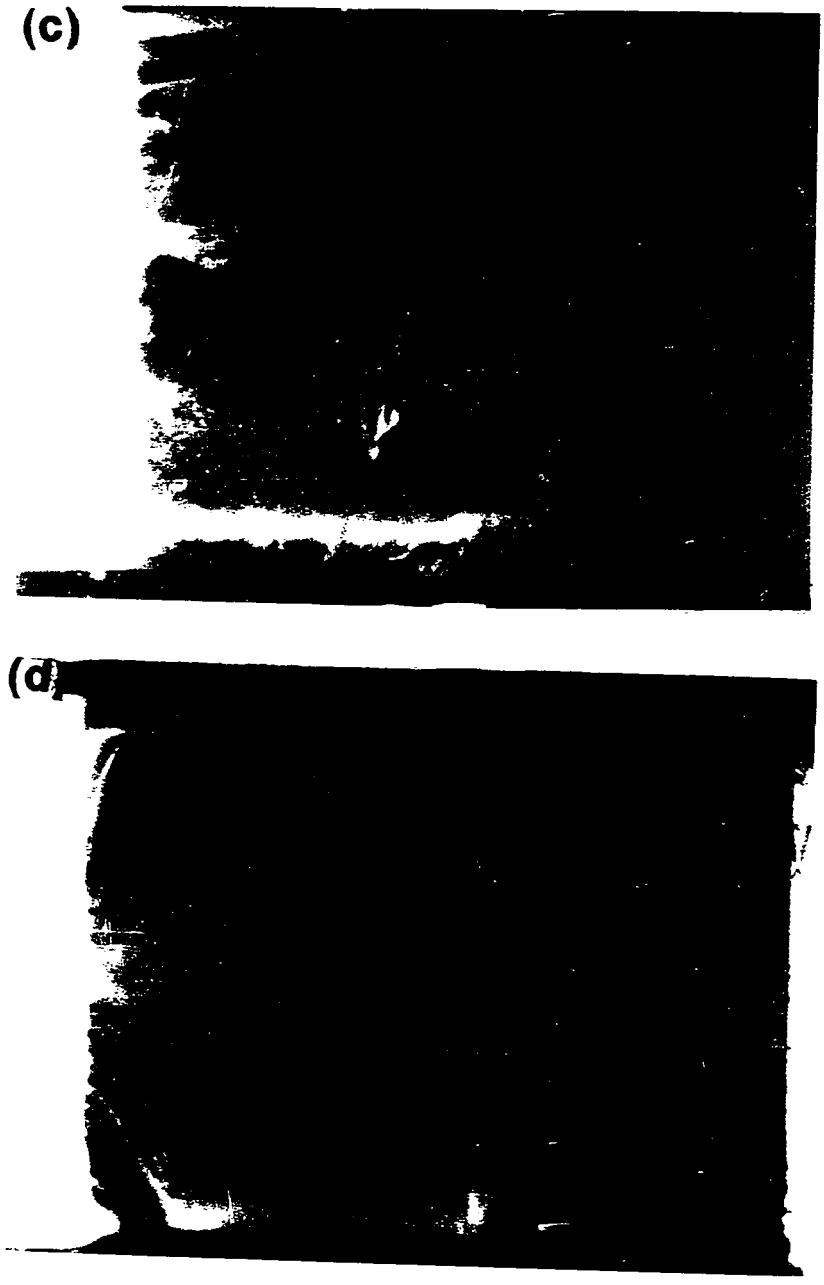


Figure 4. Fracture surface in the ductile-to-brittle transition region with a crosshead speed of 229 mm/min as viewed in the stereoscan optical microscope.(c)50/50 at -50°C (d)30/70 at -25°C

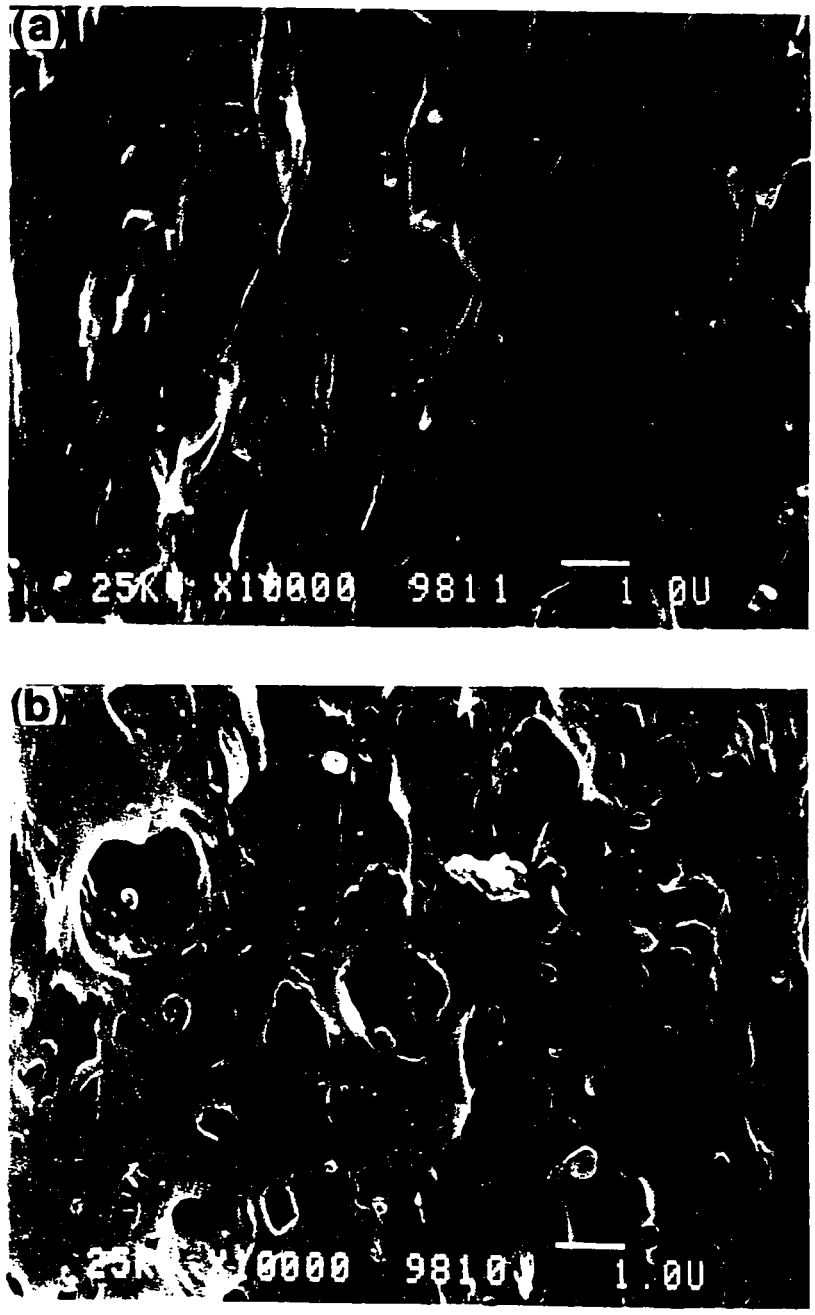


Figure 5. Scanning electron micrographs of the fracture surface in Figure 4a of PC/ABS 90/10(a)the ductile region near the center (b)the same area of the matching fracture surface

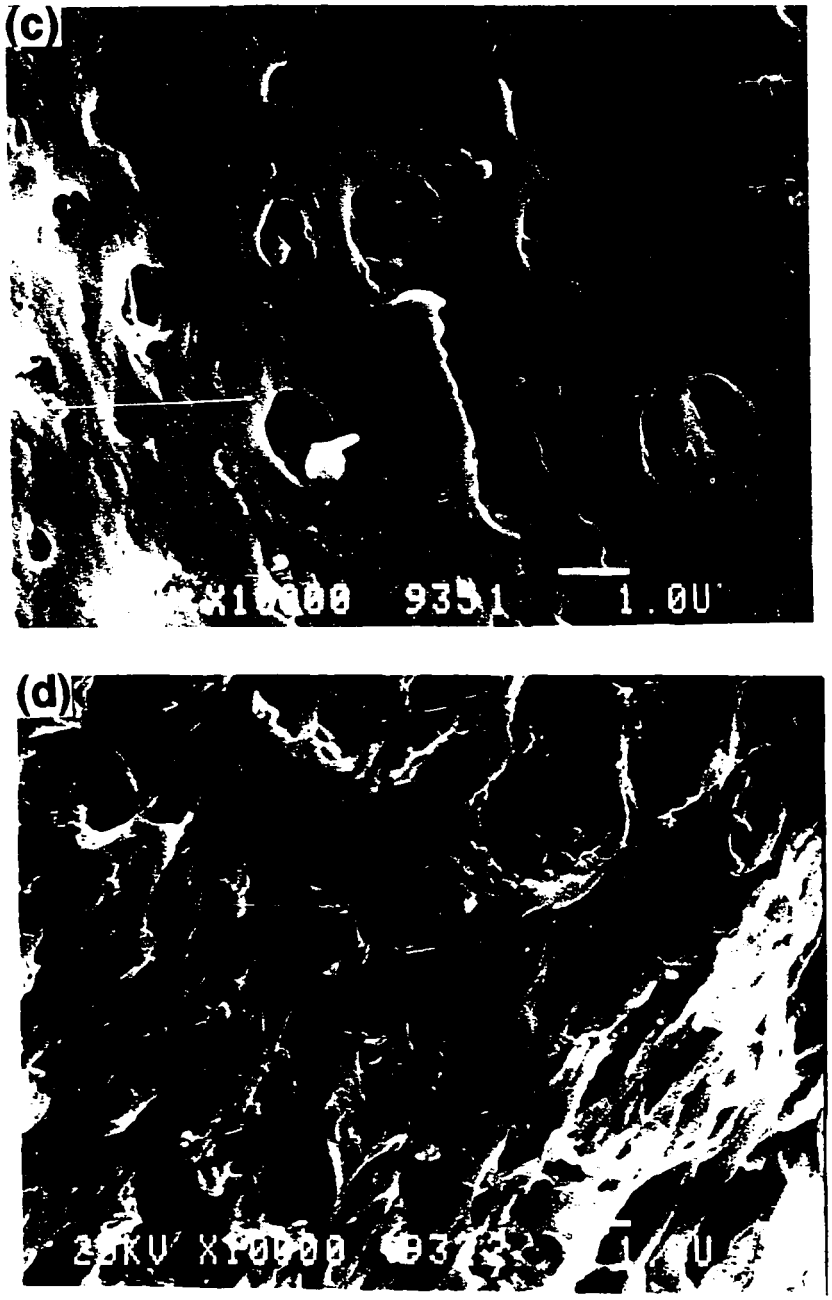


Figure 5. (c)the ductile region near the center, (b) the same area of the matching fracture surface after etching with KOH. The direction of crack propagation was top-to-bottom on the micrographs

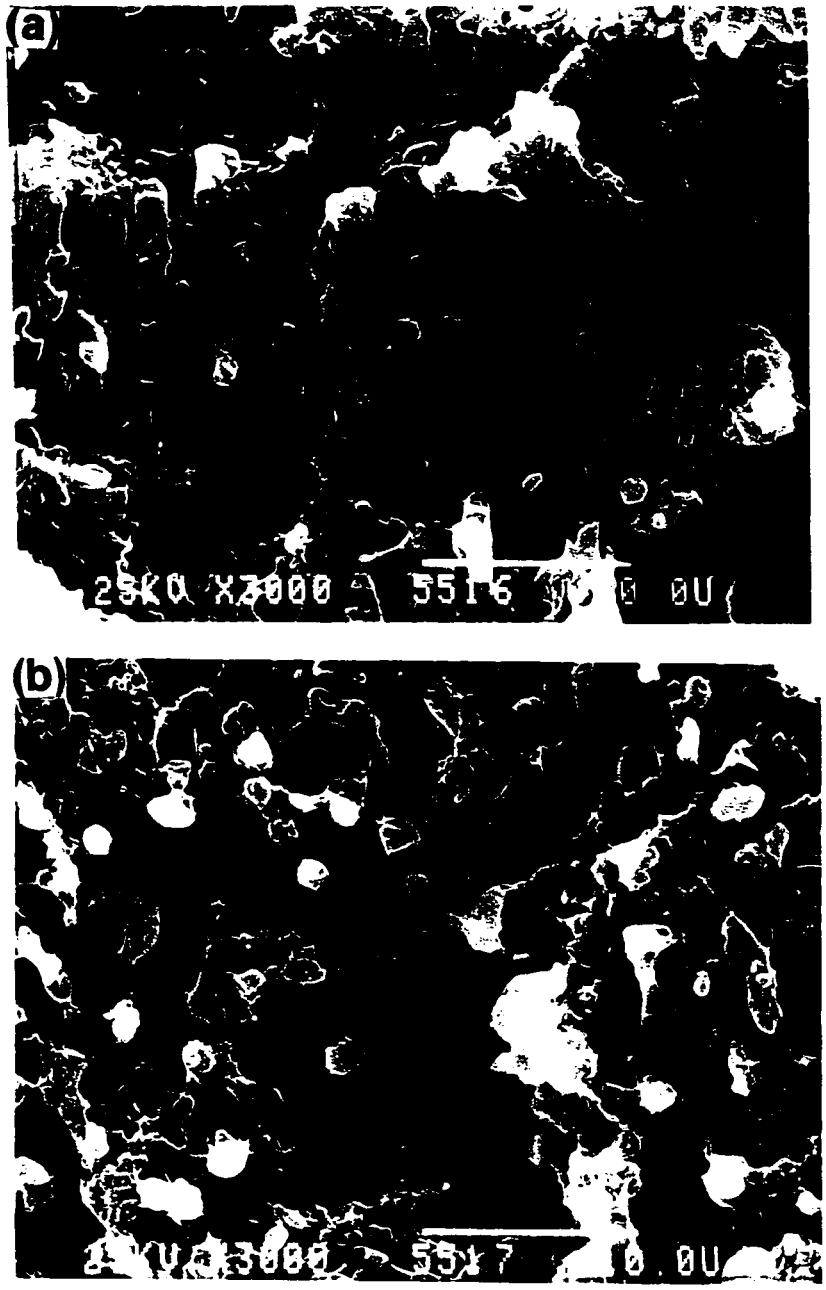


Figure 6. Scanning electron micrographs of a fracture surface of PC/ABS 50/50 obtained at -65°C and a crosshead speed of 229 mm/min. The position of the micrographs are indicated on the inset (a) the featureless brittle fracture brittle fracture region (b)near the tip of the pop-in region

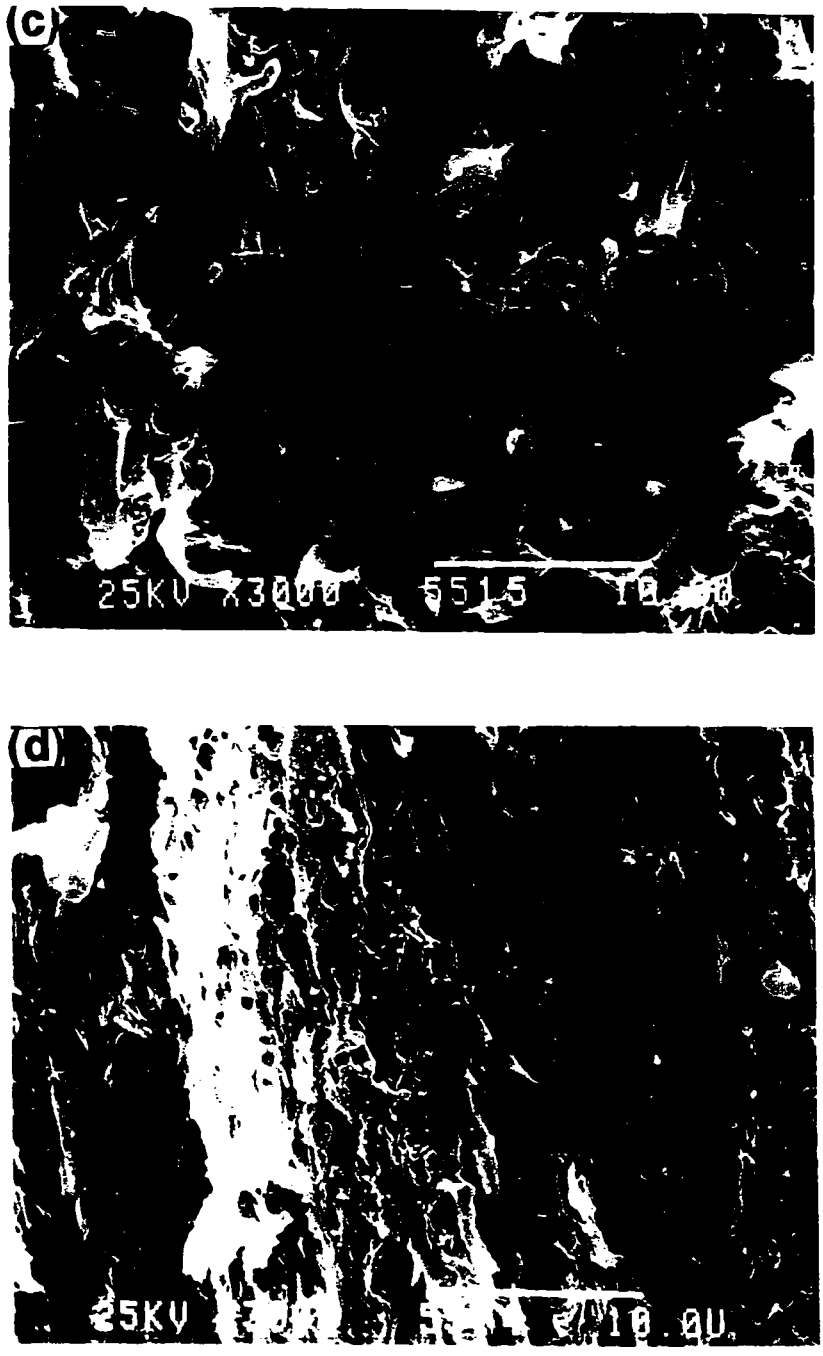


Figure 6. (c)the pop-in region, and (d)the shear lips near the edge. The direction of crack propagation was top-to-bottom on the micrographs

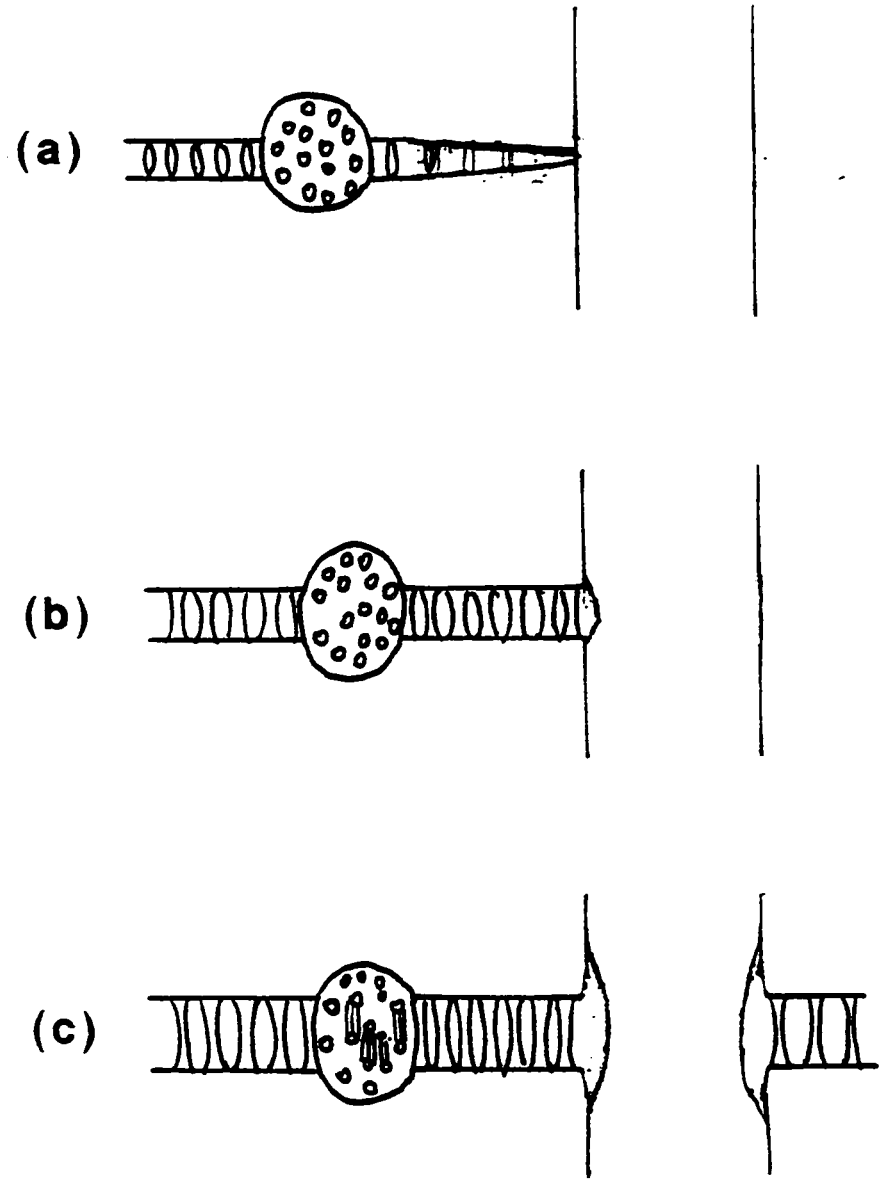


Figure 7. Schematic representation of craze growth in the pop-in region.(a) impingement of a craze on a PC domain to create a local stress concentration, and(b) craze growth and plastic deformation of the PC domain, and (c) crack propagation with local drawing and separation of the PC domain.

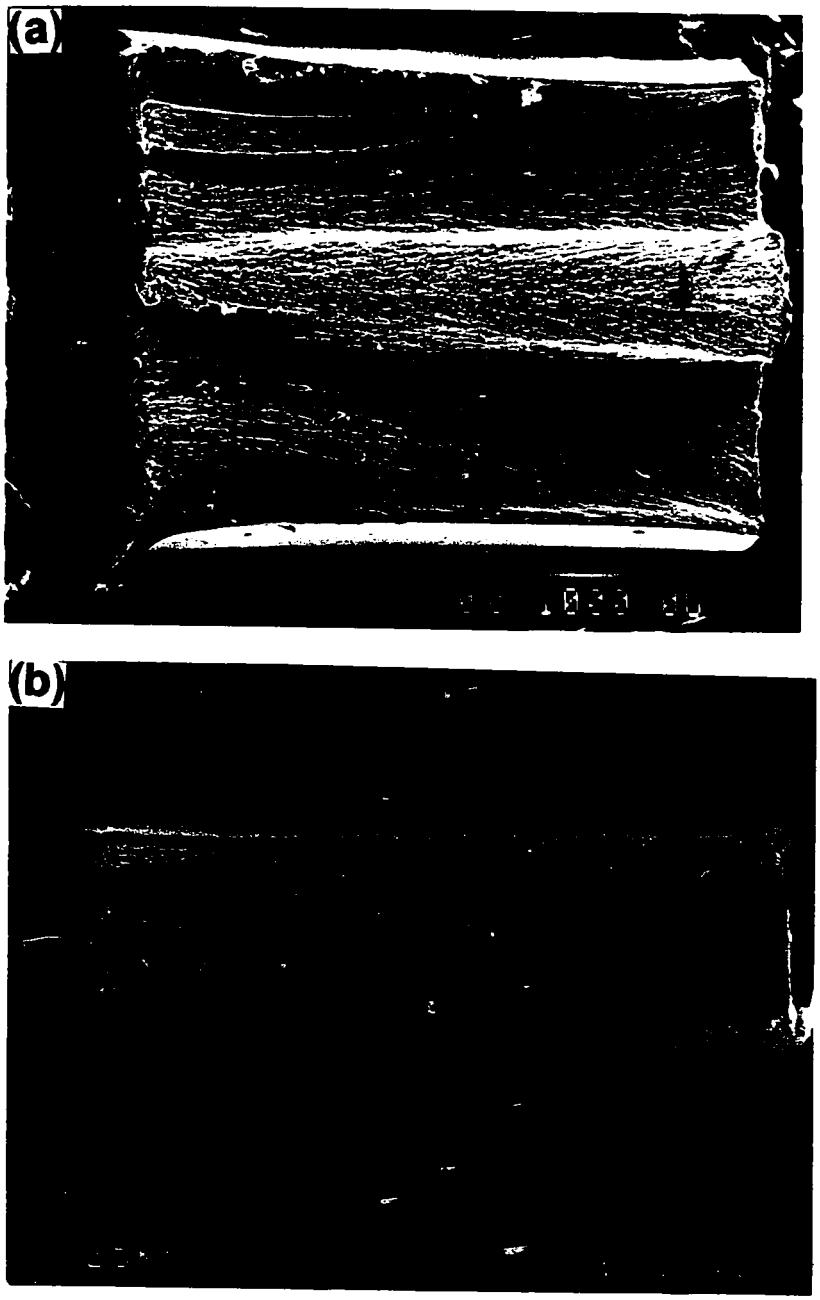


Figure 8. Scanning electron micrographs of fracture surfaces of PC/ABS 50/50 obtained at room temperature with a crosshead speed of 0.1 mm/min. (a)a specimen machined from the entire thickness, (b) a 1mm thick specimen from the center

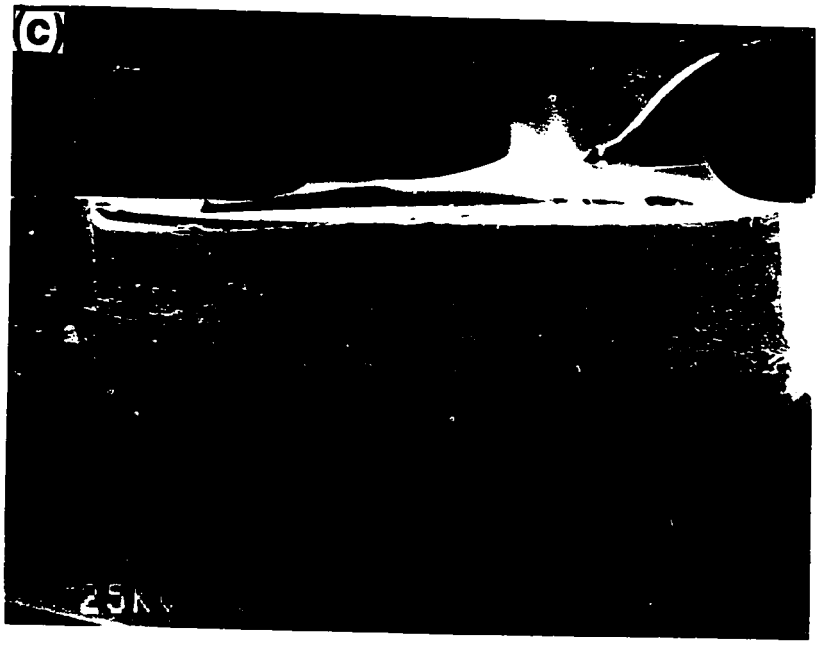


Figure 8. (c) a 1mm thick specimen from the edge

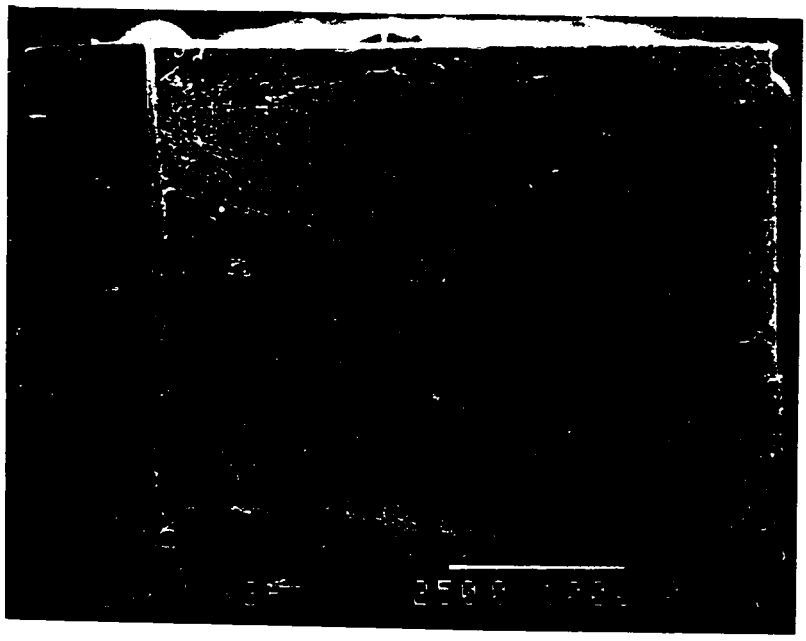

Figure 9 Scanning electron micrograph of the fracture surface of a PC/ABS 50/50 specimen machined perpendicular to the injection direction and tested at -10°C with a crosshead speed of 229mm/min.

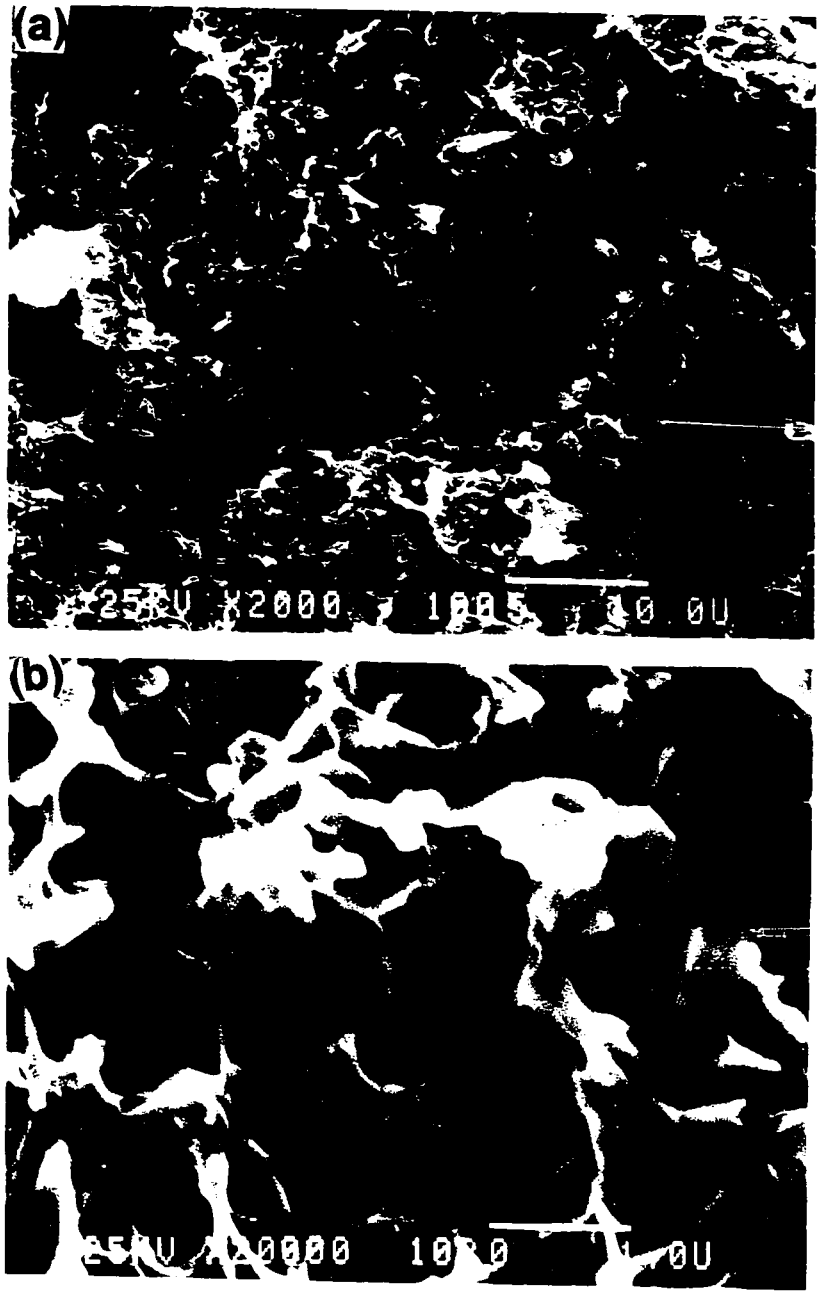


Figure 10. Scanning electron micrographs of the herringbone fracture surface of PC/ABS 30/70 obtained at -25°C and a crosshead speed of 229mm/min.(a) the center ridge of the herringbone, (b) and (c) higher magnification views of (a)

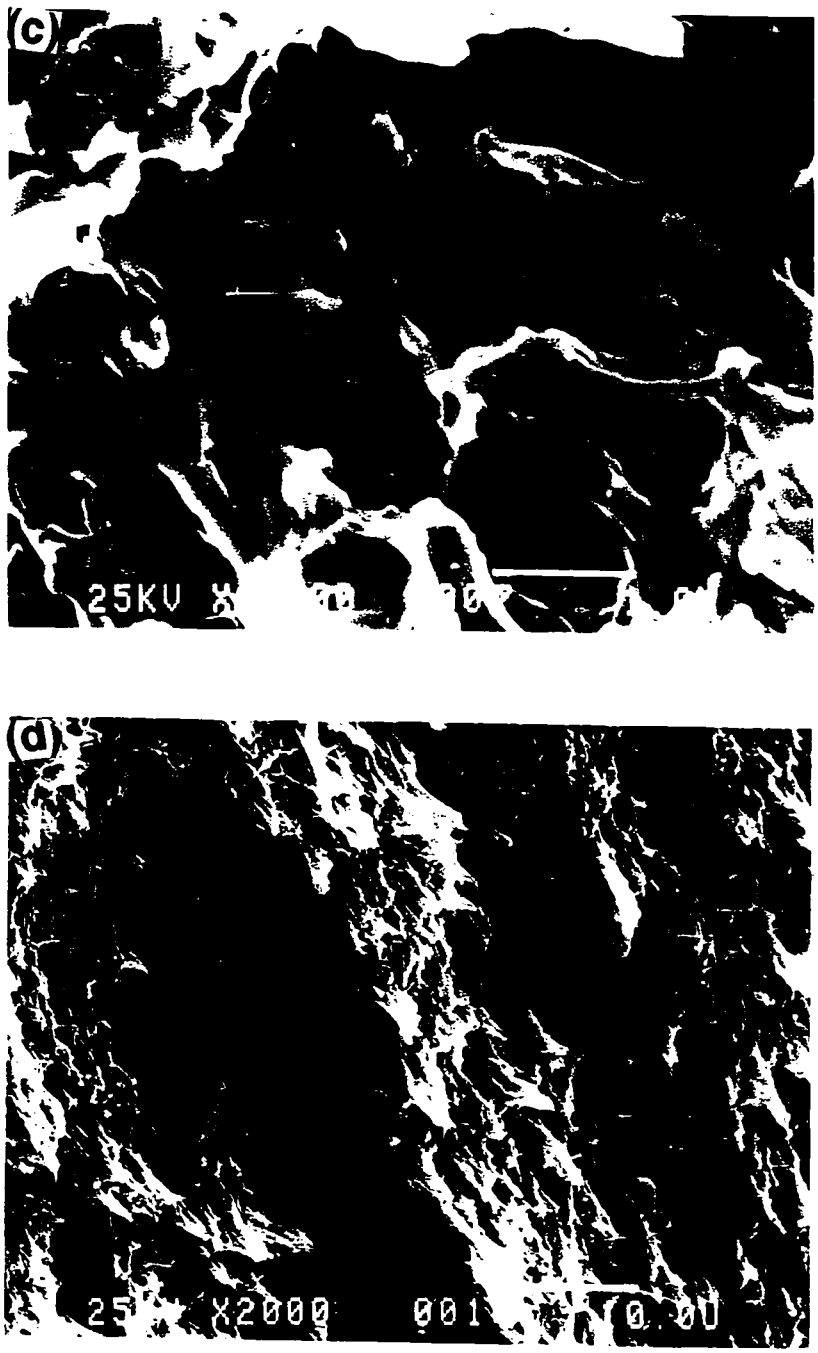


Figure 10. (d) radial ridge of the herringbone pattern. The direction of crack propagation was left-to-right on the micrographs

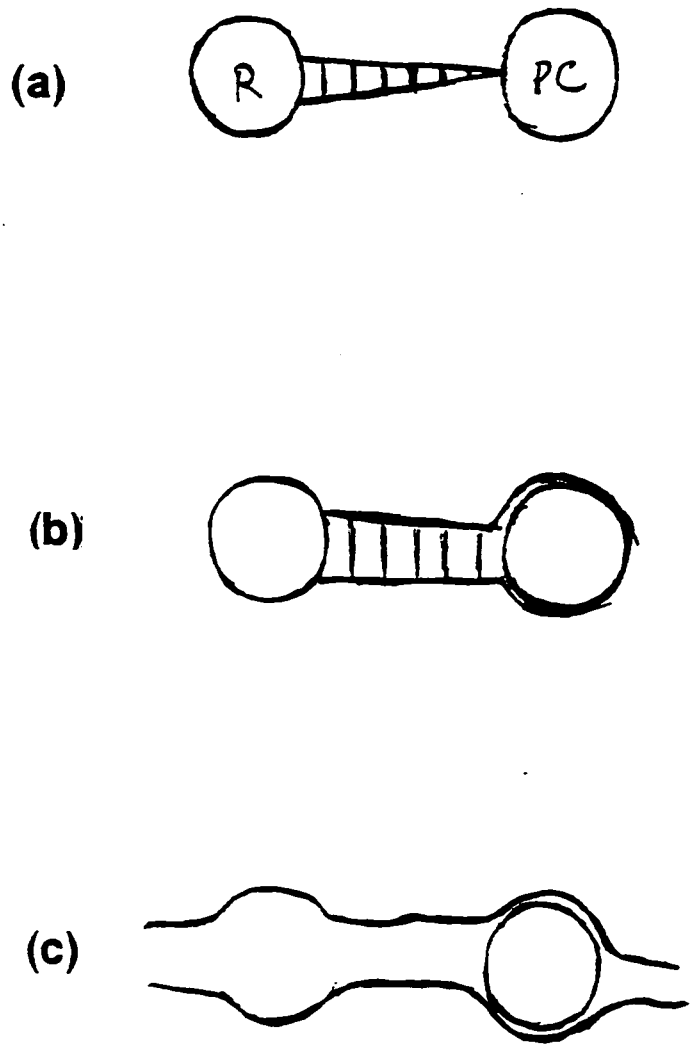


Figure 11. Schematic representation of craze growth in the crack initiation region of the herringbone. (a) impingement of a craze on a PC domain to create a local stress concentration, (b) interfacial separation to create a void, and (c) crack propagation through the void.

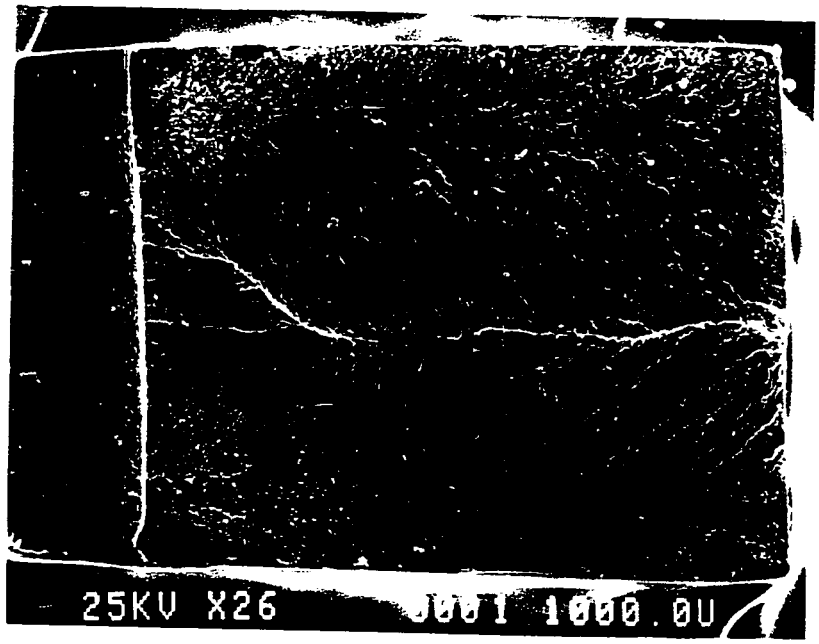


Figure 12. Scanning electron micrograph of the reverse herringbone fracture surface of a PC/ABS 30/70 specimen machined perpendicular to the injection direction and tested at -10°C and a crosshead speed of 229mm/min.

## CHAPTER 4

# THE HERRINGBONE FRACTURE OF A POLYCARBONATE/ABS BLEND

## 1. INTRODUCTION

Fractography is widely used in post-failure analysis of metals and glasses where it is generally possible to identify from the appearance of the surfaces where fracture originated, in which direction it propagated and whether it was ductile or brittle. In a previous paper, the fracture surface markings of injection molded polycarbonate/ABS blends were described as the composition was systematically varied (1). Ductile fracture of blends with 10 to 30 wt. percent PC was characterized by the so-called "chevron" of "herringbone" pattern which has only received passing mention in the plastics literature but has been studied extensively in mild steels (2,3). In particular, the characteristic V-shaped ridges pointing toward the origin of the running crack are associated with fracture of mild steel plate. Although the herringbone pattern was widely considered to be indicative of brittle and therefore unsatisfactory behavior in steel ship plate, even more brittle materials such as cast iron and high-alloy tool steel, do not exhibit the herringbone pattern.

It has been pointed out that many times the markings on fracture surfaces, including the herringbone, can best be explained by multiple fracture initiations that propagate and unite to complete separation. The markings owe their visibility to the existence of sharp changes in level and for this reason are often called level-difference lines. The herringbone pattern observed in sheet is then a particular case where the concentration of fracture initiation sites is along the center line. Shearing observed along the herringbone ridges, suggesting that the fracture lags or hesitates in the final joining up of the crack fronts, is evidence of plastic deformation before and during fracture(4,5).

Fracture behavior of polymers is complicated by flow-induced anisotropy which is a pervasive feature of injection molded pieces. Injection molding of thermoplastics usually produces moldings with some degree of anisotropy due to orientation of the polymer molecules. When the polymer system is a blend of immiscible phases, injection molding can produce another type of anisotropy caused by orientation of the phases along melt flow lines. Thus, elongational flow at the wall produces a skin layer with more or less elongated domains (6-10), while in multiple-gated injection moldings, blends often exhibit especially weak knit or weld lines(11,12). The most dramatic evidence for effects of morphological anisotropy is in the area of fracture phenomena. Anisotropy in the fracture of injection molded

blends is widespread and in extreme cases the strength of injection moldings is more related to melt flow patterns than to bulk material properties. It is the purpose of this paper to examine more closely the fracture behavior of the PC/ABS 30/70 wt. percent blend and in particular to provide an explanation for a herringbone patterned fracture surface as related to the anisotropic phase morphology.

## 2. EXPERIMENTAL

A blend of 70% by weight ABS and 30% by weight polycarbonate (PC) was provided by The Dow Chemical Company in the form of 5in (12.7 cm) x 3in (7.6 cm) x 1/8in (0.3 cm) plaques. The polymer and injection molded condition were described previously (1). Tensile specimens were cut to the ASTM-1708 geometry either parallel or perpendicular to the injection direction. These were subsequently referred to as parallel and perpendicular specimens respectively. A single edge notch (SEN) was machined at the midpoint of the gauge length, the notch was 0.037in (0.094cm) in depth with a 0.010in (0.025cm) notch radius and 45° flank angle.

Tensile tests were carried out in an Instron machine. The crosshead

speed was varied from 0.458 mm/min to 229 mm/min and the test temperature was varied from -70° to 25°C. In some cases crack propagation in the thickness direction was viewed end-on from either the notched or unnotched end with a Panasonic WV-1800 video camera. In other cases an Inframetrics infrared imaging radiometer was focused on either the notched or the unnotched end of the specimen in order to record temperature changes in the thickness direction during fracture. With the Thermoteknix software from Inframetrics Inc., the data were presented in the form of two-dimensional isothermal contours.

Fracture surfaces were examined with an Olympus Model SZH stereoscan optical microscope in the reflection mode, then coated with gold and viewed in a JEM 35CF scanning electron microscope (SEM). Cross-sectional slices 0.5mm thick were cut with a diamond wafering blade from the Buehler Company for viewing in the optical microscope.

For morphology studies, parallel and perpendicular tensile specimens were notched and fractured in the Instron at -70°C with a crosshead speed of 229 mm/min. The specimens were cut and notched in such a way that the location of the fracture surfaces corresponded to the midpoint of the plaque. The cryogenic fracture surfaces were subsequently selectively etched by immersion in 30% by weight aqueous potassium hydroxide for

5 hours to remove the PC phase, then washed in water for 2 hours, dried, coated with gold and examined in the scanning electron microscope (13). Alternatively, some of the etched specimens were stained with a 1 weight percent aqueous solution of osmium tetroxide for 1 week, then coated with gold and examined in a JEOL 840A scanning electron microscope in the backscattered mode. For transmission electron microscopy, specimen blocks cut from the plaque were stained with 1 weight percent aqueous osmium tetroxide for one week at room temperature then sectioned with an RMC MT-6000 ultramicrotome at room temperature. Sections as thin as 60nm were cut in the thickness direction from the region about 0.2 to 0.7mm from the edge. The sections were made with the knife cutting parallel to the injection direction. Sections were placed on copper grids and viewed in a JEOL 100CX transmission electron microscope.

## 3. RESULTS AND DISCUSSION

### 3.1 Stress-Displacement Behavior

SEN specimens of the PC/ABS 30/70 blend were loaded to fracture at various temperatures, -70° to 25°C, and at one temperature -60°C with various crosshead speeds, 0.458 to 229mm/min. Typical curves, Figure 1,

showed significant nonlinearity which usually indicates there is some level of ductility. The maximum stress achieved with specimens cut parallel to the injection direction was in the range of 40-45 MPa. The maximum stress was always lower for specimens cut perpendicular to the injection direction and while there was considerable scatter in this case, no consistent trend with changing temperature was observed. Crack growth began near the maximum stress. With the experimental conditions used to obtain the curves in Figure 1, fracture was virtually instantaneous for the perpendicular specimen, while the stress-displacement curve of the parallel specimen included a region of decreasing stress during which slow crack propagation occurred.

### 3.2. Fractography of Parallel Orientation

The markings on the fracture surfaces of parallel specimens tested at temperatures between room temperature and -20°C were characteristic of the chevron or herringbone pattern that has been described in steel ship plate (2,3). Surface markings consisted of a series of ridges that curved outward from the center towards the edges, Figure 2a. When the temperature was decreased to -25°C the herringbone pattern did not cover the entire surface, Figure 2b. The region furthest from the notch took on a featureless appearance with no stress-whitening that was characteristic

of fast brittle fracture. The length of the herringbone region decreased as the testing conditions became increasingly severe until at the lowest temperature -70°C only the crack initiation region was apparent as an area of stress-whitening at the notch in the center of the fracture surface, Figure 2c.

Although the herringbone has been identified as a brittle fracture mode, it has also been recognized that some level of plastic deformation occurs in the formation of the ridges (4). Further evidence that plastic deformation accompanied the herringbone in the PC/ABS blend was provided by visible stress-whitening of the herringbone region when the fracture surface was viewed from above or from the side. A cross-section of the fracture surface showed that the herringbone pattern did not extend to the edges of the fracture surface. When the fracture surface in Figure 2b was sectioned through the herringbone region about 0.2cm from the notch, shear lips near the edges where the stress state approached plane stress were clearly observed. Stress-whitening within the shear lips away from the fracture surface indicated that these regions experienced more plastic deformation than the center herringbone region.

Early observations on the fracture of steel plate showed that the fracture front at the center proceeds the edges (3,5). The same

characteristic was seen in the PC/ABS blend when the notch was photographed end-on during testing at -60°C with a crosshead speed of 0.5 mm/min. The final frames in Figure 3 taken 0.03 second apart show the notch before fracture initiated, 0.03 second later when fracture had started in the center, and finally complete fracture. From these photographs the average crack speed in the thickness direction in the herringbone region was estimated to be at least 25 mm/sec. A similar experiment was carried out at room temperature with the photographs taken from the unnotched end which was possible in this case because the entire fracture surface was herringbone. The results were the same except that the average crack speed was almost two orders of magnitude slower, approximately 0.4 mm/sec, at the same crosshead speed.

### 3.3. Fractography of Perpendicular Orientation

The fracture surface of a perpendicular specimen also showed the ridges of a herringbone pattern but instead of pointing toward the notch, the ridges pointed away to form a reverse herringbone pattern, Figure 4a. The reverse herringbone pattern covered the entire fracture surface when the temperature was -10°C or higher. When the temperature was decreased to -20°C, the distinct center ridge of the reverse herringbone curved off toward one edge as if one of two simultaneous crack fronts had grown slightly

faster than the other, and about half the surface had a smooth featureless appearance, Figure 4b. At -70°C the fracture surface was characteristic of a more conventional brittle fracture although two areas of stress-whitening at the notch revealed that crack initiation occurred at two locations near the edges, Figure 4c.

This method of notched tensile testing did not produce a sharp ductile-to-brittle transition temperature, rather the transition from herringbone, or reverse herringbone, to fast brittle fracture occurred gradually. Nevertheless, comparison of the fracture surfaces in Figure 4 with those of the parallel specimens in Figure 2 indicted that the blend was slightly less brittle in the parallel geometry when the crack growth was perpendicular to the injection direction.

The reverse herringbone pattern has been obtained when side scratches on a cellulose acetate plate induced the fracture to lead from the edges (2). Evidence that the fracture front proceeded from the edges inward to the center was obtained by careful examination of the Y-shaped center ridge. Figure 5a shows the fracture surface in Figure 4b viewed in the SEM. The center ridge was much more prominent than in the stereo optical micrograph although the ridges and valleys of the reverse herringbone were not as clearly defined. A region of the ridge in Figure 5a

is shown at higher magnification in Figure 5b. It consisted of an abrupt step such as would have occurred when cracks that were growing in different planes met. In this region, the fracture plane at the top of the micrograph was above that at the bottom. Closer to the notch, the situation was reversed as shown in the schematic drawing, Figure 5c. The Y-shape of the center ridge at the notched end suggested that a crack initiated in the center in addition to the cracks that initiated near the edges. Apparently, since the initial crack speed was relatively slow, a center crack had time to start before the crack fronts from the edges met. As the cracks accelerated, the edge cracks dominated while growth of the center crack ceased.

Overall, fracture was much faster when crack propagation was of the reverse herringbone type parallel to the injection direction (perpendicular specimens) than when it was of the herringbone type perpendicular to the injection direction (parallel specimens). In the former case, fracture occurred too rapidly to see by the technique used to obtain the photographs of the parallel specimen in Figure 3, even when relatively mild conditions were used to produce the reverse herringbone pattern over the entire fracture surface (room temperature and a crosshead speed of 0.5 mm/min.). This meant that the average crack speed in the thickness direction exceeded 50 mm/sec, compared to about 0.4 mm/sec for the parallel specimens under the same conditions. The shear lips were at least partially responsible for

the slower crack speed of the parallel specimens. Shear lip formation in the perpendicular specimens was inhibited since crack initiation occurred near the edges.

To confirm the surface initiation of the reverse herringbone in the PC/ABS blends, temperature readings were made from the unnotched end as a specimen was fractured. The infrared temperature profiles in Figure 6 were made at 0.03 sec. intervals as the specimen fractured, the location of fracture was indicated by a temperature rise over the background, The first two profiles show the specimen during fracture; The edge initiation was confirmed by the location of the highest temperature contours near the left edge in Figure 6a and the right edge in Figure 6b. In Figure 6c, where the specimen had fractured completely, the highest temperature was in the center which fractured last. The final result was not caused by faster heat loss from the edges for in a similar experiment with a parallel specimen the highest temperature occurred at the edges after fracture.

### 3.4. Formation of Herringbone and Reverse Herringbone Patterns

This description of the fracture process that created the herringbone pattern used the concepts put forth by Boyd (3) in discussing the similar fracture mode in steel plate. The fracture was discontinuous and proceeded

by initiation of secondary cracks in front of the primary crack so that impingement of the expanding crack fronts created the characteristic radiating ridges. The formation of one ridge is shown schematically in Figure 7a. The primary crack initiated at time $t_1$ and grew radially in all directions. At time $t_2$ a secondary crack initiated on the center line in front of the primary crack. It also grew radially at approximately the same speed as the primary crack. If the secondary crack had not grown at a comparable speed, for example if it had grown more slowly, the main crack would have rapidly overtaken the secondary crack and the pattern of a closed ellipse would have appeared on the fracture surface. The two cracks intersected along a line that extended at an angle outward toward the surface. Since the two cracks grew in slightly different planes, a tearing ridge was formed where they intersected. It has been predicted that the markings should make an angle of 72° with the center line (3). In general, the observed angles have agreed quite well with this prediction as was also the case with the PC/ABS blend where the angle was about 68° except near the edges where the shear lips cut off the herringbone pattern.

Sequential crack initiation along the center line is shown in Figure 7b. The n-th branch of the herringbone markings was formed by the intersection of the n-th and $n+1$-th crack fronts initiated at times $t_n$ and $t_{n+1}$ respectively. If n was large enough and the initiation sites were close

enough, the crack front could be considered as a parabolic envelope enclosing many discrete cracks all growing radially. It has been pointed out that in some cases, when a critical crack width is reached, shearing can occur at the surfaces to create the shear lips that were observed along with the herringbone in the PC/ABS blends (3,5).

As pointed out above, although the herringbone is sometimes considered a brittle fracture mode, the crack speed was slowed somewhat by a level of plastic deformation. As the test speed was increased or the temperature decreased, this level of ductility was lost and the crack speed increased until it was too fast for secondary cracks to initiate and grow. The critical point was identified on the fracture surfaces by the transition from the herringbone to the markings of parabolic crack front. The location of this transition moved closed to the notch as the test conditions became more severe.

Formation of the reverse herringbone pattern occurred by a similar mechanism except that the multiple initiation sites occurred near the edges of the specimen. Figure 8a shows schematically how the primary and secondary cracks impinged to produce a radial ridge of the reverse herringbone. In this case, the crack front could be considered a combination of the opposite halves of two parabolic crack fronts, Figure 8b. The center

ridge was formed where the two crack fronts, which might have been growing in slightly different planes, met. When the initiation time was insignificant compared to the overall crack speed, simultaneous growth of two crack fronts produced a symmetrical reverse herringbone pattern. However when the temperature decreased into the ductile-to-brittle transition region and the crack speed correspondingly increased, the reverse herringbone became asymmetric as in Figure 4b if the two cracks initiated at slightly different times or if one crack propagated slightly faster than the other.

## 3.5. Morphology

Typical unetched cryogenic fracture surfaces from the middle of the plaque show views parallel to the injection direction from the center and near the edge, Figures 9a and b. In the center of the plaque the PC formed more or less spherical domains about 1 micron or less in diameter, while near the edge the PC domains were highly elongated in the injection direction. Separation of the phases that was apparent in the micrographs suggested that the dewetting occurred during the fracture.

Etched surfaces from four positions through the thickness in Figure 10 show views parallel and perpendicular to the injection direction. Near

the center, Figures 10a and e, the morphology appeared the same in the two directions with spherical holes where the PC domains were etched away. The holes were the same size, 1 micron or less, as the spherical domains in Figure 9a. Toward the edge the holes which revealed the size and shape of the PC domains were thinner and elongated in the injection direction. This was particularly apparent in the views parallel to the injection direction, Figures 10c and d. The holes were less elongated when viewed perpendicular to the injection direction. Even in Figure 10g, which shows a region only 0.5mm from the edge, the PC domains appeared from the shape of the holes to be more or less circular in cross-section although the diameter had decreased to correspond to the width of the elongated holes in Figure 10c. In this region of the plaque it appeared that the PC domains were predominantly fibrillar or rod-shaped and oriented in the injection direction. In the view perpendicular to the injection direction closest to the edge, Figure 10h, most of the holes were elongated which suggested that close to the edge the PC domains were lamellar or sheet-like as well as rod-shaped. Not shown in the micrographs was a featureless outer layer which extended less than 0.1 mm inward from the edge. Although in this region no domain morphology on the micron size scale was revealed by etching the fracture surfaces, when the mold-contacting edge of the plaque was etched, very long, thin rod-shaped domains of PC about 0.05 micron or less in diameter were observed, Figure 11.

A three-dimensional model of the PC morphology, Figure 12, was constructed from the morphological observations. It shows the more-or-less isotropic morphology in the center region with spherical PC domains 1 micron or less in diameter dispersed in the ABS matrix. Toward the edge the PC domains became elongated in the injection direction and close to the edge took on a sheet-like shape. This model is similar to that described for injection molded polypropylene blends (6) although the distinct gradient in concentration of the dispersed phase through the thickness of the polypropylene blend was not readily apparent in the PC/ABS blend.

The ABS phase was not homogeneous; the composite rubber particles were evident in stained sections viewed in the transmission electron microscope, Figure 13a. Only composite particles were observed, these were fairly uniform in size with a diameter of about 0.7 to 1 micron. Very near the edge, the rubber particles were slightly elongated, Figure 13b. The size and shape of the rubber particles at various locations through the thickness were determined by viewing $OsO_4$-stained cryogenic fracture surfaces in the SEM in the backscattered mode. Only in a very narrow region that extended about 50 microns inward from the edge were the rubber particles slightly elongated in the injection direction; through the remainder of the plaque thickness the rubber particles were spherical.

The length to width ratio of the PC domains and the composite rubber particles, Figure 14, shows the change in shape through the thickness at the midpoint of the plaque. There was a very thin skin region of about 50 microns where the PC domains had on the average a very high aspect ratio and the rubber particles were also elongated. This region was produced when the melt at the front of the fountain flow pattern contacted the cold mold surface and solidified immediately. Crosslinking in the rubber particles prevented them from being more extended, but the PC domains were highly drawn under the elongational flow at the melt front. Behind the melt front, the PC domains were elongated by shear flow in the mold or elongational flow in the gate entrance region. The gradient in aspect ratio through the plaque depended on the shear rate profile through the thickness, which determined the amount of elongation in the melt, and the cooling rate after mold filling, which controlled the amount of melt relaxation before solidification. Under the conditions used in this study, these factors produced a region that extended from the skin about 0.7mm or half way to the center where the PC domains were extended with an average aspect ratio of about 12; in this region, the rubber particles were spherical. The morphology in the center half of the thickness was isotropic with spherical PC domains.

### 3.6. Microstructure of Fracture Surfaces

Deformation at the size scale of the domains in this compatible blend was observed when fracture surfaces were viewed at higher magnification in the SEM. The fracture surface of the parallel specimen tested at -25°C with a crosshead speed of 229 mm/min in Figure 2b had a herringbone region adjacent to the notch and further away from the notch, a featureless region of brittle fracture. The brittle region was indistinguishable from the -70°C fracture surface, Figures 10a and b, and showed the undeformed domain morphology including occasional separation of the PC particles from the ABS continuous phase. At higher magnification, undeformed composite rubber particles of the ABS were also discernable. Closer to the notch, a view of the multiple crack initiation zone at the center of the herringbone region, Figure 15a, revealed spherical cavitated rubber particles, Figure 15b, as well as cavitation of the matrix around the PC domains, Figure 15c. In this views, the plastically deformed matrix was not adhered to the PC particles which retained their more or less spherical shape. A radial ridge of the herringbone away from the initiation zone, Figure 15d, showed obliquely slanted peaks characteristic of shear or tear failure (16). In general the rubber particles were obscured by the pulled-out ABS and only occasionally was a cavitated rubber particle that had been pulled along the tear direction visible.

The domain morphology was essentially isotropic in the center, so

similar triaxial stress conditions would have been required to initiate a crack in the center regardless of whether the specimen orientation were parallel or perpendicular. The consistently lower failure stress of the perpendicular specimens suggested that fracture initiated at a weaker site before the required conditions were achieved at the center. The perpendicular fracture surface obtained at -70°C, Figure 4c, had two small stress-whitened regions about 0.45mm in from the edges which marked the fracture initiation sites. The stress-whitening was produced by profuse cavitation, Figure 16a. The pulled-out tufts of material were composed of ABS because they were not removed by etching. Cavitated rubber particles were seen in this region at higher resolution, Figure 16b, and in addition, rod-shaped holes that corresponded to the size of the PC domains suggested that interfacial separation had occurred. This specimen had an otherwise featureless brittle fracture surface.

An example of a ductile fracture where the entire fracture surface was the reverse herringbone was the perpendicular specimen tested at -10°C and a crosshead speed of 229 mm/min, Figure 5a. This fracture surface also had two stress-whitened regions near the edges where cracks initiated but in this case they were somewhat larger. Higher resolution showed essentially the same features as the crack initiation region of the -70°C fracture surface. The plastic deformation did not extend into the

crack propagation region of the reverse herringbone. When the ridges of the reverse herringbone were viewed at higher magnification their appearance at th size scale of the domain morphology was indistinguishable from the brittle fracture surface in Figure 9a with undeformed rubber particles; separation of the undeformed phases was also observed.

Since fracture would not have initiated at this unusual site in an isotropic material, some feature of the anisotropic domain morphology resulted in weakness in the perpendicular orientation near the edges that caused premature crack initiation at this location. The major anisotropic feature of these blends was the morphology of the PC domains especially toward the edges where they were elongated in the injection direction. The microscopic evidence suggested that the initial event in crack initiation was separation of the interface between ABS and PC to create a site at which a void could grow and eventually coalesce with other voids to initiate a crack. When the fracture occurred parallel to the injection direction, the interfacial area in the crack plane was greater near the edges where the PC domains were elongated, than at the center where the domains were spherical. Although the elongated shape of the PC domains facilitated crack initiation, the precise location of crack initiation was not where the PC domains had the highest aspect ratio, which was near the mold surface, but approximately 0.45mm inward from the edge where the condition would

have been closer to plane stress and the triaxiality would have increased the tendency toward cavitation. When the crack initiated and the crack speed was slow enough, deformation around the crack occurred by cavitation of rubber particles and pull-out of the ABS phase to create the stress-whitened zones that marked the sites of crack initiation. As the crack speeded up, rubber cavitation ceased and on the remainder of the fracture surface interfacial separation of the domains was observed but the rubber particles were undeformed.

From the evidence provided by the fracture surfaces, crack initiation appeared to be essentially the same for both parallel and perpendicular fractures with separation at the interface between PC and ABS phases, cavitation of the rubber particles and, especially at the higher temperatures, some pull-out of the ABS. In the perpendicular specimens, once the crack had initiated it grew rapidly inward toward the center plane strain region, Figure 17. The rough estimates of crack speed indicated that propagation under these conditions was much faster than when the crack initiated in the center. In the latter case, as the crack grew toward the edge, it encountered the skin region where the elongated PC domains were oriented perpendicular to the advancing crack front, Figure 17. This would have had a crack blunting effect (19). Additionally, as the crack neared the edges, shear lips formed where the conditions approached plane stress and this

would have further slowed the crack. Although the difference in crack speed of parallel and perpendicular specimens was expected, it was nevertheless noteworthy that it was clearly evident on the fracture surfaces. While the crack initiation region showed cavitation and plastic deformation of the matrix in both cases, the ridges and valleys of the reverse herringbone had the appearance of brittle fracture while those of the herringbone revealed ductile tearing fracture.

## 4. CONCLUSIONS

A fractographic and morphological study led to the following conclusions regarding the fracture of an injection molded blend of PC and ABS :

1. Fracture of a PC/ABS 30/70 blend occurred by a herringbone mechanism perpendicular to the injection direction and by a reverse herringbone mechanism when fracture occurred parallel to the injection direction. The blend was somewhat less tough in the latter configuration.

2. The herringbone pattern arose from interaction of the main crack with secondary cracks initiated along the center line. Reverse herringbone

fracture occurred by a similar mechanism but crack initiation occurred near the edges.

3. Directional differences in the fracture behavior were attributed to the processing induced oriented skin morphology.

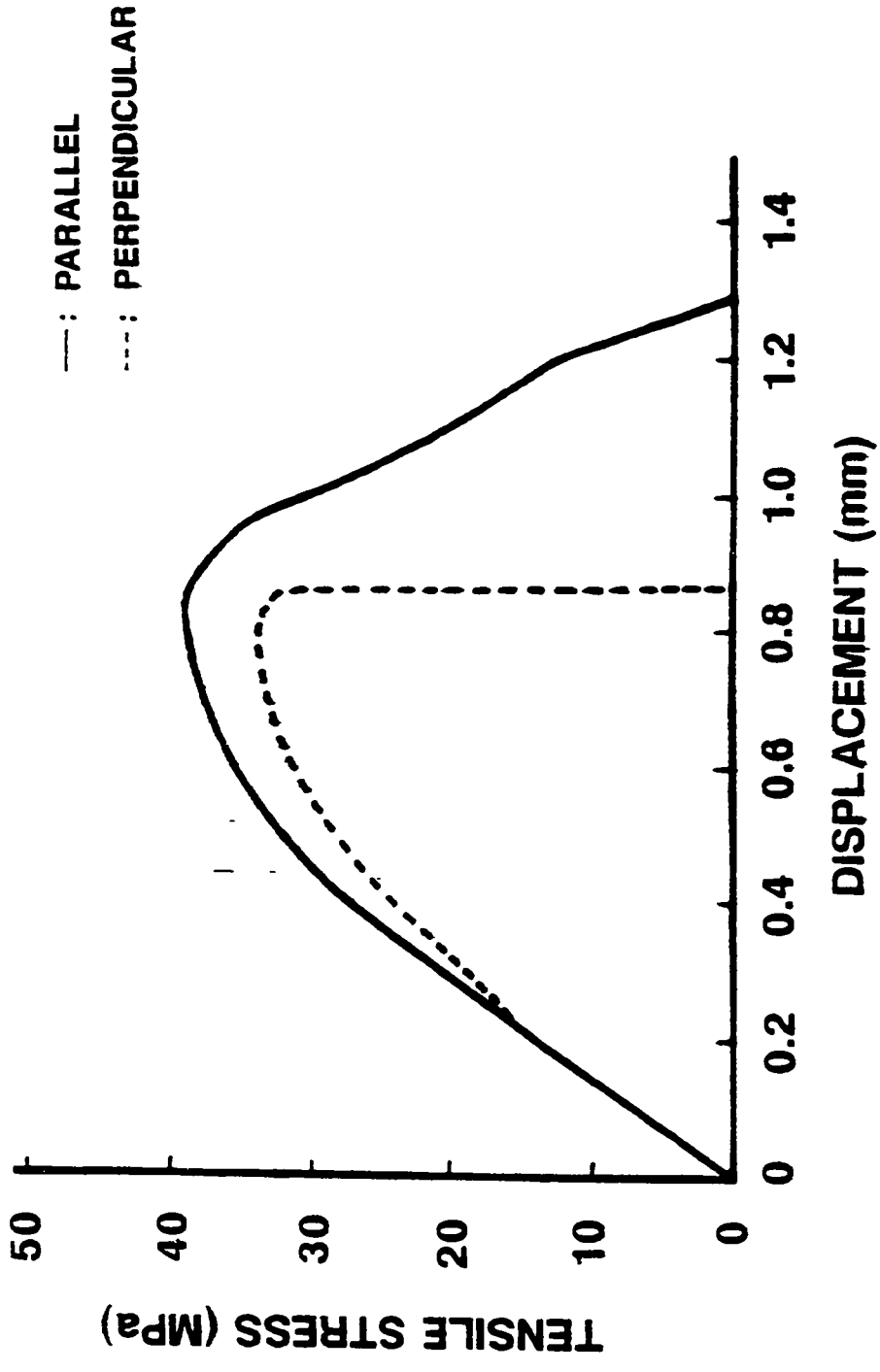


Figure 1. Typical stress-displacement curves for parallel (solid line) and perpendicular (dashed line) specimens tested at room temperature with a crosshead speed of 0.5mm/min.

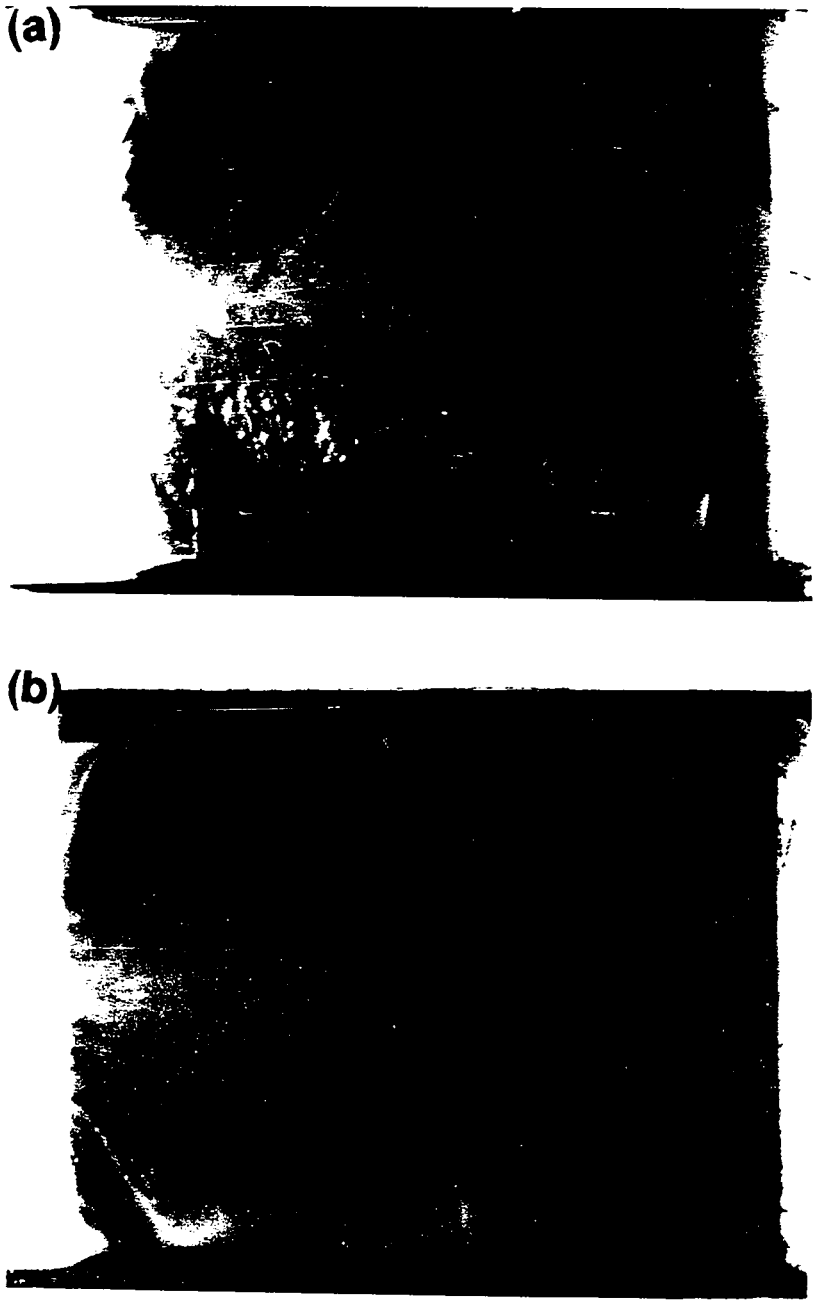


Figure 2. Typical fracture surfaces of parallel specimens tested at a crosshead speed of 229mm/min and various temperatures: (a) and (b)stereoscan optical micrographs at -20° C and -25° C respectively. The crack propagated from left to right

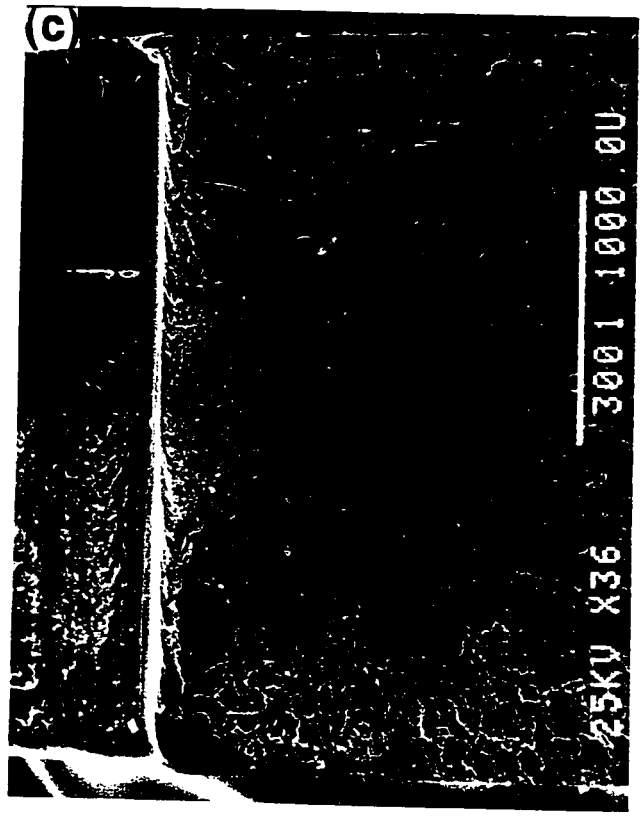


Figure 2. Typical fracture surfaces of parallel specimens tested at a crosshead speed of 229mm/min and various temperatures : (c) scanning electron micrograph at -70°C. The crack propagated from left to right

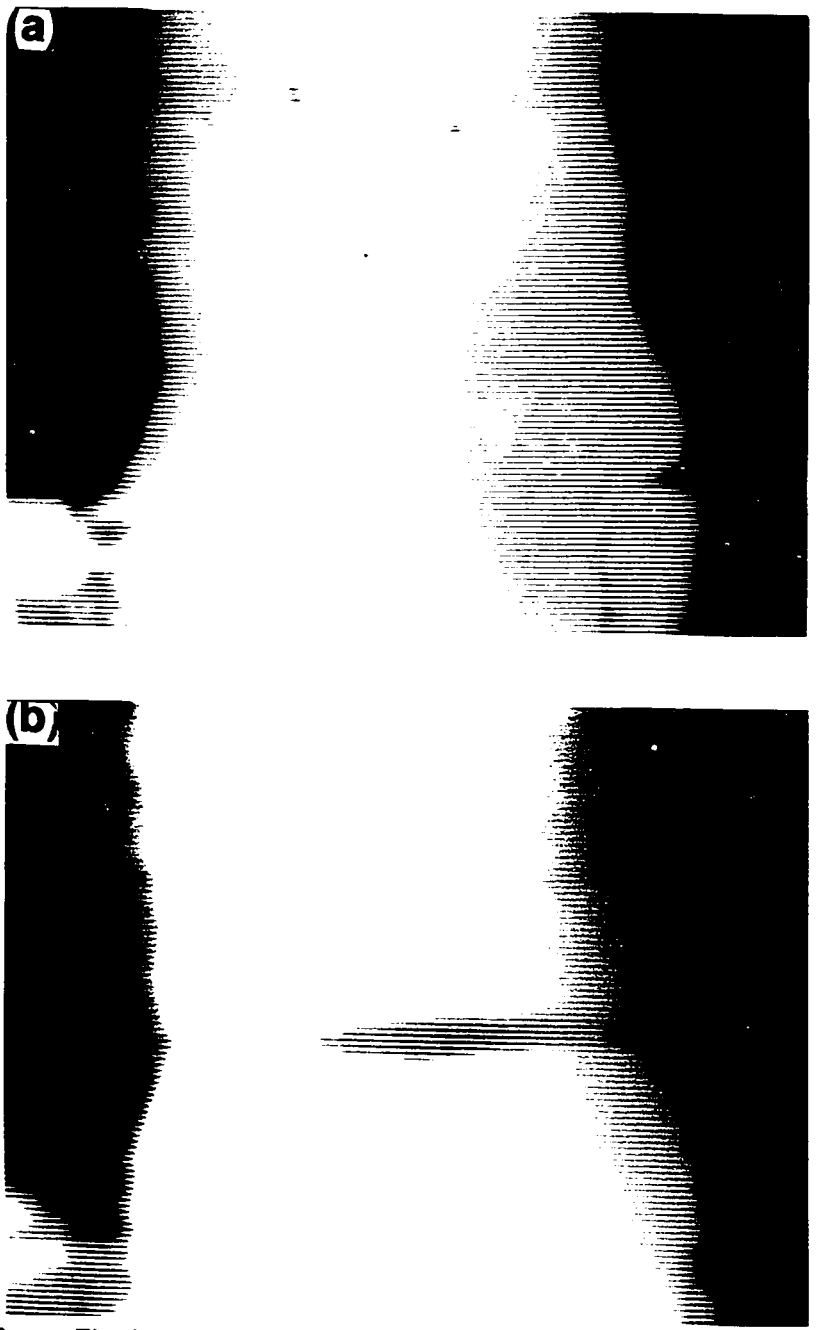


Figure 3. Final three frames showing fracture of a parallel specimen viewed end-on from the notched end. Testing was carried out at -60°C with a crosshead speed of 0.5 mm/min: (a) 0.06sec before complete fracture.(b)0.03sec before complete fracture

Figure 3. Final three frames showing fracture of a parallel specimen viewed end-on from the notched end, (c) fracture

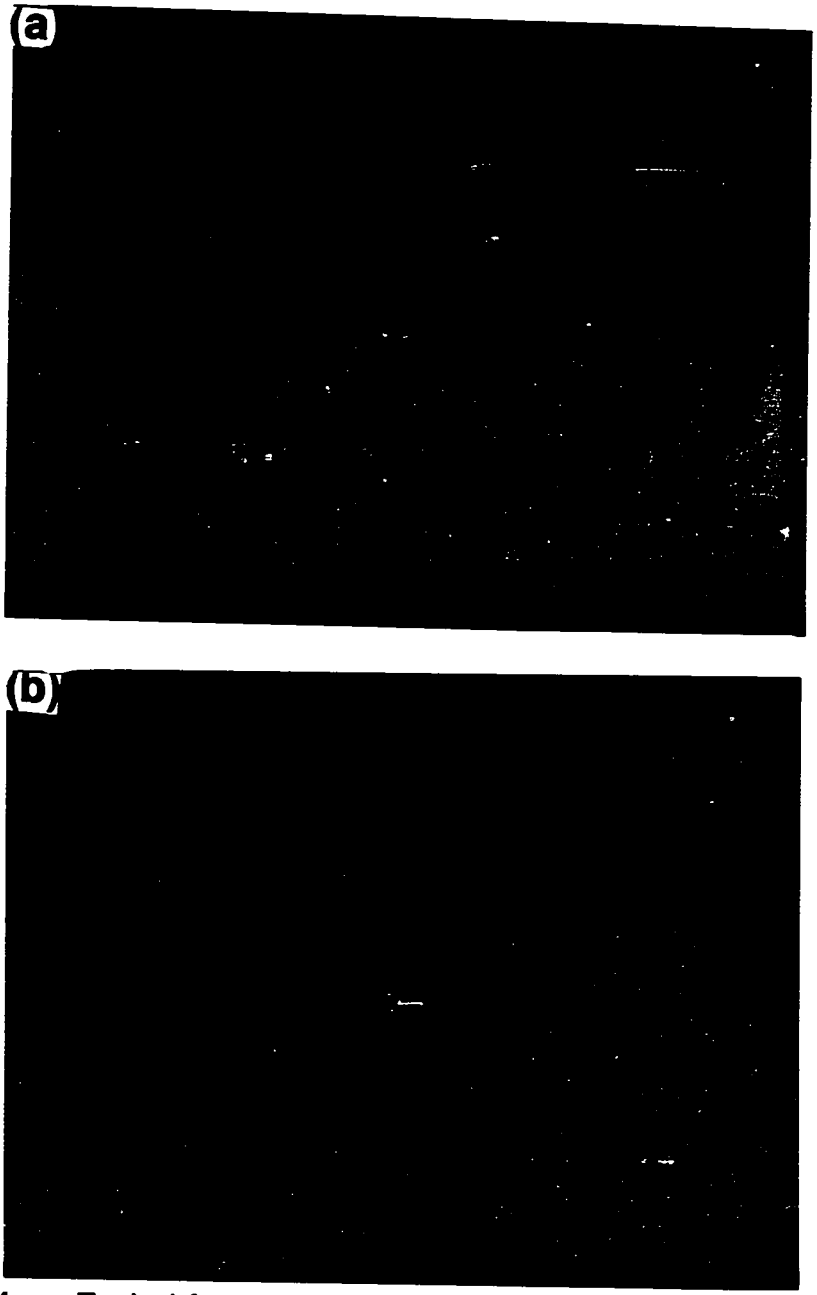


Figure 4. Typical fracture surface of perpendicular specimens tested at a crosshead speed of 229mm/min and various temperatures: (a) and (b) stereoscan optical micrographs at -10°C and -20°C respectively

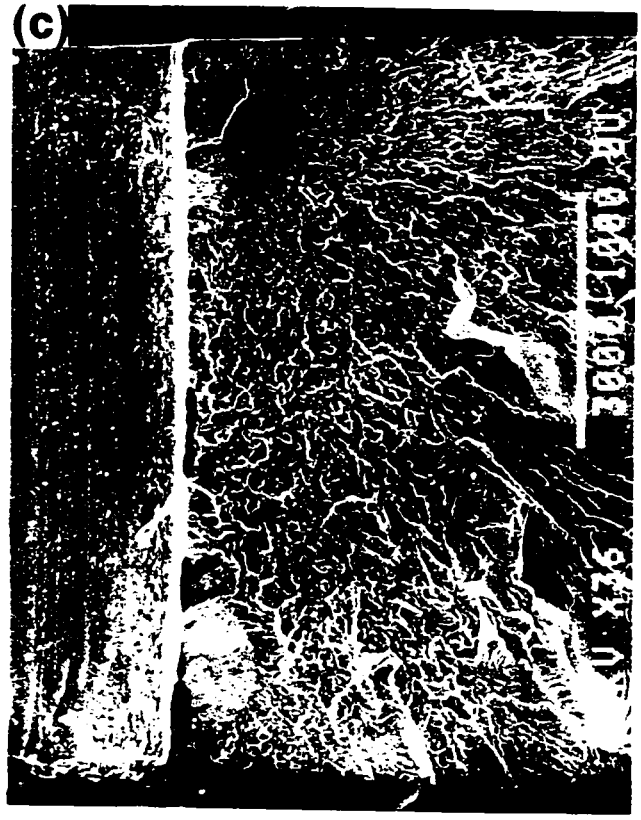


Figure 4. Typical fracture surfaces of perpendicular specimens tested at a crosshead speed of 229 mm/min and various temperatures (c) scanning electron micrograph at -70°C. The crack propagated from left to right

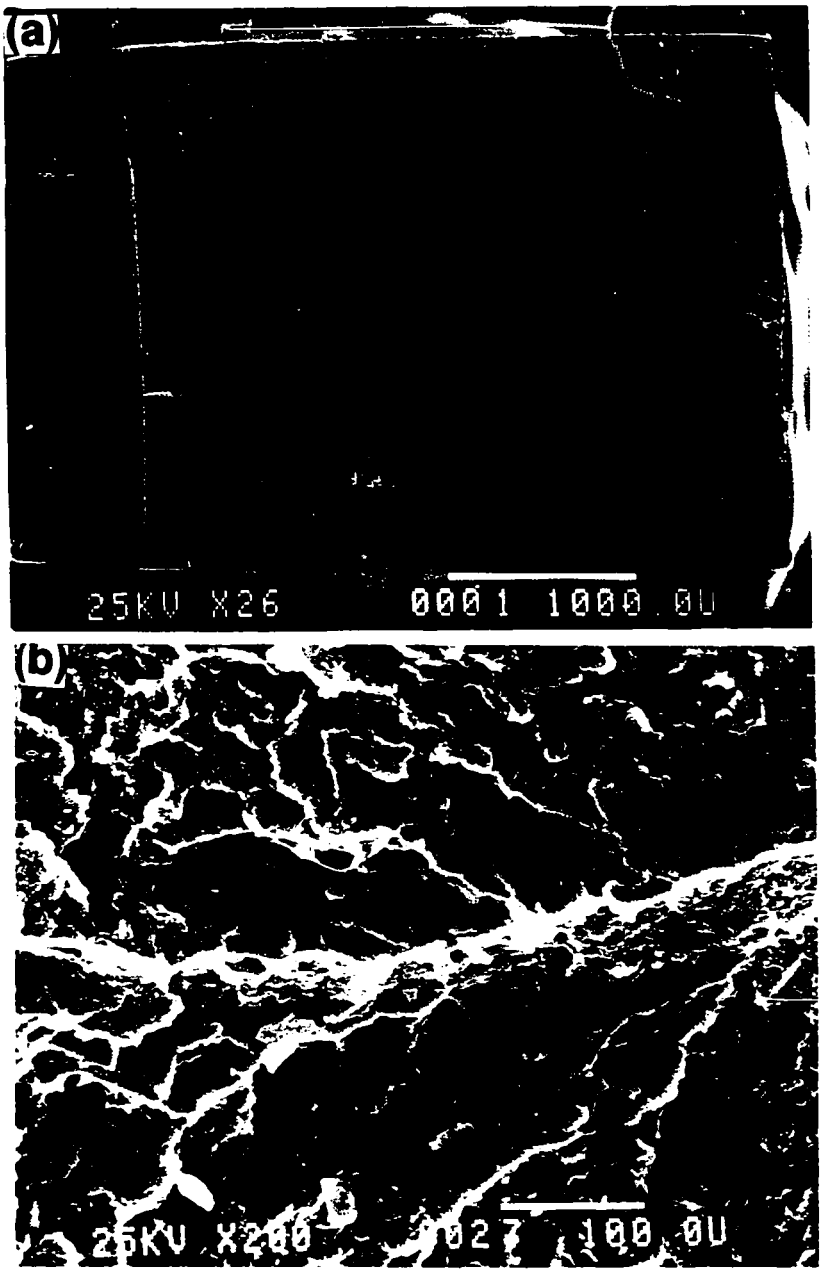


Figure 5. The reverse herringbone pattern: (a) the fracture surface in Figure 4a of a perpendicular specimen tested at -10°C with a crosshead speed of 229mm/min as viewed in the SEM, (b)a higher magnification of the center ridge region indicated in (a)

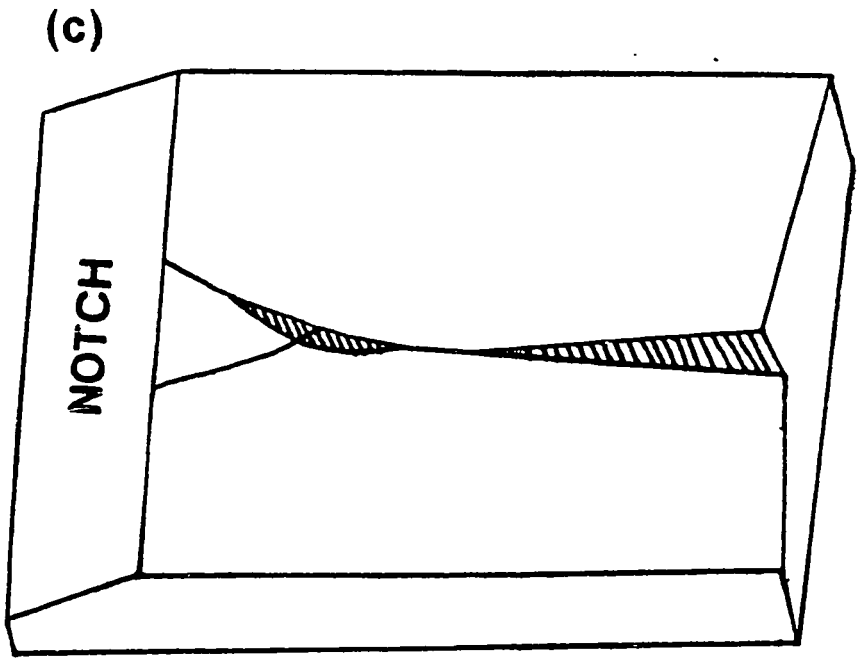


Figure 5. The reverse herringbone pattern: (c) a schematic representation of the center ridge

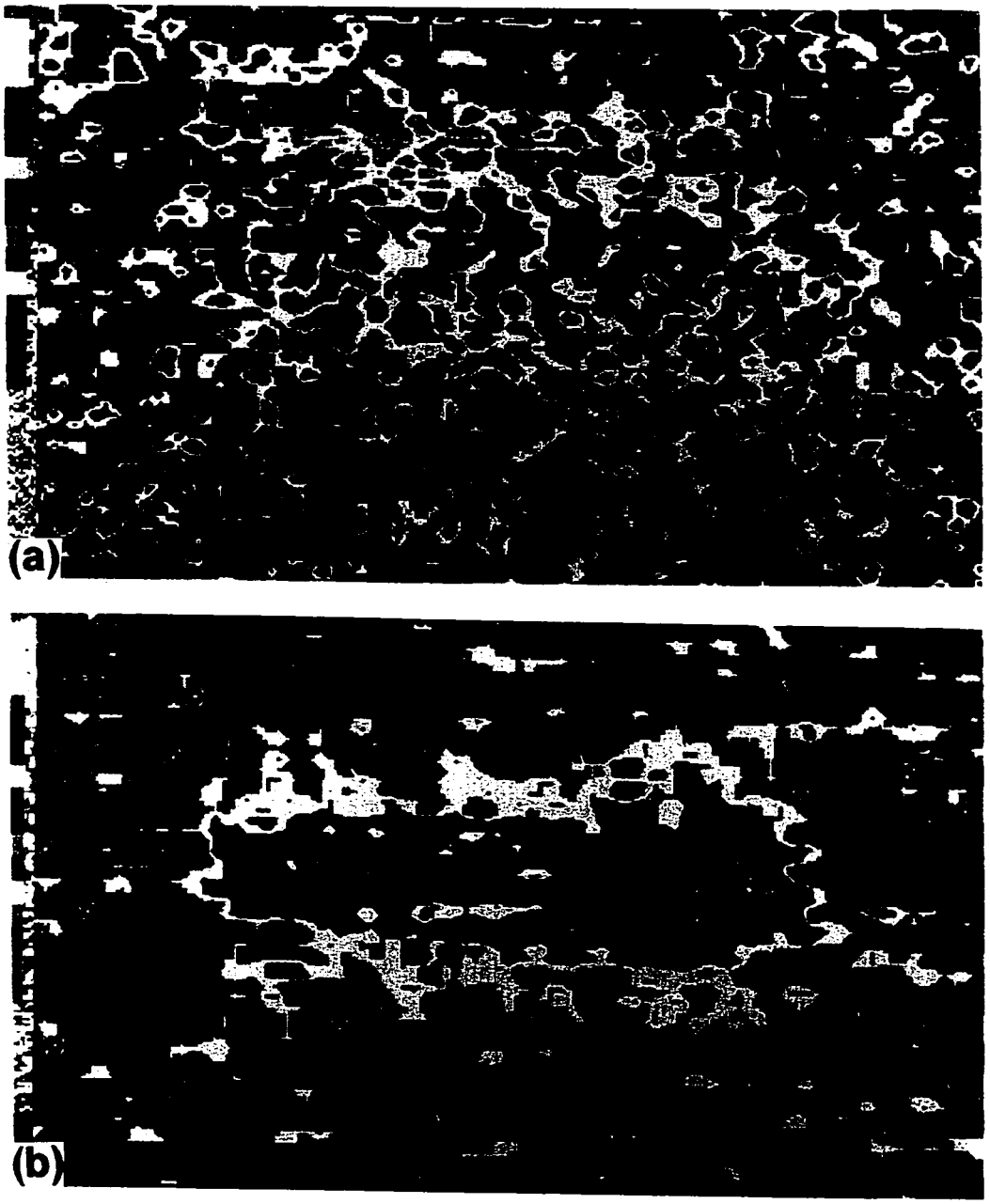


Figure 6. Temperature contours showing fracture of a perpendicular specimen viewed end-on from the unnotched end. Testing was carried out at room temperature with a crosshead speed of 0.5 mm/min. Each color on the scale to left of the thermogram represents a temperature increment of 0.5°C : (a)0.06sec before complete fracture, (b) 0.03 sec before complete fracture

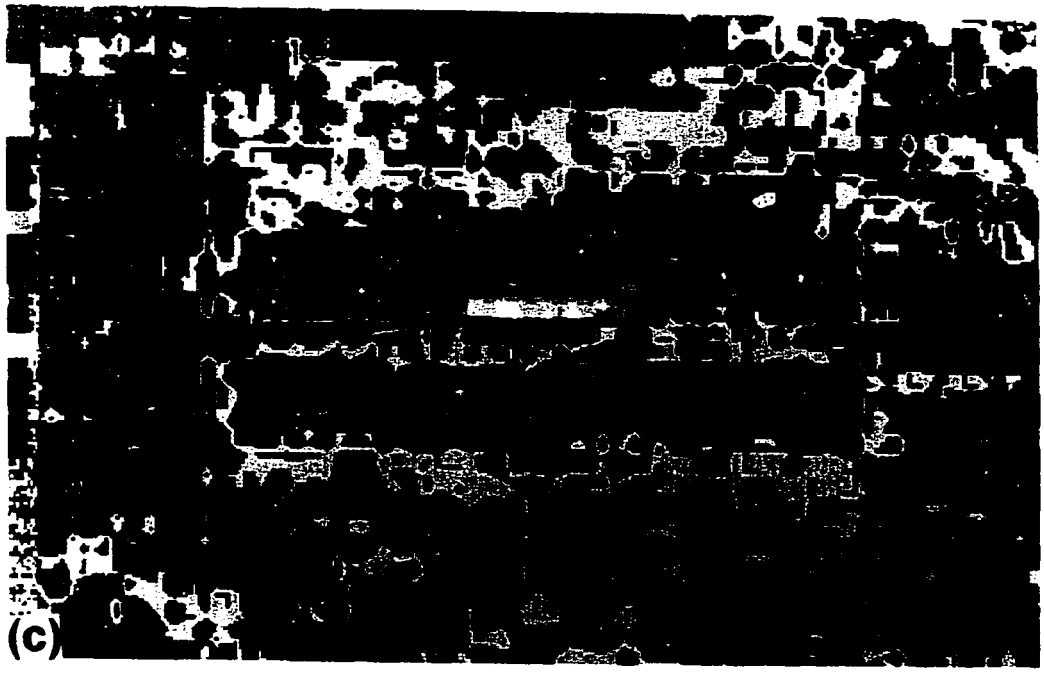


Figure 6. Temperature contours showing fracture of a perpendicular specimen viewed end-on from the unnotched end. Each color on the scale to left of the thermogram represents a temperature increment of 0.5°C :(c) fracture, the arrow indicates the region of highest temperature.

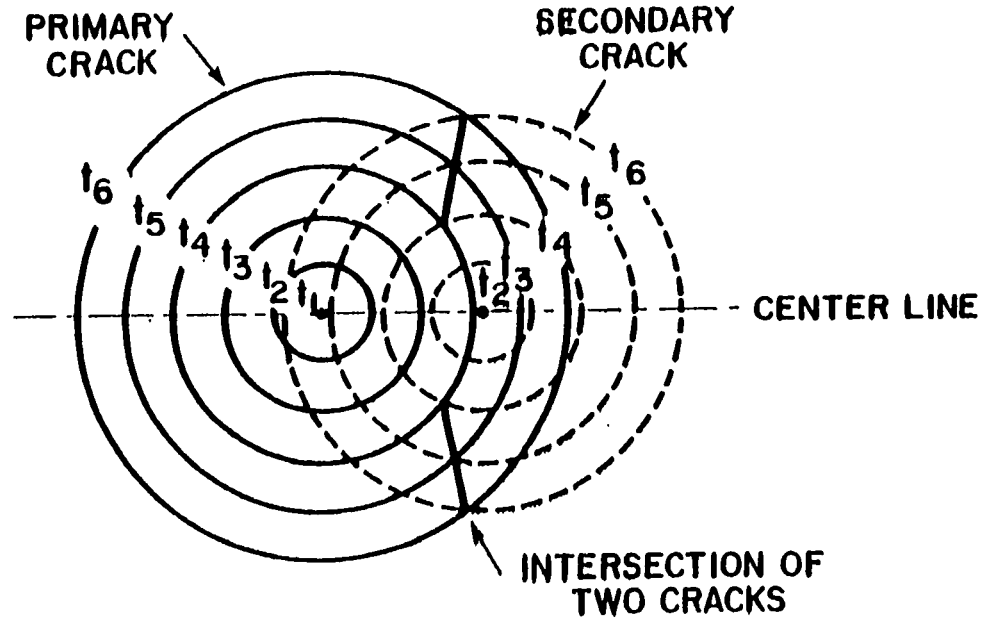


Figure 7. Proposed mechanism for formation of the herringbone pattern: (a) schematic representation of formation of one pair of radial marking

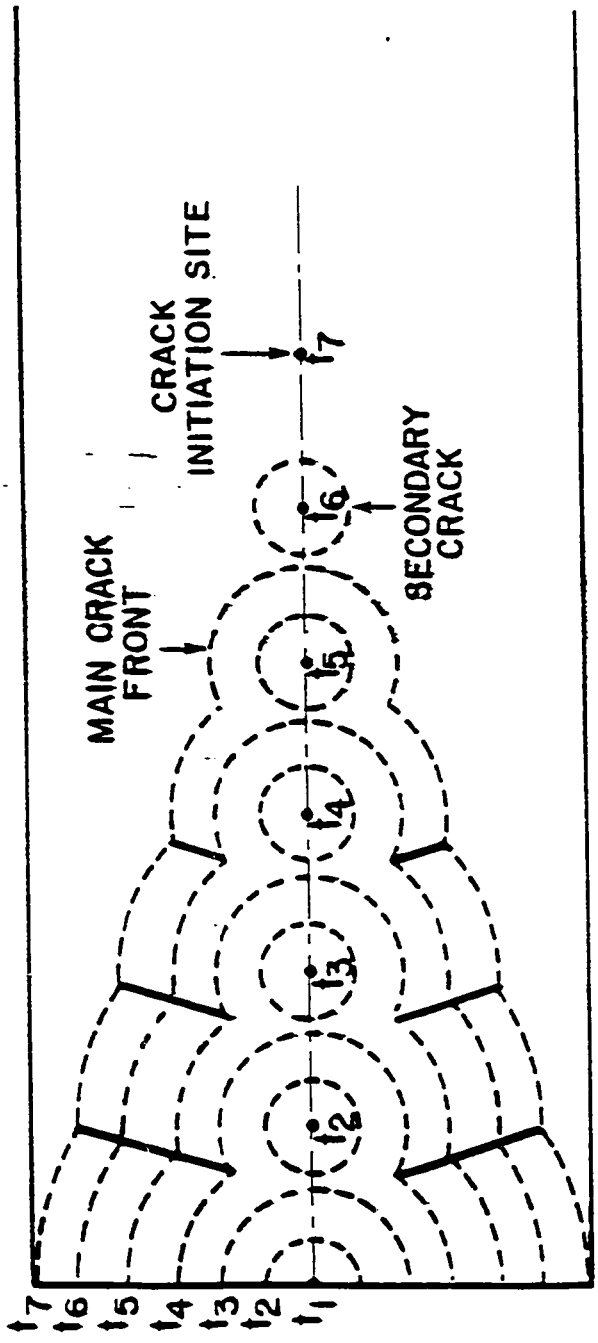


Figure 7. Proposed mechanism for formation of the herringbone pattern: (b) schematic illustration of formation of the herringbone pattern.

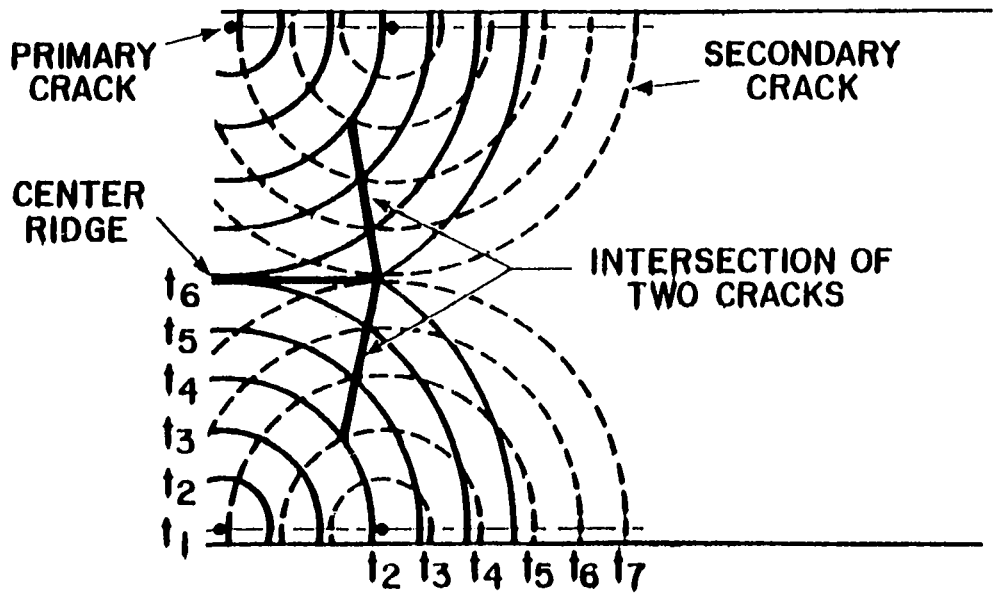


Figure 8. Proposed mechanism for formation of the reverse herringbone pattern: (a) schematic representation of formation of one pair of radial markings

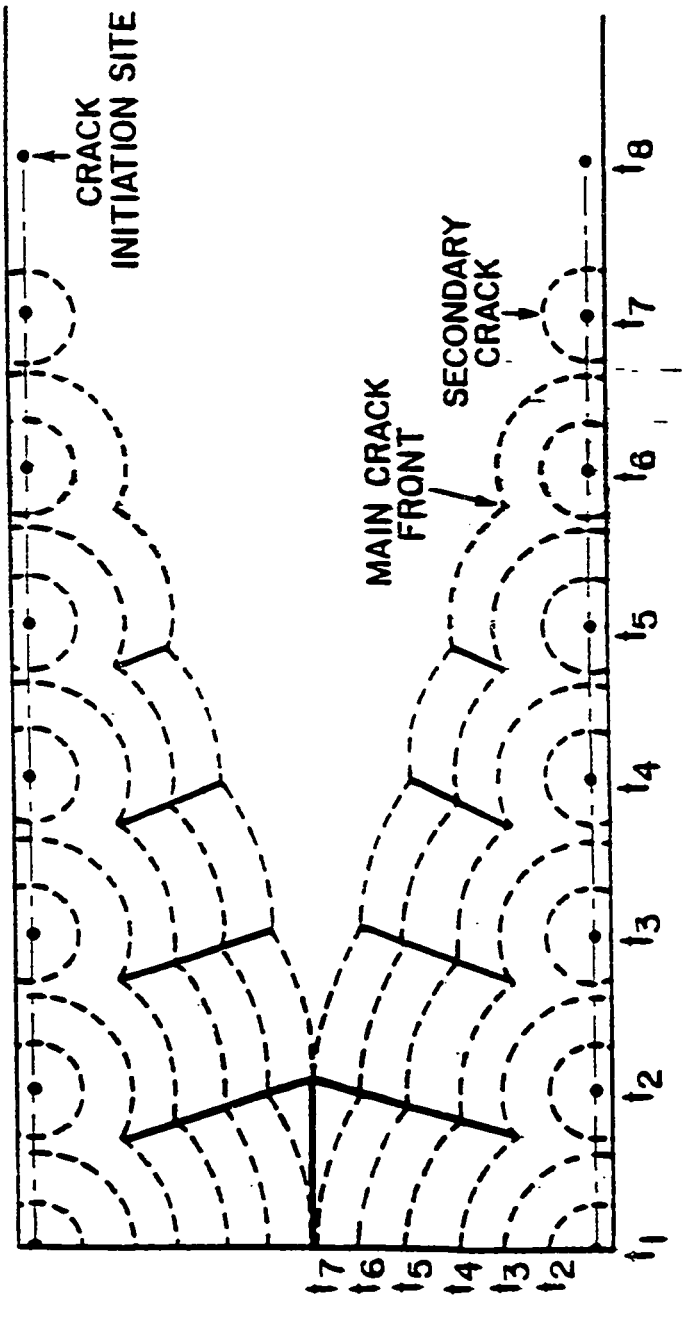


Figure 8. Proposed mechanism for formation of the reverse herringbone pattern: (b)schematic illustration of formation of the reverse herringbone pattern.

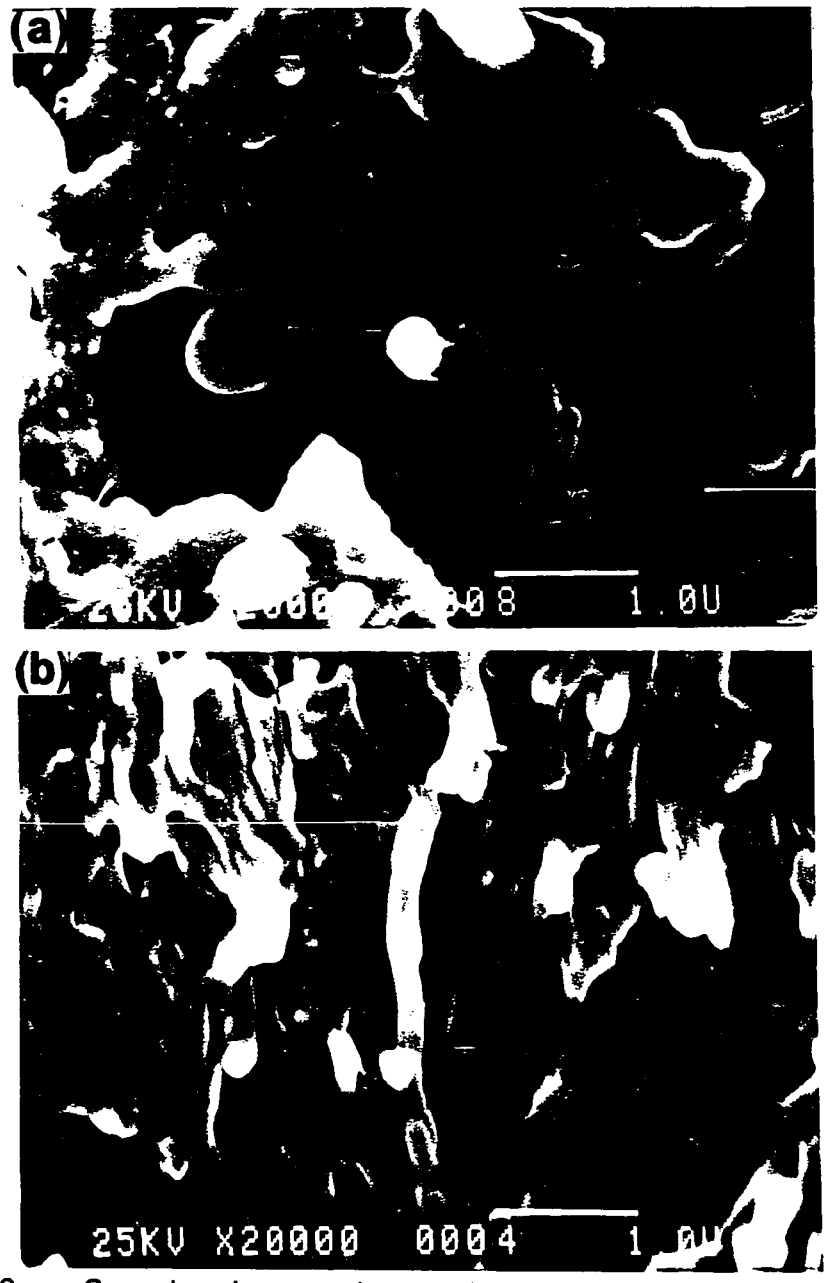


Figure 9. Scanning electron micrographs of the unetched fracture surface of a perpendicular specimen tested at -70°C with a crosshead speed of 229mm/min : (a) a region in the center, and (b) a region near the edge. The injection direction is from top to bottom

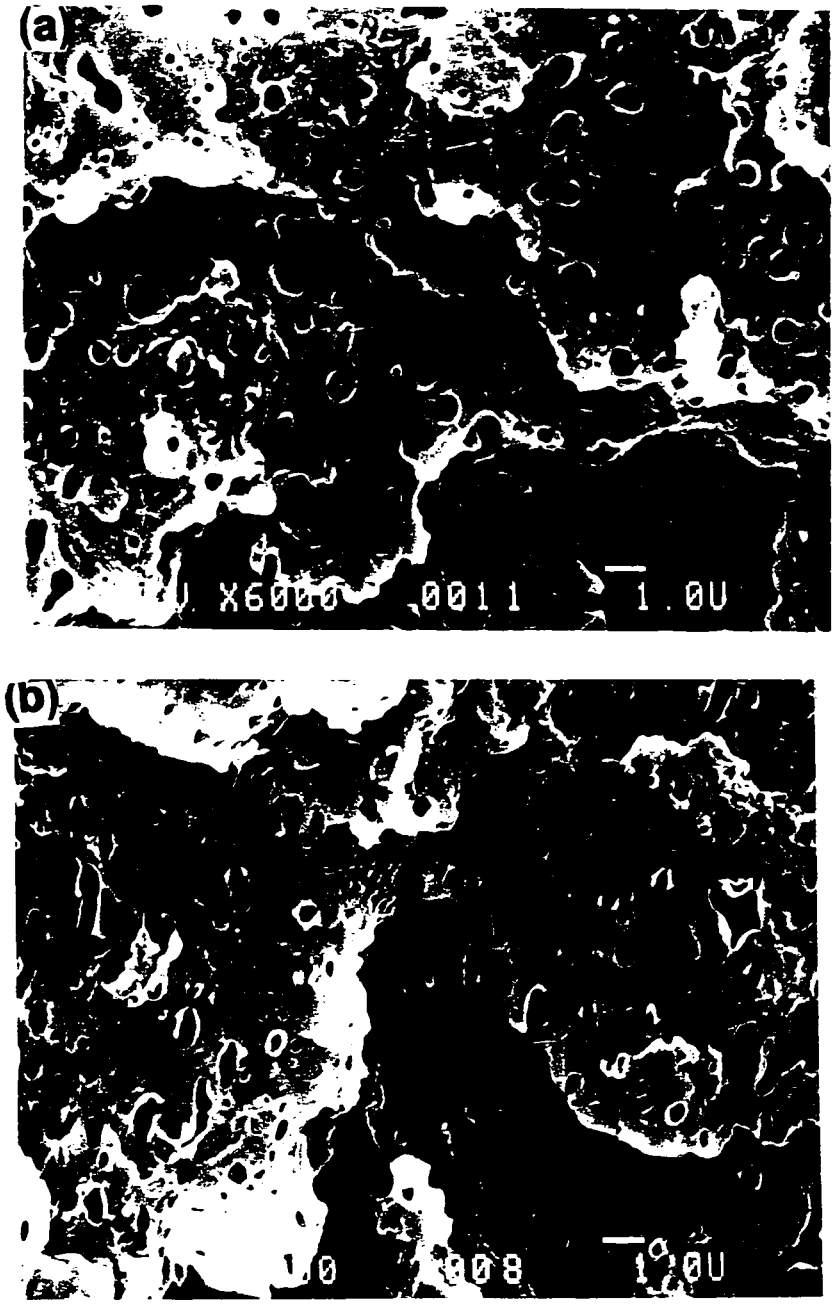


Figure 10. Scanning electron micrographs of etched cryogenic fracture surface at various positions through the thickness :(a),(b)in the injection direction and (a)d = 1.5 mm (b) d = 0.85 mm, d : distance from the edge of the 3mm thick plaque

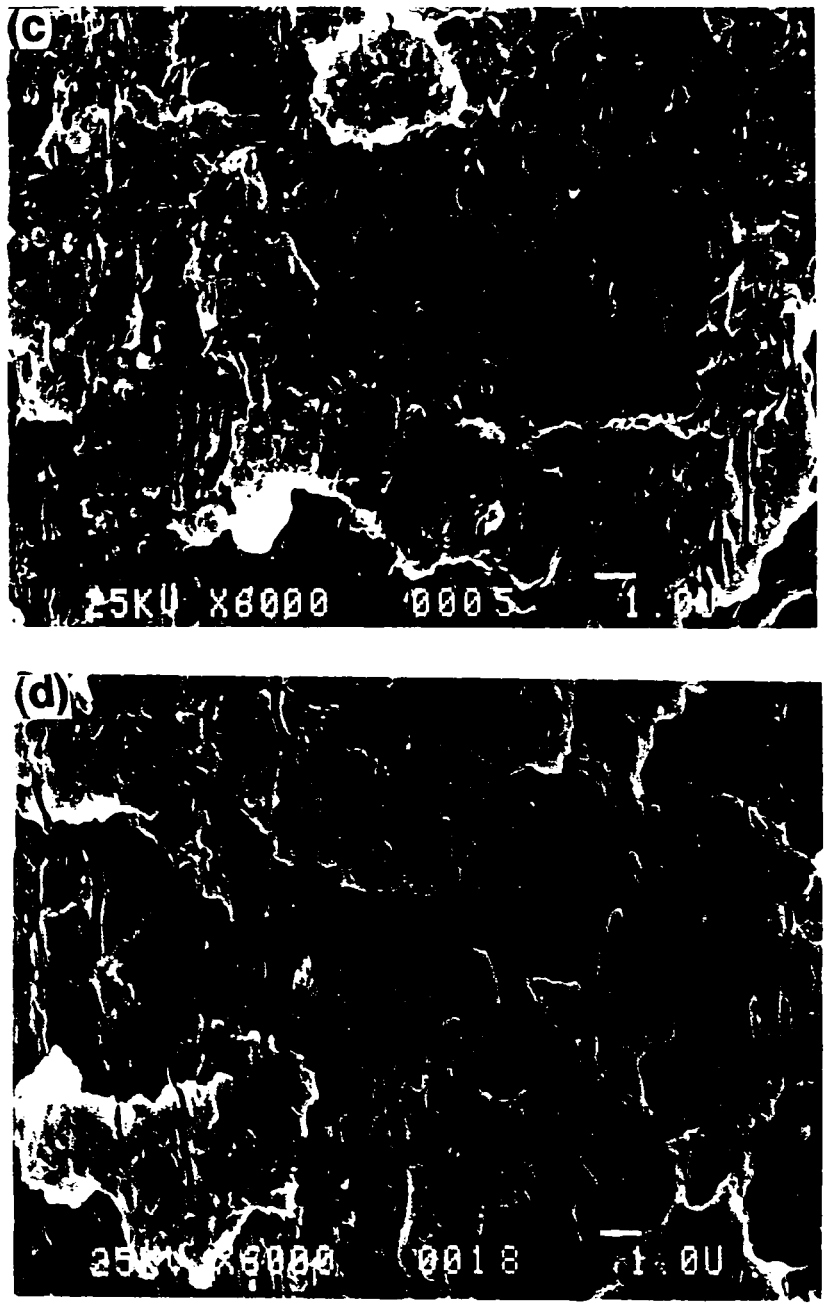


Figure 10. Scanning electron micrographs of the etched cryogenic fracture surface at various position through the thickness : (c),(d) in the injection direction and (c)d = 0.54mm (d) d = 0.12mm, d : distance from the edge of the 3mm thick plaque

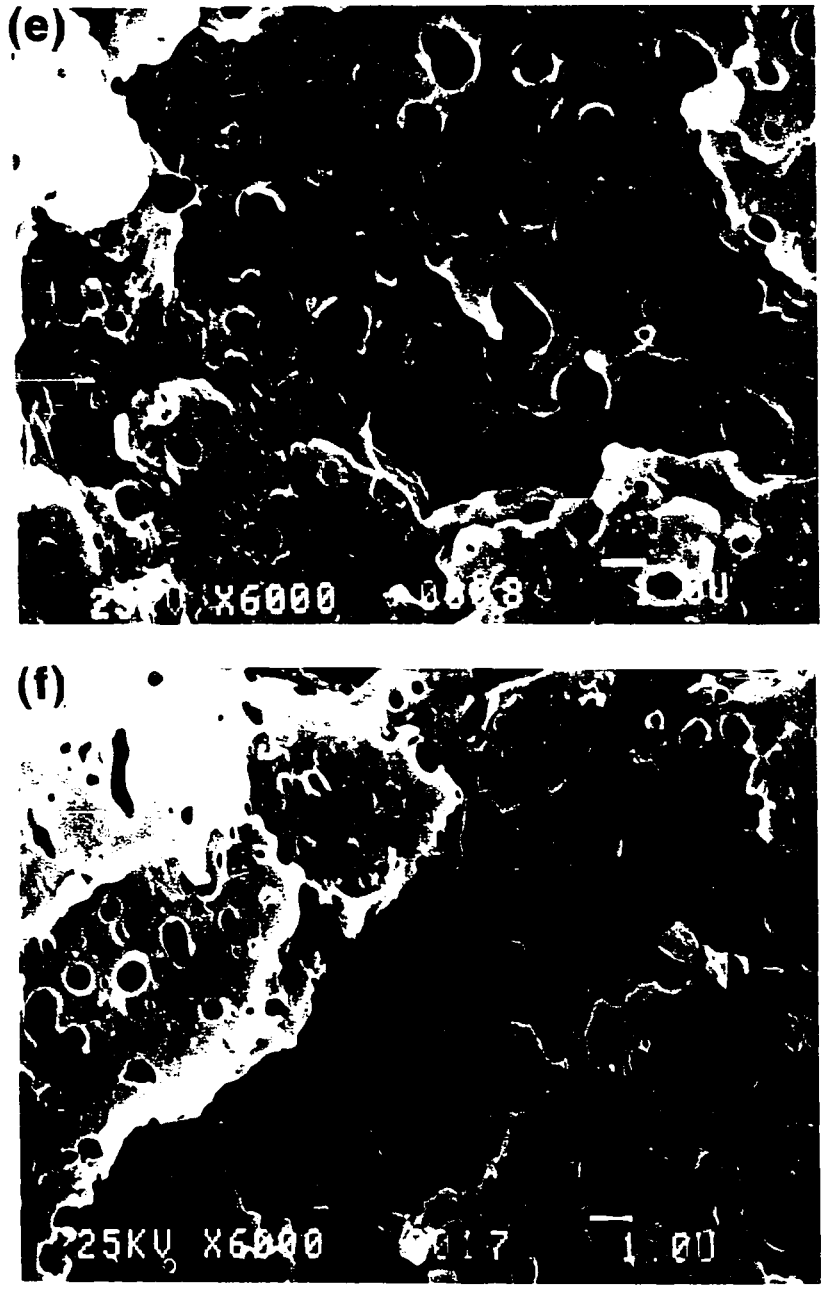


Figure 10. Scanning electron micrographs of etched cryogenic fracture surfaces at various positions through the thickness :(e),(f) perpendicular to the injection direction and (e) d = 1.5mm (f) d = 0.81mm, d: distance from the edge of the 3mm thick plaque

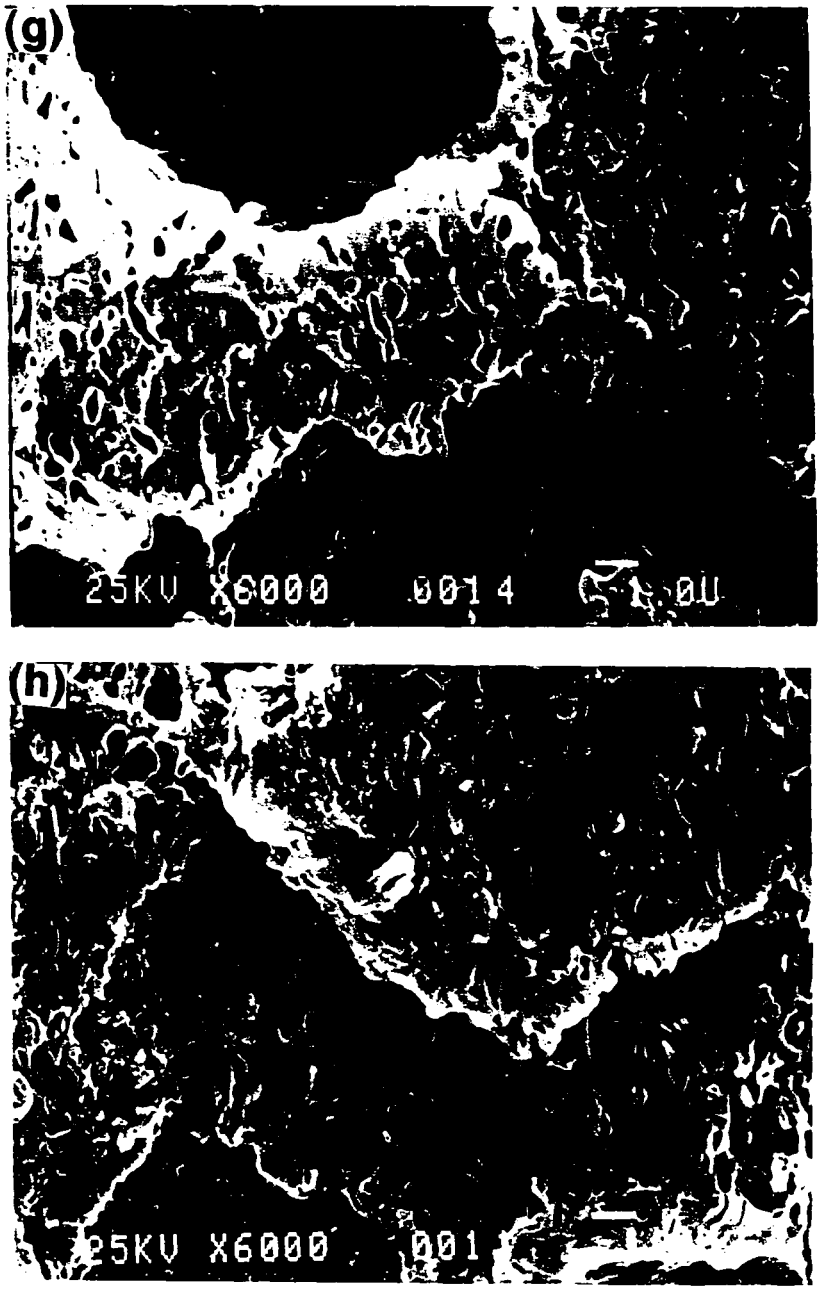


Figure 10. Scanning electron micrographs of etched cryogenic fracture surfaces at various positions through the thickness: (g),(h): perpendicular to the injection direction and (g)d = 0.53mm (h) d = 0.11mm,d: distance from the edge of the 3mm thick plaque

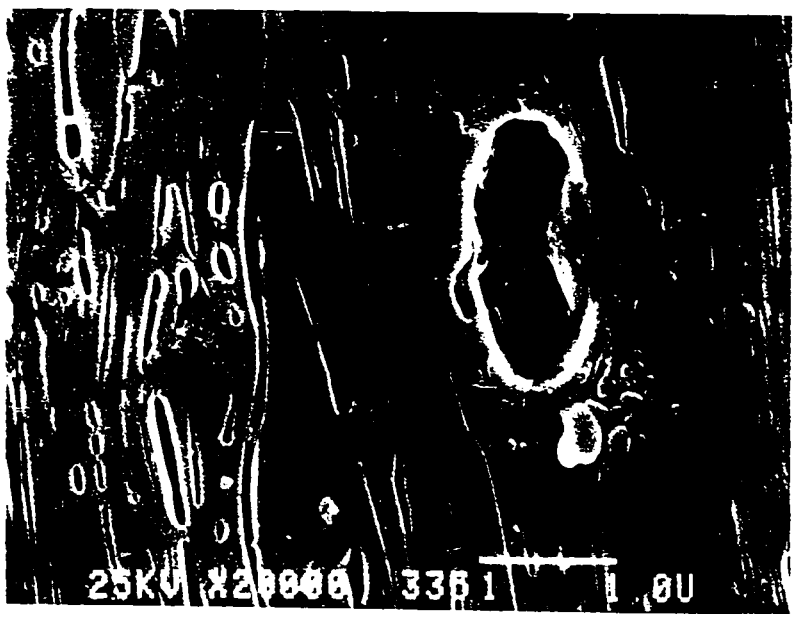

Figure 11. Scanning electron micrograph of etched mold-contacting edge. The injection is from top to bottom

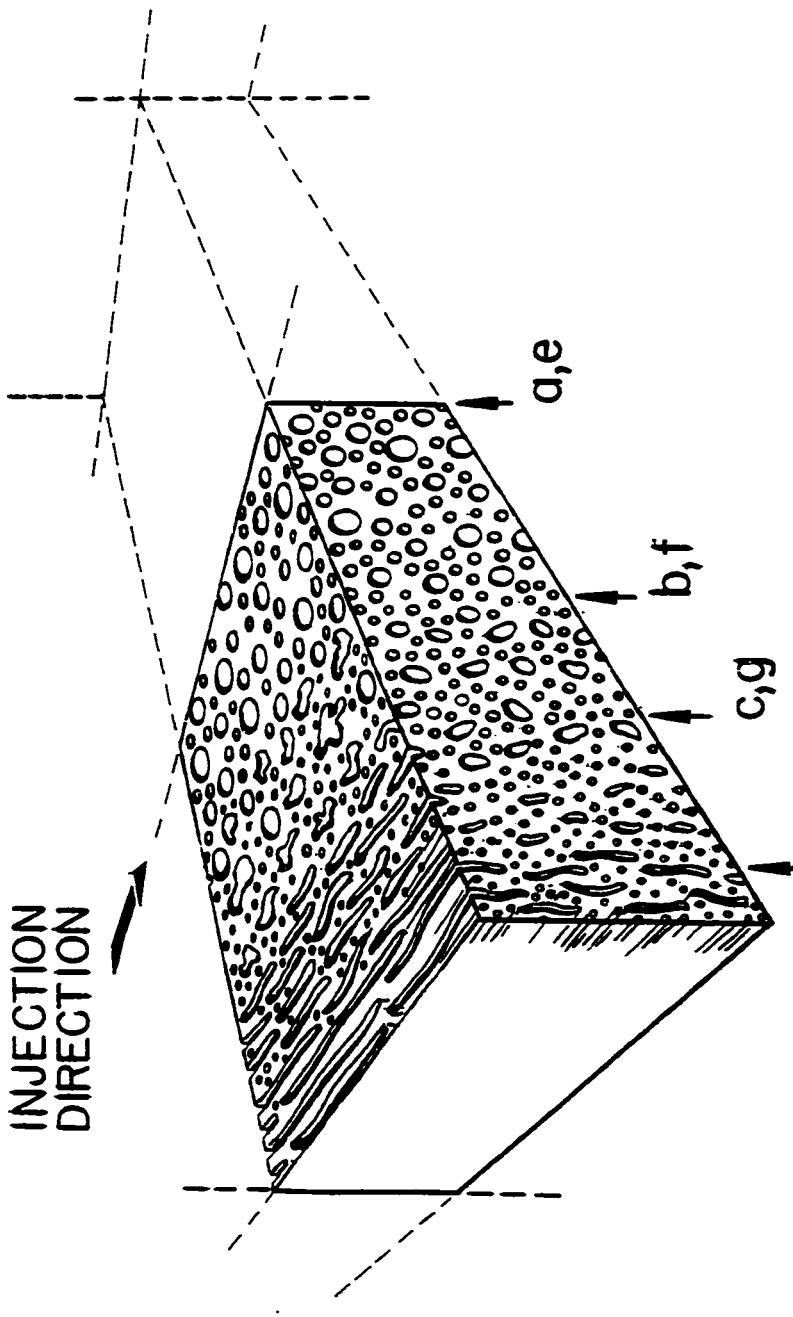


Figure 12. Schematic representation of the morphology. The position of the micrographs in Figure 10 are indicated

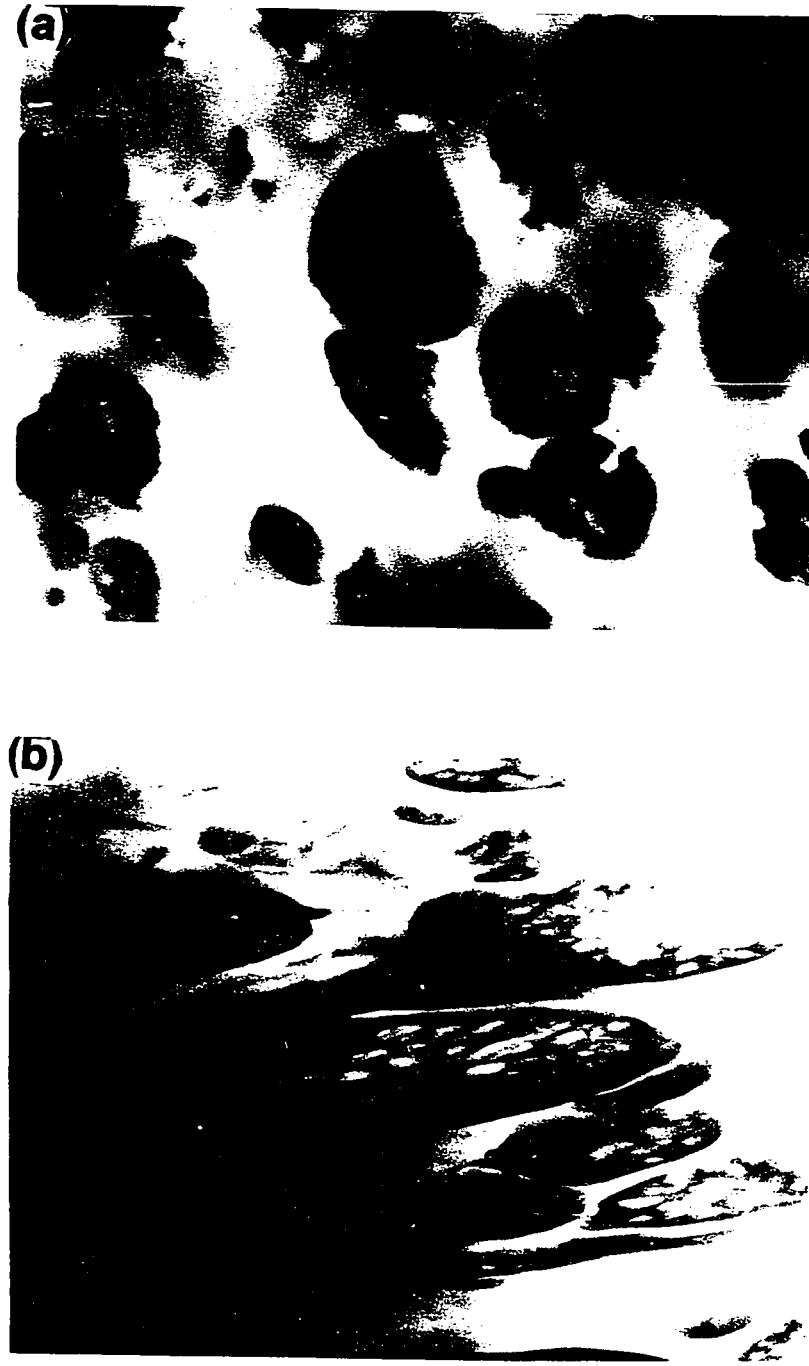


Figure 13. Transmission electron micrographs of $OsO_4$-stained sections: (a) from the center and (b) near the edge

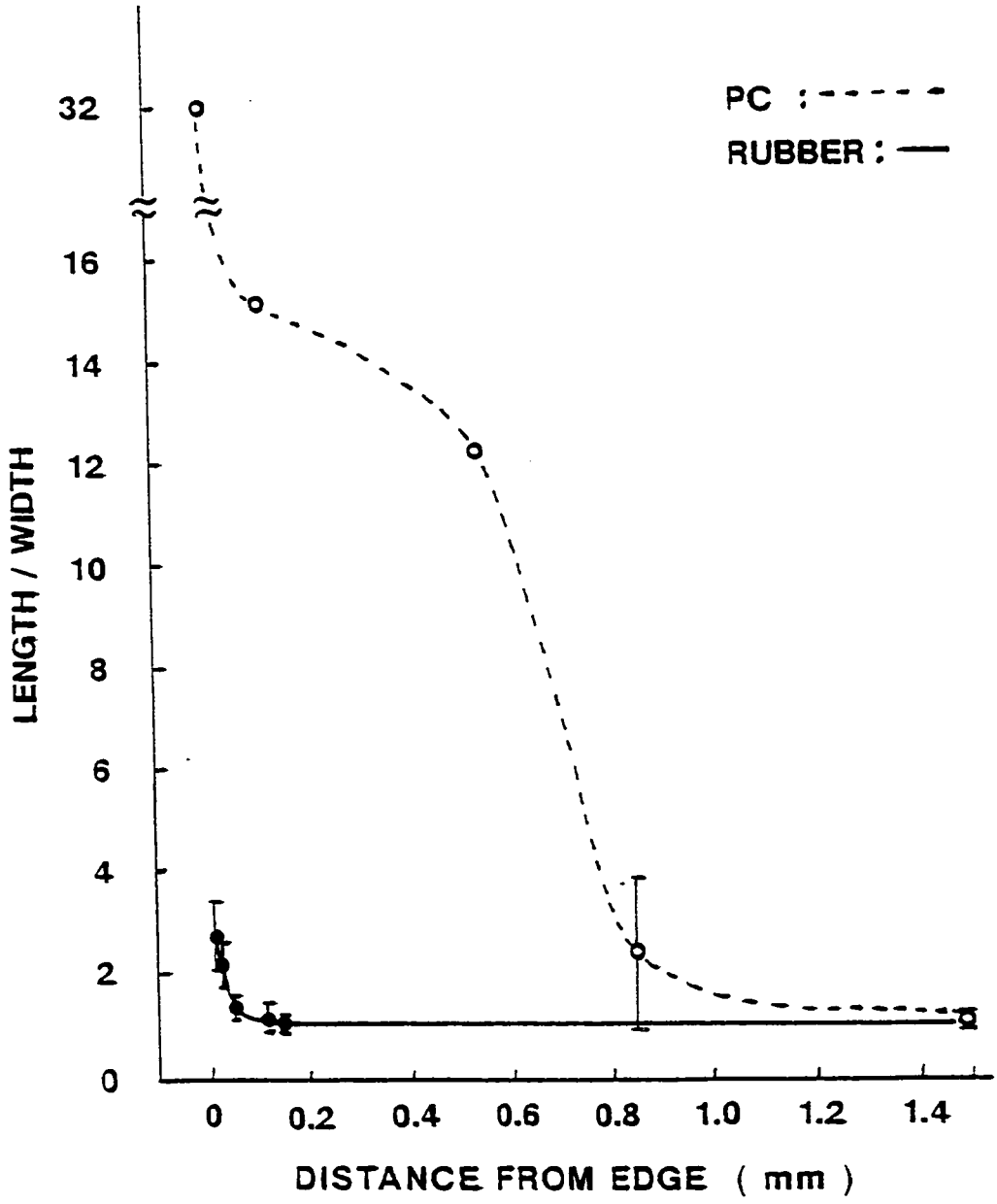


Figure 14. The length to thickness ratio of the PC domains and the rubber particles through the thickness of the 3mm thick plaque at its midpoint.

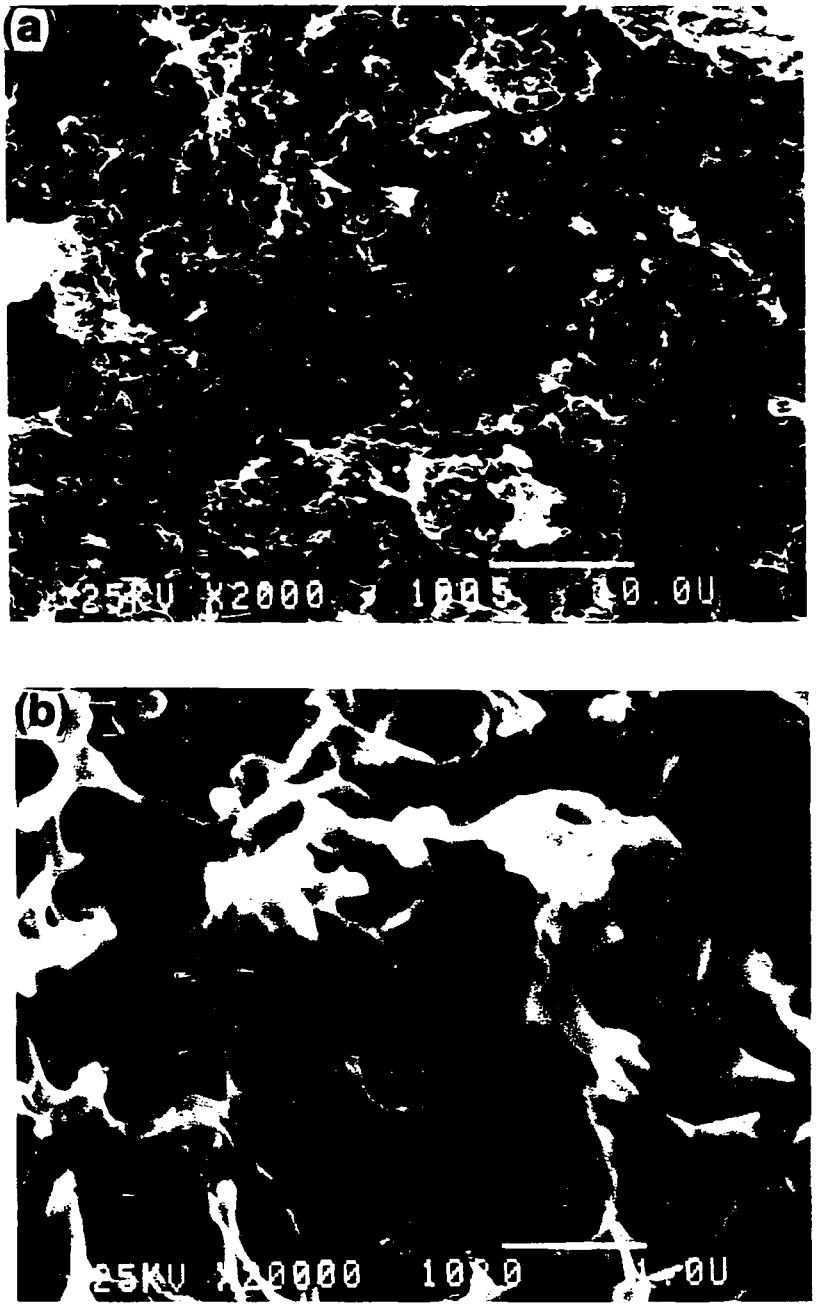


Figure 15. Scanning electron micrographs showing various regions of the fracture surface in Figure 2b, a parallel specimen tested at -25°C with a crosshead speed of 229 mm/min: (a) the center region of the herringbone, (b) higher magnification of (a)

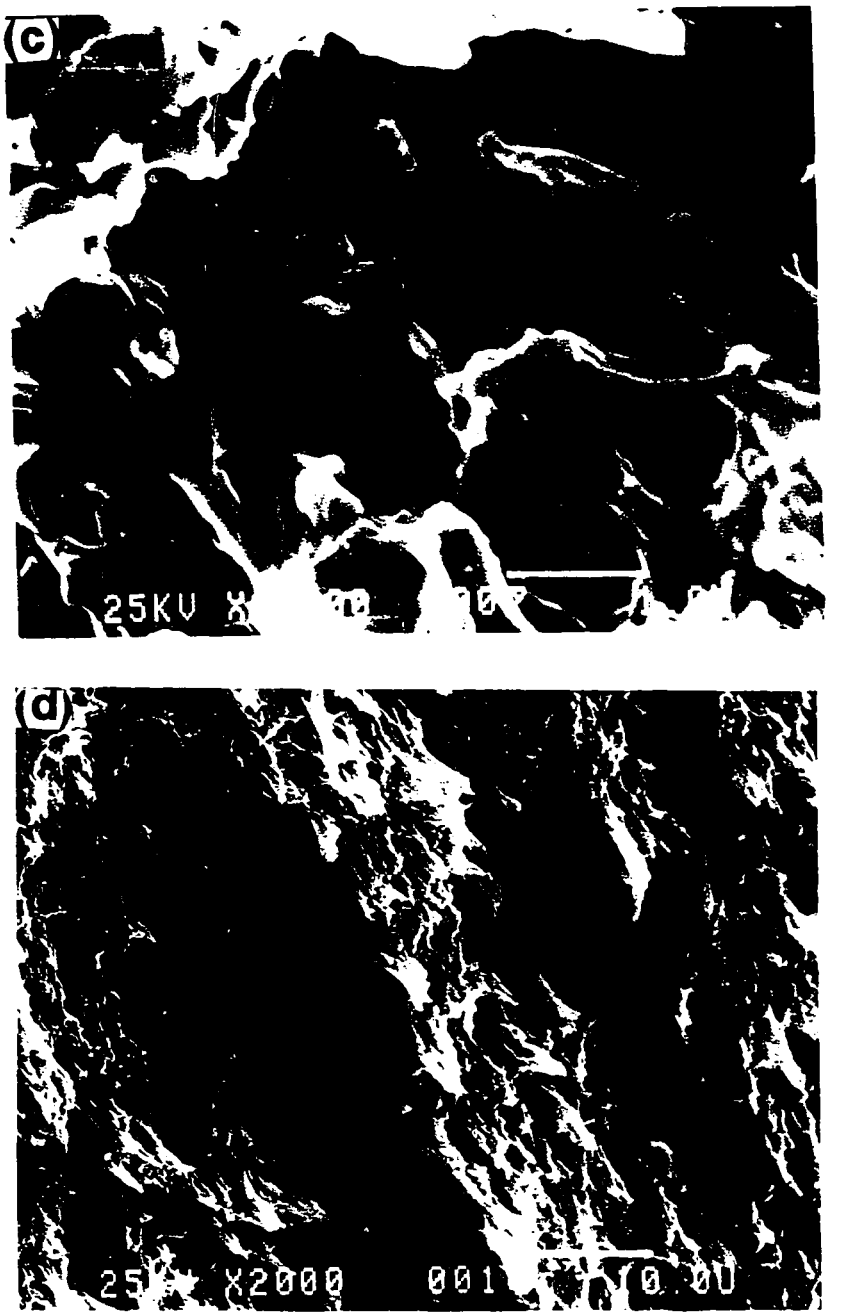


Figure 15. Scanning electron micrographs showing various regions of the fracture surface in Figure 2b, (c) higher magnification of (a), (d) a radial ridge in the outer portion of the herringbone. The crack propagated from left to right.

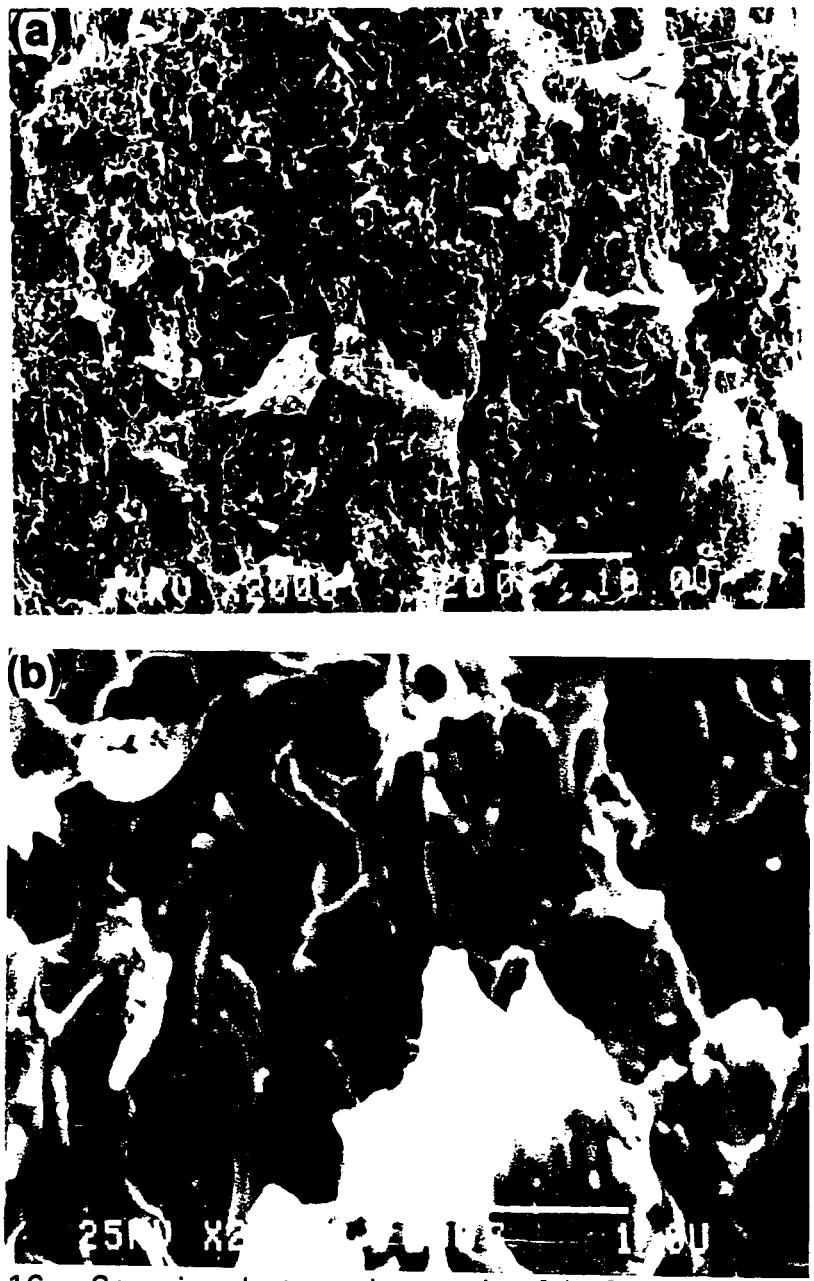


Figure 16. Scanning electron micrographs of the fracture surface in Figure 4c, a perpendicular specimen tested at -70°C with a crosshead speed of 229 mm/min: (a) the crack initiation region near the edge, and (b) a higher magnification of (a). Both the crack propagation direction and the injection direction were from top to bottom.

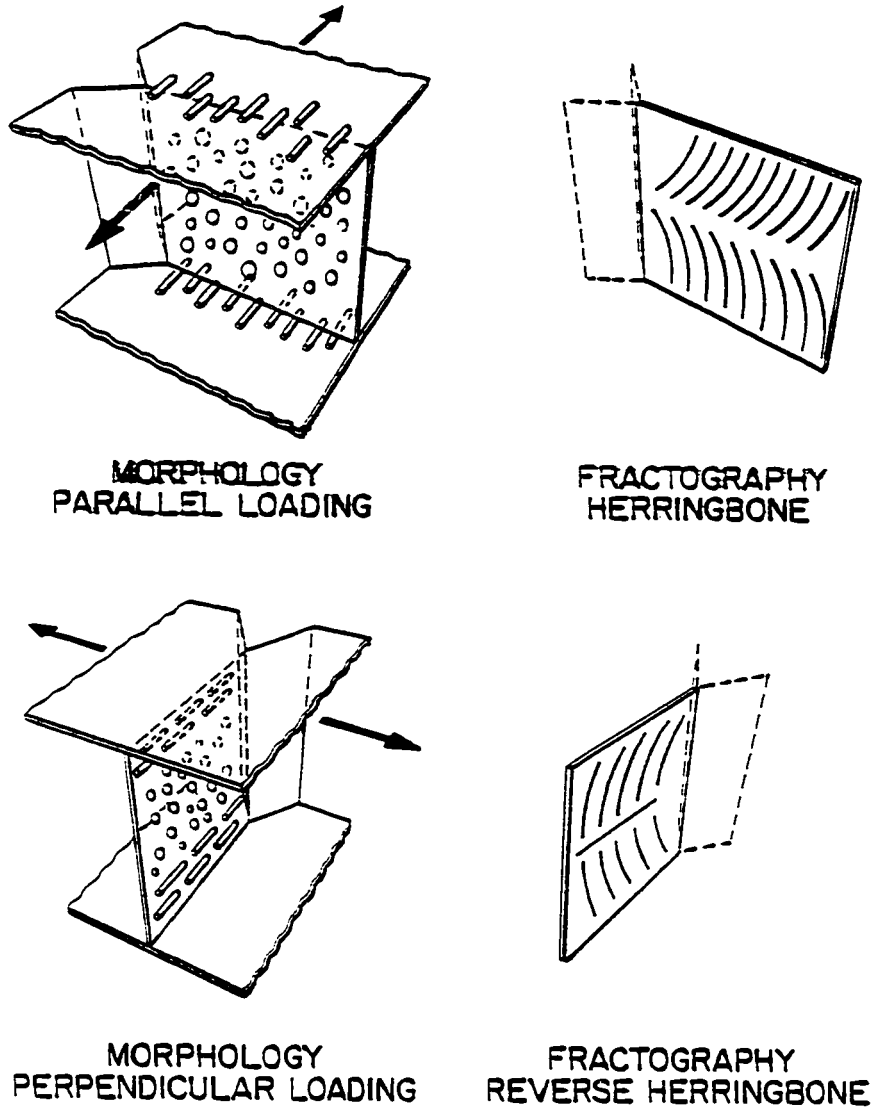


Figure 17 Schematic representation showing how the anisotropic morphology produced the herringbone and reverse herringbone fracture. The arrows indicate the tensile loading direction

## REFERENCES

### REFERENCES OF CHAPTER 1


1. Tadmore, Z., J. Appl. Polym. Sci., vol.18, p.1753 (1974)

2. Karger-Kocsis, J. and Csikal, I., Polym. Eng. Sci., vol.27, p.241 (1987)

3. Skochdopole, R. E., Finch, C. R. and Marshall, J., Polym. Eng. Sci., vol.27, p.627 (1987)

4. McLaughlin, K. W., Polym. Eng. Sci., vol.29, p.1560 (1989)

5. Tsebrenko, M. V., Rezanova, N. M. and Vinogradov, G. V., Polym. Eng. Sci., vol.20, p.1023 (1980)

6. Quintens, D., Groeninckx, G., Guest, M. and Aerts, L., Polym. Eng. Sci., (in press)

7. Karger-Kocsis, J., Kallo, A. and Kuleznev, V. N., Polymer, vol.25, p.279 (1984)

8. Elmendorp, J. J., Polym. Eng. Sci., vol.26, p.418 (1986)

9. Rayleigh, J. W. S., Proc. Roy. Soc., vol.29, p.71 (1879)

10. Taylor, G. I., Proc. Roy. Soc. (London), vol.A146, p.501 (1934)

11. Tomotika, S., Proc. Roy. Soc. (London), vol.A150, p.322 (1935)

12. Tomotika, S., Proc. Roy. Soc. (London), vol.A153, p.308 (1936)

13. Kurauchi, T. and Ohta, T., J. Mater. Sci., vol.19, p.1699 (1984)

14. Suarez, H., Barlow, J. W. and Paul, D. R., J. Appl. Polym. Sci., vol.29, p.3253 (1984)

15. Kim, W. N. and Burns, C. M., Polym. Eng. Sci., vol.28, p.1115 (1988)

16. Moore, L. D., Moyer, W. W. and Frazer, W. J., J. Appl. Polym. Sci., Appl. Polym. Sci. Symp., No.7, p.57 (1968)

17. Post, M. A., J. Paint Tech., vol.38, p.336 (1966)

18. Wexler, A. S., Anal. Chem., vol.36, p.1829 (1964)

19. Weir, A. P., Williams, D. A. and Woodstock, J. D., Chem. Ind., No. 35(August 28), p.990 (1971)

20. Casale, A., Moroni, A. and Spreafico, C., ACS Polym. Preprint, vol.15(1), p.334 (1974)

21. Mendelson, R. A., Polym. Eng. Sci., vol.16, p.690 (1976)

22. Shenoy, A. V. and Saini, D. R., Rheologica Acta., vol.23, p.368 (1984)

23. Saini, D. R. and Shenoy, A. V., J. Macromol. Sci.-Phys., vol.B22, p.437 (1983)

24. Ide, Y. and White, J. L., J. Appl. Polym. Sci., vol.20, p.2511 (1976)

25. Torza, S., Cox, R. G. and Mason, S. G., I. Colloid Interface Sci., vol.38, p.395 (1972)

26. Rumscheidt, F. D. and Manson, S. G., J. Colloid Sci., vol.16, p.238 (1961)

27. Tsebrenko, M. V., Yudin, A. V., Ablazova, T. I. and Vinogradov, G. V., Polymer, vol.17, p.831 (1976)

28. Elmendorp, J. J. and Van der Vegt, A. K., Polym. Eng. Sci., vol.26, p.1332 (1986)

29. Stone, H. A. and Leal, L. G., J. Fluid Mech., vol.198, p.399 (1989)

30. Rumscheidt, F. D. and Mason, S. G., J. Colloid Sci., vol.17, p.260 (1962)

31. Stone, H. A. and Leal, L. G., J. Fluid Mech., vol.206, p.223 (1989)

32. Goedde, E. F. and Yuen, M. C., J. Fluid Mech., vol.40, p.495 (1970)

33. Kamal, M. R. and Kenig, S., Polym. Eng. Sci., vol.12, p.302 (1972)

34. White, J. L., Polym. Eng. Sci., vol.15, p.44 (1975)

35. Barrie, I. T., Plast. Polym., vol.37, p.463 (1969)

36. Churchill, S. W. and Evans, L. B., J. Heat Transfer, vol.93, p.234 (1971)

37. White, J. L. and Dietz, W., Polym. Eng. Sci., vol.19, p.1081 (1979)

38. Carslaw, H. S. and Jaeger, J. C., "Conduction of Heat in Solids", 2nd., Oxford University Press, New York (1973)

39. Tadmor, Z. and Gogos, C. G., "Principles of Polymer Processing", Wiley-Interscience, Chap. 5, p 132 (1979)

REFERENCES OF CHAPTER 2

1. Plochocki, A. P., Polym. Eng. Sci., vol.23, p.618 (1983)

2. Karger-Kocsis, J., Kallo, A. and Kuleznev, V. N., Polymer, vol.25, p.279 (1984).

3. Howe, D. V. and Wolkowicz, M. D., Polym. Eng. Sci., vol.27, p.1582 (1987)

4. Wu, S., Polym. Eng. Sci., vol.27, p.335 (1987)

5. Karger-Kocsis, J. and Csikai, I., Polym. Eng. Sci., vol.27, p.241 (1987)

6. Thamm, R. C., Rubber Chem. Tech., vol.50, p.24 (1977)

7. White, J. L. and Dietz, W., Polym. Eng. Sci., vol.19, p.1081 (1979)

8. Tadmor, Z., J. Appl. Polym. Sci., vol.18, p.1753 (1974)

9. Kurauchi, T. and Ohta, T., J. Mater. Sci., vol.19, p.1699 (1984)

10. Kim, W. N. and Burns, C. M., Polym. Eng. Sci., vol.28, p.1115 (1988)

11. Suarez, H., Barlow, J. W. and Paul, D. R., L. Appl. Polym. Sci., vol.29, p.3253 (1984)

12. Stefan, D. and Willians, H. L., J. Appl. Polym. Sci., vol.18, p.1451 (1974)

13. Lee, M. P., Hiltner, A. and Baer, E., Polymer, (in press)

14. Chalkley, H. W., Cornfield, J. and Park, H., Science, vol.110, p.295 (1949)

15. Quintens, D., Groeninckx, G., Guest, M. and Aerts, L., Polym. Eng. Sci., (in press)

16. Vanoene, M., J. Colloid Interface Sci., vol.40, p.448 (1972)

17. Stone, H. A. and Leal, L. G., J. Fluid Mech., vol.198, p.399 (1989)

18. Heikens, D. and Barentsen, W., Polymer, vol.18, p.69 (1977)

REFERENCES OF CHAPTER 3

1. Broek, D., "Elementary Engineering Fracture Mechanics", 4th Ed., Kluwer Academic, (1987)

2. Kinloch, A. J. and Young, R. J., "Fracture Behavior of Polymers", Elsevier-Applied Science, London, (1983)

3. Boyle, R. W., Sullivan, A. M. and Kraffy, J. M., Welding J. Res. Suppl., vol.41, p.428 (1962)

4. Key, P. L. and Katz, Y., Int. J. Fract. Mech., vol.5, p.63 (1969)

5. Boyd, G. M., Engineering, vol.175, p.65 (1953)

6. Tipper, C. F., J. Iron Steel Inst., vol.185, p.4 (1957)

7. Tipper, c. F., Met. Revs., vol.2, p.195 (1957)

8. Lee, M. P., Hiltner, A. and Baer, E., Polymer, (in press)

9. Lee, M. P., Hiltner, A. and Baer, E., Polymer, (in press)

10. Mills, N. J., J. Mater. Sci., vol.11, p.363 (1976)

11. Pitman, G. L., Ward, I. M. and Duckell, R. A., J. Mater. Sci., vol.13, p.2092 (1978)

12. Parvin, M. and Williams, J. G., J. Mater. Sci., vol.10, p.1883 (1975)

13. Fraser, R. A. W. and Ward, I. M., J. Mater. Sci., vol.12, p.459 (1977)

14. Parvin, M. and Williams, J. G., Int. J. Fract., vol.11, p.963 (1975)

15. Bucknall, C. B., "Toughened Plastics", Applied Science Publishers, London, (1977)

16. Donald, A. M. and Kramer, E. J., J. Mater. Sci., vol.17, p.1765 (1982)

17. Yee, A. F., J. Mater. Sci., vol.12, p.757 (1977)

18. Engel, L., Klingele, H., Ehrenstein, G. W. and Schaper, H., "An Atlas of Polymer Damage", Prentice-Hall, Englewood Cliffs, N. J.

19. Kusy, R. P. and Turner, D. T., Polymer, vol.18, p.391 (1977)

20. Hull, D., J. Mater. Sci., vol.5, p.357 (1970)

21. Murray, J. and Hull, D., J. Polym. Sci. vol.8(A-2), p.583 (1970)

22. Hull, D. and Owen, T. W., L. Polym. Sci., Polym. Phys. Ed., vol.11, p.2039 (1973)

23. Kies, J. A., Sullivan, A. M. and Irwin, G. R., J. Appl. Phys., vol.21, p.716 (1950)

24. Keitz, J. D., Barlow, J. W. and Paul, D. R., J. Appl. Polym. Sci., vol.29, p.3131 (1984)

25. Ma, M., Vijayan, K., Hiltner, A. and Baer, E., J. Mater. Sci., vol.25, p.2039 (1990)

REFERENCES OF CHAPTER 4

1. Lee, M. P., Hiltner, A. and Baer, E., J. Mat. Sci. (submitted)

2. Kies, J. A., Sullivan, A. M. and Irwin, G. R., J. Appl. Phys., vol. 21, p. 716 (1950)

3. Boyd, G. M., Engineering, vol.175, p.65 and p.100 (1953)

4. Tipper, C. F., J. Iron Steel Inst., vol.185, p.4 (1957)

5. Tipper, C. F., Met. Revs., vol.2, p.195 (1957)

6. Karger-Kocsis, J. and Csikai, I., Polymer. Eng. Sci., vol.27, p.241 (1987)

7. Kato, K., Polymer, vol.8, p.33 (1967)

8. Kato, K., Polymer, vol.9, p.225 (1968)

9. Henery, L. H., Polym. Eng. Sci., vol.14, p.167 (1974)

10. Koiwa, S., J. Appl. Polym. Sci., vol.19, p.1625 (1975)

11. Hagerman, E. M., Plast. Eng., vol.50, p.67 (1973)

12. Thamm, R. C., Rubber Chem. Tech., vol.50, p.24 (1977)

13. Estman, G. C. and Smith, E. G., Polymer, vol.14, p.509 (1973)

14. Tadmor, Z., J. Appl. Polym. Sci., vol.18, p.1753 (1974)

15. Katti, S. S. and Schultz, J. M., Polym. Eng. Sci., vol.22, p.1001 (1982)

16. Engel, L., Klingele, H., Ehrenstein, G. W. and Schaper, H., An Atlas of Polymer Damage, Prentice-Hall, Englewood Cliffs, NJ. p.147

17. Cook, J. and Gordon, J. E., Proc. Roy. Soc.,(London), vol.A282, p.508 (1964)